



# Advances, challenges, and environmental impacts in metal–air battery electrolytes



Manuel Salado <sup>a, \*\*, \*</sup>, Erlantz Lizundia <sup>a, b, \*</sup>

<sup>a</sup> BCMaterials, Basque Center for Materials, Applications and Nanostructures, UPV/EHU Science Park Leioa, 48940, Spain

<sup>b</sup> Life Cycle Thinking Group, Department of Graphic Design and Engineering Projects, University of the Basque Country (UPV/EHU), Plaza Ingeniero Torres Quevedo 1 Bilbao, Biscay, 48013, Spain

## ARTICLE INFO

### Article history:

Received 14 March 2022

Received in revised form

25 May 2022

Accepted 26 May 2022

Available online 2 June 2022

### Keywords:

Metal–air batteries

Electrolyte

Gel polymer electrolyte

Environmental impact

Life cycle assessment

## ABSTRACT

Efficient energy storage technologies are vital in the current efforts towards decarbonisation. Batteries, as one of the most versatile electrochemical energy storage systems, have the potential to shape the transition from the current climate crisis scenario to a carbon neutral and sustainable future. In particular, metal–air batteries are gaining scientific and industrial interest as promising contenders to the ubiquitous lithium-ion batteries. The electrolyte plays a critical role in metal–air batteries as it determines the battery performance, its safety and the operating lifespan. The low-density, ease of processing, good thermal and electrochemical stability, mechanically stiff but ductile character, electrically insulating properties and tailor-made chemistry make polymers singularly interesting to be applied as a separator/liquid electrolyte pair, gel-electrolytes or solid-electrolytes. Accordingly, in this work the current bottlenecks and challenges in metal–air batteries are presented, with particular emphasis on the electrolyte design. The implementation of aqueous liquid electrolytes, organic liquid electrolytes, polymer membranes soaked in liquid electrolytes, gel-like electrolytes and solid-state electrolytes is discussed and the environmental impacts associated with metal–air batteries are analysed within a Circular Economy perspective. We expect this work can guide future efforts in the development of potentially sustainable next generation metal-air batteries.

© 2022 The Author(s). Published by Elsevier Ltd. This is an open access article under the CC BY license (<http://creativecommons.org/licenses/by/4.0/>).

## 1. Introduction

Nowadays, lithium-ion batteries (LIBs) are the preferred commercial technology available to fulfill the demanded requirements (e.g. energy-to-weight ratios, high open circuit voltage, low self-discharge rate, no memory effect and a slow loss of charge when not in use) [1]. However, this technology presents different limitations such as cost and safety issues (e.g. thermal runaway due to electrolyte degradation/evaporation) [2]. Although LIBs have been available for many years, this technology still has several drawbacks to overcome through different strategies (e.g. solid-state electrolyte) [3]. It is indeed expected that the future expansion of electric vehicles (EVs) will multiply by a factor of nine the lithium (Li) demand for the production of LIBs in the next ten years [4].

Consequently, it will be a notable increment in the consumption of some certain materials (e.g. cobalt, manganese, nickel...) used in their fabrication, especially of the cathode [5].

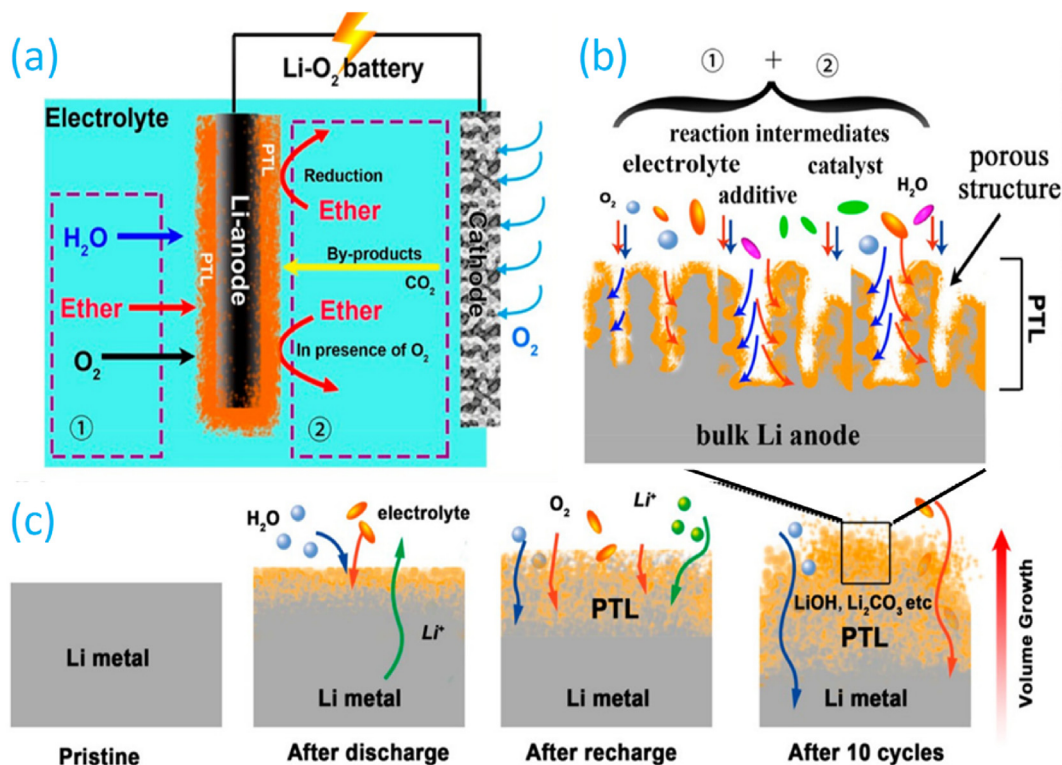
In this scenario, metal–air batteries (MABs) are considered as a viable future alternative to LIBs. However, several challenges and drawbacks need to be faced for their practical implementation [6]. For instance, high charge voltages and reactive oxygen intermediates such as superoxide and singlet oxygen can lead to the decomposition of the cathode material and the electrolyte [7]. Therefore, a careful selection of the electrolyte is of central importance given its pivotal role in the battery cell safety and its electrochemical properties.

It should be considered that the reactivity of the metal anode influences the nature of the electrolyte (aqueous or non-aqueous); nevertheless, carbon dioxide (CO<sub>2</sub>), nitrogen (N<sub>2</sub>), and oxygen (O<sub>2</sub>) present as dissolved species in the liquid electrolyte, strongly affecting the discharge mechanism and the stability of the metal anode. Sun et al. [8], investigated the effect of Li anode degradation by in-situ X-ray and neutron tomography. As summarised in Fig. 1a, the species in the electrolyte induce the formation of an irreversible

\* Corresponding author.

\*\* Corresponding author.

E-mail addresses: [manuel.salado@bcmaterials.net](mailto:manuel.salado@bcmaterials.net) (M. Salado), [erlantz.lizundia@ehu.eus](mailto:erlantz.lizundia@ehu.eus) (E. Lizundia).



**Fig. 1.** Mechanisms for Li anode degradation in a Li-air battery. (a) Li anode transformation in the presence of an ether-based electrolyte, that is, the chemical path as indicated by ① and the electrochemical path indicated by ②. (b) and (c) Illustration of the morphological evolution during long-term electrochemical cycling conditions [8]. Copyright © 2019, American Chemical Society.

Li porous-structuralised transition layer under various chemical conditions. More specifically, Fig. 1b and c depict as the lithium anode suffers progressively a severe morphological degradation (e.g. a large volume expansion) when it is exposed to ten charge-discharge cycles.

This significant corrosion or degradation is not a particular case of Li metal. Indeed, sodium (Na), potassium (K), and zinc (Zn) metals have also shown this behaviour in their corresponding MAB configurations [9–11]. Therefore, the excellent theoretical energy density of the metal anode cannot be fully exploited if it suffers from a fast degradation during cycling. On the other hand, the assembly of a desired MAB testing results a complex task. Particularly challenging is the development of new cathode materials (for the three components: a catalyst layer, a current collector and a gas diffusion layer) to efficiently increase the  $O_2$  diffusion. Among the three components, the development of novel morphology and composition of a catalyst material has attracted the attention of researchers. Recently, a core-shell  $CuMo_2ON@NG$  nanohybrid cathode has been designed through a simple, scalable, cost-effective, and eco-friendly pyrolysis strategy for Zn-air batteries [12]. A specific capacity of  $736 \text{ mAh} \cdot \text{g}_{Zn}^{-1}$  and a remarkable energy density of  $800.75 \text{ Wh} \cdot \text{kg}^{-1}$  were achieved. Another method proposed [13] consisted in FeNi alloy nanoparticles (NPs) encapsulated in N-doped carbon nanotubes (NCNT) grown onto a cotton pad (FeNi@NCNT-CP) by a self-jet vapour-phase growth approach. This method provided a better peak power density ( $200 \text{ mW} \cdot \text{cm}^{-2}$ ) compared to the previous pyrolysis process ( $176.3 \text{ mW} \cdot \text{cm}^{-2}$ ).

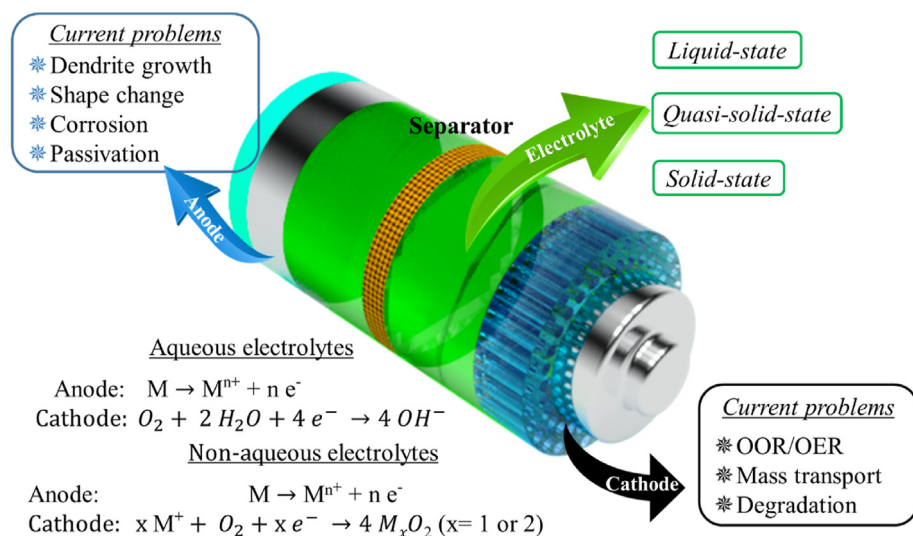
Although, extensive research has been done in this area [14], the research community has been aware of the importance of electrolyte chemistry in the final performance of the batteries. In this direction, a dual-solvent system has been recently studied by mixing fluorinated 1,6-dimethoxyhexane (FDMH) and 1,2-

dimethoxyethane (DME) [15]. In this system, the FDMH provides electrolyte oxidative stability (6 V) while the co-solvent DME enables improved ionic conductivity and reduced interfacial resistance ( $\sim 75 \Omega \cdot \text{cm}^{-1}$ ). Besides, the development of novel electrolytes can allow the suppression of metal dendrites. For instance, prefixed  $CO_2$  in a poly(vinyl alcohol) (PVA) electrolyte via ionisation to avoid the poisoning effect of  $CO_2$  as well as significantly suppress the Zn dendrite growth and ZnO deposition [16]. As a result, even with a concentration of  $CO_2$  of 22.7% in the atmosphere, the battery with the modified electrolyte was twelve times more stable than the one containing a neat PVA electrolyte.

Taking into account these concepts, the scope of this review comprises firstly a brief description of the main issues that limit the full implementation of MABs and secondly, the different strategies that could be considered during the design of novel electrolytes to overcome these problems.

## 2. Metal-air batteries: Structure and mechanism

Current post Li-ion technologies follow a similar working principle of metal batteries of Li-ion/metal, with the substitution of other alkali metals (e.g.  $Na^+$ ,  $K^+$ ), divalent ( $Ca^{2+}$ ,  $Mg^{2+}$ ) or trivalent metals ( $Al^{3+}$ ) [3,17]. However, the sluggish ionic transport or the poorly reversible metal plating/stripping at the anode of multivalent batteries are in sharp contrast with the features usually found in LIBs, mainly due to the lack of suitable electrolytes [18]. In contrast to the physically closed system of a LIB [19], the MAB is featured with an open cell structure as shown in Fig. 2. Basically, the cell configuration possess the same structure than a LIB (a metal anode, a separator and an electrolyte), but with a porous cathode [20]. The presence of  $O_2$  and electrolyte impurities yield side reactions (e.g. redox reactions that produce reduced oxygen species such as superoxides) on the



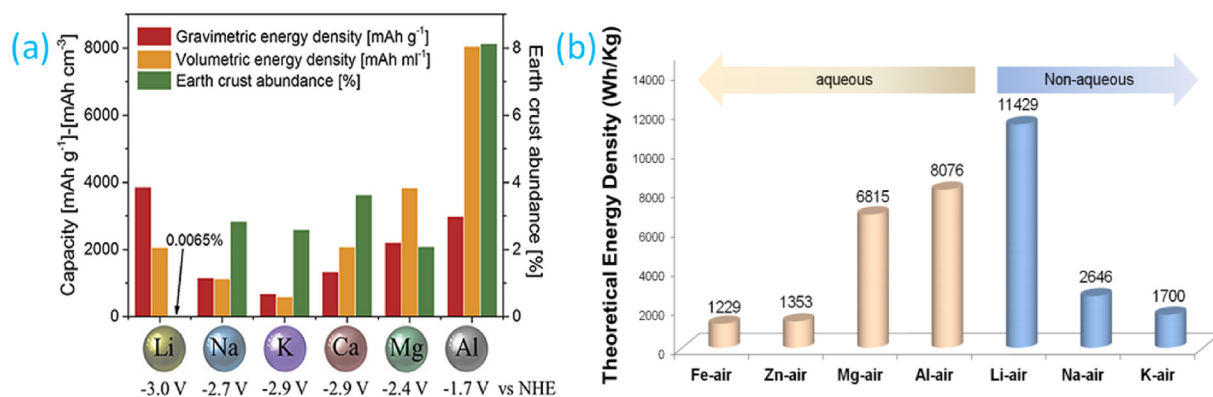
**Fig. 2.** General configuration of a metal–air battery, highlighting the main issues associated to the cathode and the anode and the chemical reactions depending on the type of liquid electrolyte.

metal electrode, which usually result in the corrosion of the metal anode by the electrolyte, electrolyte degradation, or blockage of cathode reaction sites because of electrolyte decomposition [21]. As a consequence, metal electrodes in MABs suffer from metal dendrite growth, shape change, corrosion and surface passivation [22]. In the case of non-aqueous batteries, generally a solid electrolyte interphase (SEI) is formed on the anode surface inhibiting further electrolyte decomposition. However, for aqueous batteries, the lithium metal is isolated avoiding self-discharge reaction with the oxygen and allowing the application of acidic or neutral electrolytes that are not susceptible to carbonation processes.

Among the different *anode metals* previously described, Li-air batteries are the most studied batteries within the MAB technology because of their high energy density of about  $3458 \text{ Wh} \cdot \text{kg}^{-1}$ , which is several times higher than that of conventional LIBs ( $250\text{--}300 \text{ Wh} \cdot \text{kg}^{-1}$ ) [23]. Due to the high reactivity of Li in aqueous electrolytes, Zn metal has been deeply studied as an anode choice in MABs. As a result, enhanced safety and lower costs are achieved at expenses of a lower energy density of  $1084 \text{ Wh} \cdot \text{g}^{-1}$ . Nevertheless, other metal-air systems have also been developed as summarised in Fig. 3a. Among them and bearing in mind the (theoretical) energy density, the good availability of the raw

material and its high safety, Al can be considered a promising metal anode to replace both Zn-air and Li-air batteries. Nevertheless, up-to-date only Zn-air batteries can be electrically recharged in aqueous electrolyte. In the case of the Al- or Mg-air batteries, as they cannot be directly reduced from ions to metals, a mechanical method has to be used to change the metal anodes.

To ensure an efficient ionic transport between electrodes and avoid the short-circuit of the battery a thin electrically insulating physical *separator* is used. Typically, this consists on a single- or multi-layer of polyethylene (PE), polypropylene (PP) or glass-fibre mats [25]. In this sense, renewable polymer-based compounds have been promising used as a separator in Li-ion batteries [26], or Na-ion batteries [27], and MABs [28]. Other approaches such as the modification of commercial separators by changing their surface chemical properties and pore structure [29] have been also pursued. Lee et al. carried out a modification of the separator using redox mediators (5,10-dihydro-5,10-dimethylphenazine), achieving a round-trip efficiency of 90% in a Li–O<sub>2</sub> battery over 20 cycles [30]. Recently, Hu et al. summarised the state-of-the-art bi-dimensional (2D) materials for separators [31]. Among those materials, an ultrathin layer of graphene nanosheet suppressed dendrite formation as well as improved the dimensional stability at elevated temperatures [32].



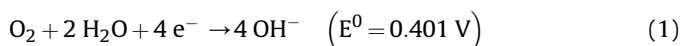
**Fig. 3.** Energy density in batteries. (a) Comparison between gravimetric and volumetric capacities, standard reduction potential and Earth's crust abundance of metal negative electrodes used or proposed for application in electrochemical storage systems. Fig. reproduced with permission from Leisegang et al. [24] Copyright © 2019. (b) Theoretical energy densities for different types of metal–air batteries. Fig. reproduced with permission from Li et al. [22]. Copyright © 2017, Royal Society of Chemistry.

Regarding the *cathode*, an air-cathode is desired to benefit from the abundant oxygen in the air as an electron acceptor. Nevertheless, H<sub>2</sub>O together with some trace of CO<sub>2</sub> in ambient air contributes to the formation of carbonates in the first few cycles and consequently, accelerates the aforementioned degradation processes. Since the formation of these carbonates occurs mainly in strong alkaline electrolytes, the use of acidic electrolytes based on Leclanché electrolytes can mitigate the problem [33–35]. Nevertheless, low pH electrolytes entail the appearance of other issues (e.g. the lack of formation of ZnO in the case of Zn-air batteries or physical deterioration of the cell). Consequently, neutral electrolytes are preferred even if the cathode stability is affected. In any case, reaching a compromise between capacity and electrode stability is of paramount relevance to develop efficient MABs [36,37]. Extensive research has been focused on the optimisation of the air catalyst and cathode architecture as it plays a decisive role in improving battery performance. Currently, the use of noble-metal-free catalyst entails dissolution, sintering, and agglomeration processes during the operation of the cathode [38]. Besides, for a rechargeable battery, different strategies need to be developed for an efficient oxygen electrode with dual catalytic activity for oxygen reduction reaction (ORR) and oxygen evolution reaction (OER). Among them, transition-metal-based electrocatalysts exhibit relatively satisfactory bi-functional performances in comparison to their alloy counterparts with metal-free carbon-based catalysts. For instance, Yang et al. developed Fe<sub>2</sub>N/Fe<sub>3</sub>C NPs nanoparticles to improve the ORR performance in acidic media while keeping good stability and high current density. As a result, a half-wave potential of 0.764 V (vs. RHE) and high current density in acidic electrolytes were achieved [39].

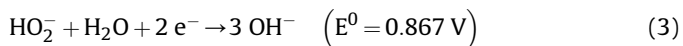
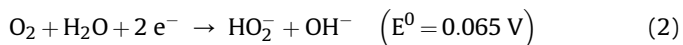
ORR and OER are defined as the basic electrochemical reactions at the air cathode, which correspond to the discharging and charging process, respectively. Although the reaction path depends on diverse parameters such as the catalyst used [40], generally ORR can be divided into a four-electron transfer process and 2-plus-2 electron transfer process. The two-electron transfer process requires a lower overpotential compared to four-electron transfer process, and the intermediate HO<sub>2</sub><sup>-</sup> formation entails a fast degradation of the cathode. OER presents a complex mechanism that similarly to ORR, requires a high overpotential in practical application to break the O=O bond (which is broken during discharge). The steps of ORR and OER are shown below:

Oxygen reduction reaction:

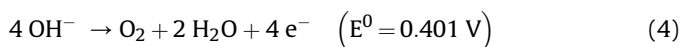
1: 4-electron reaction process:



2: 2-plus-2 electron reaction process



Oxygen evolution reaction



In this regard, metal-organic frameworks (MOFs)-based materials are promising catalysts to promote the ORR and OER at the air electrode, thus reducing the overpotential of charge/discharge reaction and increasing the circulation stability of the battery. The synergistic effect between the large surface area, the large variety of chemically available linkers and the hollow framework morphology of the metal-free carbon-based electro-catalyst improves the O<sub>2</sub>

adsorption. This kind of morphology also boosts the electronic conductivity and mass transport, causing enhanced catalytic activity and stability of the catalysts. For instance, Sindhe et al. studied the use of a hexaiminobenzene-based MOF (Mn/Fe-HIB-MOF) as a bi-functional oxygen electro-catalyst in flexible Zn-air battery with functionalised cellulose electrolytes [41]. Superior bifunctional oxygen electrocatalytic activity (0.627 V vs. RHE) for oxygen reduction and overpotential (280 mV at 10 mA·cm<sup>-2</sup>) for oxygen evolution reactions were obtained. Recently, Kundu et al. also replicated the natural shape of bamboo to synthesise nitrogen-doped carbon nanotube-encapsulated Co<sub>0.25</sub>Ni<sub>0.75</sub> alloy electrocatalyst (Co<sub>0.25</sub>Ni<sub>0.75</sub>@NCNT) and its bifunctional oxygen electrocatalytic performance toward oxygen reduction and oxygen evolution reactions [42]. When the cathode material was applied to Zn-air battery, a peak power density of 167 mW cm<sup>-2</sup> was achieved with a high open-circuit voltage of 1.53 V.

Contrarily to MOFs, covalent organic frameworks (COFs) consist of porous polymers assembled by lightweight organic building blocks through stable covalent bonds to produce highly cross-linked networks with periodic skeletons and ordered pores [43]. Therefore, it is possible to uniformly disperse single-metal sites and unique ordered channels. As an example, porphyrin-based COF as an efficient cathode catalyst was synthesised according to the demand of a high-performance Li-CO<sub>2</sub> battery [44]. Taking into account the complexity to obtain excellent stability, with this approach 180 cycles at 300 mA·g<sup>-1</sup> with a fixed 1000 mAh·g<sup>-1</sup> capacity was achieved. In this sense, electrospun carbon nanofibres decorated with ZIF-67 serve as efficient bifunctional oxygen catalysts for Zn-air batteries. The application of a super-assembly method reduces the need for electrochemical catalysts based on precious metals, obtaining a Zn-air battery with a specific capacity of 1635 mAh·g<sup>-1</sup> at 20 mA·cm<sup>2</sup> [45]. These promising strategies could pave the way for the development of COF and MOF-derived carbon-based bifunctional oxygen electrocatalysts for commercial applications in MABs.

Generally, MABs can be divided into following types according to the *electrolyte* characteristics. Depending on the interactions between the anode and the electrolyte (Fig. 3b), aqueous electrolytes are applied into Fe-, Zn-, Al- or Mg- air batteries, while non-aqueous electrolytes are used into Li-, Na- or K-air batteries. Aqueous MABs are considered more environmental friendly, cost-effective and efficient. Meanwhile, non-aqueous electrolytes present a wider electrochemical window [46]. Besides, solid-state electrolytes allow the implementation of a wide range of metal anodes as well as to overcome the current risk of liquid-base electrolytes (e.g. leakage and ignition) [47]. A great effort has been carried out to improve the performance of the different parts of the MABs, indicating that the nature of the electrolyte affects the formation of the passivating SEI layer on the negative metal. In addition, the by-products formed during the reaction with the electrolytes can block the air-cathode, limiting the exploitation of remaining metal, as well as the storage characteristics of the MABs. Accordingly, Section 3 is focused on the different kinds of electrolytes aimed to overcome the current issues.

In particular, defining an appropriate electrolyte composition is one of the most important choices that MAB designers face. The electrolyte must be chemically and thermally stable, ionically conductive, and should facilitate the reactions at both the anode and the cathode. Furthermore, electrolyte composition plays a critical role during the cell ageing process. Although, only primary Zn-air batteries have been commercialised for daily life applications [48], the development of novel bi-functional catalysts capable of catalysing both the oxygen reduction (battery discharge) and oxygen evolution (battery recharge) reactions as well as suitable electrolytes that broaden the metal anodes, have

paved the path to create practically viable rechargeable MABs (e.g. NantEnergy, EOS Energy Enterprises). Zn–air configuration offers a theoretical energy density of  $1353 \text{ Wh}\cdot\text{kg}^{-1}$ , however the practically attainable energy density of Zn–air is usually between 350 and  $500 \text{ Wh}\cdot\text{kg}^{-1}$ . Commercialised Zn–air batteries present relatively poor rate capability limited by the inefficiency of air catalysts, and thus are mostly intended for low power applications such as miniature hearing aids (e.g. Phinergy, Israel) [49]. Furthermore, rechargeable Zn–air batteries suffer from poor energy efficiency (< 60%) caused by the severe degradation related to morphology changes of the anode, the precipitation of carbonates in the cathode and additional electrolyte degradation.


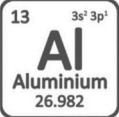




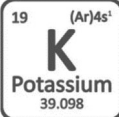
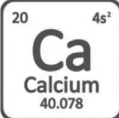
### 3. Electrolytes

In this section, the modelling tools currently available to design and optimise electrolytes for MABs are discussed to smooth the

detrimental effects previously aforementioned (Table 1). According to the nature of the electrolytes, MABs are divided into two types. From one side, a cell system using an aqueous electrolyte that is not sensitive to moisture is found. The main drawback of this configuration is its voltage window limitation. On the other side, a water-sensitive system based on an electrolyte with aprotic solvents is used. Interestingly, Zn–air battery efficiency can be significantly increased using ionic liquids (ILs) as electrolytes [50]. However, finding the best IL for a certain system is difficult without a thorough understanding of the electrochemical reactions occurring in IL-based zinc cells [51].

Aqueous electrolytes either on their own or as part of hybrid systems are widely used in the various metal–air chemistries [65]. The most common electrolytes are alkaline (e.g., KOH, NaOH), which are economically affordable and allow high performance devices. However, when they are exposed to air, dissolved  $\text{CO}_2$  reacts with the excess  $\text{OH}^-$  to form carbonate ions,  $\text{CO}_3^{2-}$ . This parasitic reaction reduces the conductivity of the electrolyte, slows

**Table 1**  
Summary of the main drawbacks of MABs depending on the nature of the electrolyte.

Metal anode	Electrolyte	Main drawbacks	Ref	
 <b>Zn</b> Zinc 65.39	<b>Aqueous</b>	<ul style="list-style-type: none"> <li>• Formation of <math>\text{Zn}(\text{OH})_4^{2-}</math> and precipitation of ZnO in alkaline electrolytes</li> <li>• Shape changes and dendrite formation</li> <li>• Precipitation of insoluble carbonates</li> <li>• Hydrogen evolution reaction (HER) due to water electrolysis that changes the cathode/electrolyte distribution</li> </ul>	[52,53]	
		 <b>Al</b> Aluminium 26.982	<ul style="list-style-type: none"> <li>• Formation of a passivating oxide layer</li> <li>• High corrosion rates in strongly alkaline electrolytes</li> </ul>	[24,54]
		 <b>Fe</b> Iron 55.847	<ul style="list-style-type: none"> <li>• Hydrogen releasing</li> <li>• Anode passivation by iron oxide films</li> </ul>	[55,56]
		 <b>Mg</b> Magnesium 24.305	<ul style="list-style-type: none"> <li>• Corrosion of the Mg anode</li> <li>• The sluggish kinetics of the ORR in the air cathode</li> </ul>	[57,58]
 <b>Li</b> Lithium 6.941	<b>Non-aqueous</b>	<ul style="list-style-type: none"> <li>• Poor cyclability</li> <li>• The sluggish reduction of <math>\text{O}_2</math> to form electrochemically active oxygen</li> <li>• Moisture from air</li> </ul>	[59–61]	
		 <b>Na</b> Sodium 22.989	<ul style="list-style-type: none"> <li>• The complexity of discharge product identification and discharge mechanism</li> <li>• Na corrosion</li> <li>• Poor conductivity and deposition of non-conductive <math>\text{NaO}_2</math> and <math>\text{Na}_2\text{O}_2</math> (discharge products) onto the porous cathode</li> </ul>	[61,62]
		 <b>K</b> Potassium 39.098	<ul style="list-style-type: none"> <li>• K dendrite formation</li> <li>• Moisture from air</li> </ul>	[63]
		 <b>Ca</b> Calcium 40.078	<ul style="list-style-type: none"> <li>• The ORR on the superoxide has not been demonstrated</li> <li>• Oxygen reduction is still rather irreversible</li> </ul>	[64]

the reaction kinetics, and can lead to unwanted precipitation of the carbonate salts within the cell. On the other hand, near-neutral electrolytes (e.g.  $\text{NH}_4\text{Cl}$ ,  $\text{NaCl}$ ) are less susceptible to the formation of carbonates and are a growing area of interest for MABs. Finally, acidic electrolytes are usually avoided due to the increased risk of corrosive self-discharge of the metal electrode. Understanding the equilibrium properties of the electrolyte is the first step to improve the performance of MABs in the dynamic battery environment. To facilitate the reading of the content in Section 3, [Scheme 1](#) summarises the different categories regarding the used electrolyte.

### 3.1. Porous membranes soaked into liquid electrolytes

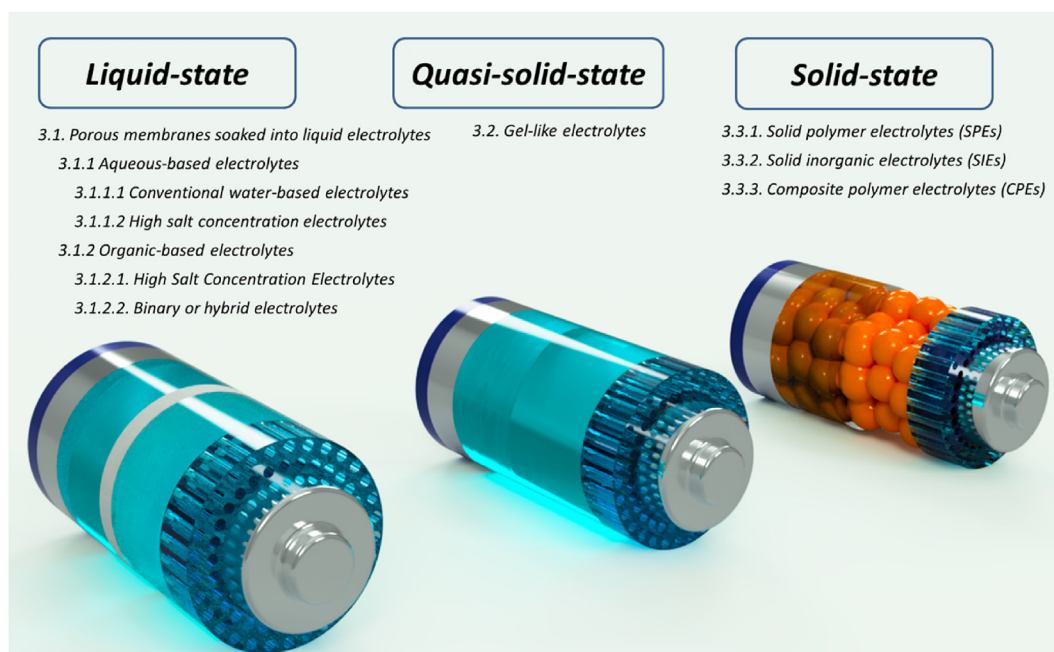
*Widely used in conventional LIBs, the configuration based on porous membranes soaked into a liquid electrolyte results in bulky batteries with serious safety issues associated to electrolyte leakage and combustion risks*

The basic function of the separator is to physically separate the anode and the cathode to prevent short-circuit. To accomplish its function, the ideal separator is a wettable porous membrane that is electrically insulating but ionically conductive; it is mechanically, dimensionally and electro-chemically stable across different environment conditions. In addition to these basic functions, separators can also limit the migration of specific ions or molecules [7]. Polymeric membranes soaked into an ionically conducting liquid electrolyte represent a common form of separator in MABs. This layer physically separates the anode and the cathode to avoid short-circuit while enables an adequate ion-diffusion between the electrodes. As occurs with conventional LIBs, microporous polyolefin membranes based on PP or PE (mainly commercialised by Celgard®) [66], or glass microfibre separators (commercialised under Whatman®) [67], are applied. These materials offer easy

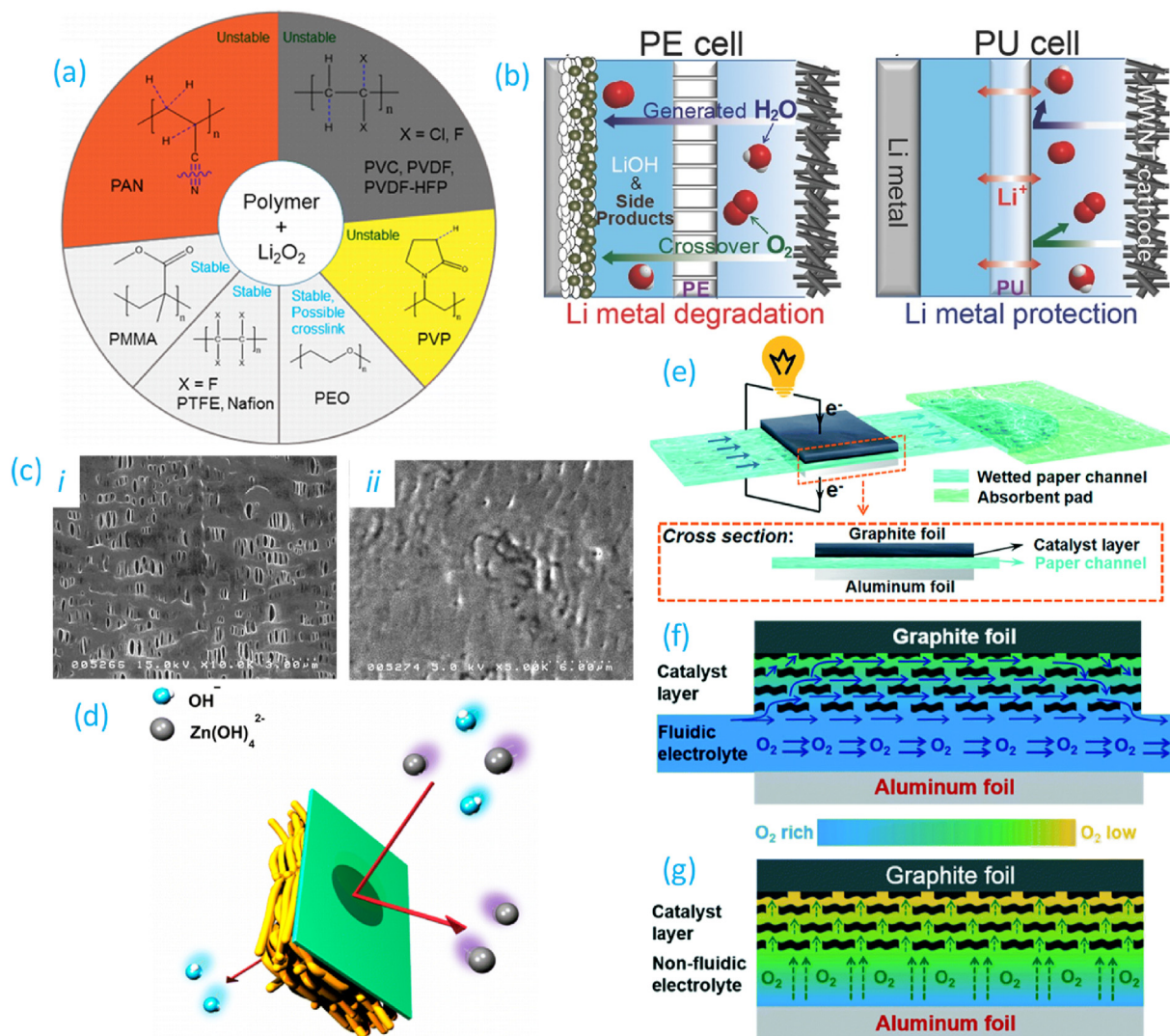
processing, mechanical/electrochemical stability and good ionic conductivities at room temperature ( $12.8 \text{ mS} \cdot \text{cm}^{-1}$  in 6 M KOH for Celgard® 3501) [68].

The seminal work by Abraham and Jiang in 1996 showed a Li– $\text{O}_2$  battery with a poly(acrylonitrile)-based polymer electrolyte reaching a specific energy of  $250\text{--}350 \text{ Wh} \cdot \text{kg}^{-1}$  [69]. However, certain instability issues were identified resulting from the irreversible decomposition of lithium hexafluorophosphate ( $\text{LiPF}_6$ ) in organic electrolytes, as non-ionised  $\text{LiPF}_6$  dissociates to  $\text{PF}_5$  and  $\text{LiF}$  in organic solvents [70]. Following this work, Amanchukwu et al. studied the stability of different polymers widely used as separators in LIBs and concluded that poly(acrylonitrile), poly(vinyl chloride), poly(vinylidene fluoride) (PVDF), and poly(vinylpyrrolidone) (PVP) show reactivity and stability issues in the presence of  $\text{Li}_2\text{O}_2$  [71]. On the contrary, Nafion, poly(tetrafluoroethylene) (PTFE) and poly(methyl methacrylate) (PMMA) showed good stability against the nucleophilic  $\text{Li}_2\text{O}_2$  attack (summarised in [Fig. 4a](#)) [71]. However, the pore size of these membrane based on those polymers is often larger than the size of solvated zincate ions ( $\text{Zn}(\text{OH})_4^{2-}$ ), so undesired species generally diffuse across the separator to the air cathode. The crossover of zincate ions in Zn–air batteries or the crossover of  $\text{H}_2\text{O}$  and  $\text{O}_2$  from the air–cathode to the Li metal, together with the presence of redox mediators is considered some of the main bottlenecks facing MABs.

As demonstrated in [Fig. 4b](#), a pore-less polyurethane separator soaked in 1 M lithium perchlorate ( $\text{LiClO}_4$ )/TEGDME effectively suppresses the crossover of water and oxygen from the air–cathode side to the Li metal in Li– $\text{O}_2$  batteries, which is in contrast with the performance provided by a conventional PE separator (an improved electrolyte wetting is achieved and the conductivity is enhanced by 34%) [72]. The polyurethane membrane also protects Li metal anodes from redox mediators used to enhance the battery reversibility, resulting in a capacity of  $600 \text{ mAh} \cdot \text{g}^{-1}$  for more than 200 cycles. Similarly, to face this issue and enable longer lasting rechargeable Zn–air batteries, Kim et al. designed an anion-repelling material with selective ion transport channels based on electrospun PVA/polyacrylic acid nanofibre mat impregnated with Nafion [68]. Nafion prevents  $\text{Zn}(\text{OH})_4^{2-}$  crossover via the Donnan exclusion effect, while



**Scheme 1.** Electrolyte types (ranging from liquid to solid-state) aiming to improve the energy density and safety in metal–air batteries.



**Fig. 4.** Porous polymeric membranes soaked into liquid electrolytes. (a) Summary of the stability of different polymers when applied as Li-air battery separators. Reproduced with permission [71]. Copyright © 2015, American Chemical Society. (b) Comparative schematic illustration of Li-O<sub>2</sub> having a conventional porous polyethylene separator and pore-less polyurethane separator. Reproduced with permission [72]. Copyright © 2016, Royal Society of Chemistry. (c) Scanning electron microscope (SEM) micrographs of sulfonated polypropylene membranes: i) before the sulfonation, ii) after 128 h. Reproduced with permission [74]. Copyright © 2008, Elsevier. (d) Schematic showing the distinctively ion transport character of polymerised ionic liquid/PP separator, where zincate ion would be prohibited and solely OH<sup>-</sup> is transported during charge/discharge. Reproduced with permission [75]. Copyright © 2016, American Chemical Society. Paper-based Al-air battery: (e) Schematic illustration of the whole battery; (f) schematic cross-section showing the O<sub>2</sub>-rich/low electrolyte distribution in Al-air batteries with paper based and (g) non-paper based (bottom) separator. Reproduced with permission [76]. Copyright © 2019, Royal Society of Chemistry.

the nanofibre mat ensure an OH<sup>-</sup> conduction ( $6.6 \text{ mS} \cdot \text{cm}^{-1}$  in 6 M KOH). As a result cycling stability is increased from 900 min (conventional PP separator) to 2500 min. Other struggling issue facing MBAs is the parasitic corrosion of Al when in physical contact with the liquid electrolyte. This effect forms a passive oxide/hydroxide layer limiting the electrochemical performance of Al-air batteries. A PP separator was applied in the form of microfluidic channels being able to deliver the liquid electrolyte via capillary action, enabling a compact cell design. A maximum discharge capacity of  $375 \text{ mAh} \cdot \text{g}^{-1}$  was achieved at a current of 30 mA using a 1 M KOH electrolyte [73]. It was found that strong alkaline solutions increase the corrosion rate (Al reacts with OH<sup>-</sup> to form Al(OH)<sub>3</sub>) and lead to poor anode utilisation, reducing the delivered capacity to nearly  $80 \text{ mAh} \cdot \text{g}^{-1}$ . A sulfonation treatment can be applied to microporous PP membranes to enhance their surface hydrophilicity (contact angle drop from 85 to 66°) and anionic conductivity in alkaline electrolytes from  $1.52 \times 10^{-2} \text{ S} \cdot \text{cm}^{-1}$  to  $3.52 \times 10^{-2} \text{ S} \cdot \text{cm}^{-1}$  [74]. Although the original pores of about  $400 \text{ nm} \times 50 \text{ nm}$  in size of the original PP membrane

in Fig. 4c provide channels for the transport of electrolytes, sulfonation enhances the Zn-air battery power density from  $20 \text{ mW} \cdot \text{cm}^{-2}$  to  $38 \text{ mW} \cdot \text{cm}^{-2}$ . At the same time, the anionic transport number was increased from 0.79 to 0.89 in 1 M KOH [74]. Membrane coating is also a commonly followed approach to enhance operating performance. Hwang et al. coated a commercial PP membrane with a polymerised IL and applied this material into a Zn-air battery (6 M KOH electrolyte) [75]. As schematically depicted in Fig. 4d, this approach keeps the anionic transfer through the separator and minimises the migration of zincate ions to the cathode compartment during charge/discharge by 96%, keeping high electrolyte conductivity and avoiding the deterioration of the catalytic activity by the formation of ZnO on the surface of the catalyst layer. As a result, the durability of the battery life was increased by 281% in comparison with the pure commercial PP membrane.

Polyolefins are characterised by relatively low melting temperatures (theoretical upper limits of 171 °C for perfectly isotactic PP and 146 °C for PE), so the risk for thermal runaway remains latent.

Additionally, separators based on PVP or PVDF can react with superoxide/peroxide and reactive intermediates to form undesired side products. To address these issues, naturally-derived polymeric membranes or inorganic separators have been used. A microfluidic Al–air battery was constructed using a cellulosic filter paper soaked into a 1.5 M KOH electrolyte [28]. The porosity and hydrophilicity of cellulose enabled the fluidic transport of the liquid electrolyte via capillary action [77], offering a maximum current of 17.4 mA with a power of 3.0 mW ( $3 \times 3 \text{ cm}^2$  battery). The design has been improved to attain an open-circuit voltage of 1.45 V and  $28 \text{ mW} \cdot \text{cm}^{-2}$  using a technical grade commercial Al-6061 anode and a MnO<sub>2</sub>-loaded carbon cloth cathode [78]. In this approach, as schematically shown in Fig. 4e, Shen et al. constructed an Al–air battery composed of an Al anode, a catalyst loaded graphite cathode, and a cellulosic paper acting as both separator and microfluidic channel able to carry the electrolytes to electrode surfaces [76]. Flowing electrolytes can mitigate the electrochemical issues related to oxygen mass transfer providing sufficient mass transfer of O<sub>2</sub> to cathode. Accordingly, in this example the paper acts as a capillary transport system to make the electrolyte flow along the paper channel in a laminar and continuous way to the cathode catalyst layer with a flow rate of  $24 \mu\text{L} \cdot \text{min}^{-1}$  (Fig. 4f). This way the fast depletion of O<sub>2</sub> near the surfaces of the cathode characteristic of conventional MABs is prevented (Fig. 4g). In addition, no external auxiliaries such as pumps are needed to circulate the electrolyte. In addition, the electrolyte flow removes the insoluble products generated during operation, preventing electrode surface passivation. However, the areal power density is lowered from  $\sim 22$  to  $\sim 13 \text{ mW} \cdot \text{cm}^{-2}$  when increasing the electrode active area from 40 to 120 mm<sup>2</sup>. This behaviour suggests a depletion of O<sub>2</sub> at the electrode due to the fact that the active centres reduce the O<sub>2</sub> amount in the electrolyte a result. Importantly, in contrast to regular Al–air batteries which have a pre-loaded electrolyte, the designed battery protects the Al anode from the electrolyte before use thanks to the porous paper that allows the flow of the electrolyte through capillarity and efficiently transports O<sub>2</sub> to the cathode side. As a result, the parasitic corrosion effects during storage are avoided, limiting the self-discharge to enlarge battery self-life, which is considered as one of the most pressing shortcomings of traditional Al–air batteries.

Generally, biopolymers ensure large electrolyte uptake and good ionic conductivity values [79]. However, the strength weakening behaviour of biopolymers soaked in electrolytes should be considered from the safety point of view as it markedly reduces both Young's modulus and tensile strength [80]. As a good film-forming cellulose derivative, the 3–10 nm pore-structure and the negatively charged surface of cellophane offers large OH<sup>−</sup> conductivity values and excludes the negatively charged Zn(OH)<sub>4</sub><sup>2−</sup> ions, enabling a lower zincate crossover than that of Celgard® 3501 in 45% KOH (pore size of 64 nm) [81]. Biopolymers have also been used in MABs as additives. A water-soluble cellulose derivative such as carboxymethyl cellulose (CMC), in conjunction with ZnO, has been proven efficient to mitigate the corrosion of the aluminium anode (4 M NaOH electrolyte) [82]. The carboxyl groups adsorbed onto Al surface afford a stable protecting layer formed via the interaction between CMC and Zn<sup>2+</sup> ions. As a result, the anode utilisation increases from 91.1% to 94.1%, which is translated into a capacity increase from 2710 mAh·g<sup>−1</sup> to 2824 mAh·g<sup>−1</sup>.

Inorganic separators generally offer a good electrolyte adsorption together with the subsequent retention of electrolytes thanks to their highly porous structure. Ceramic separators have a better stability against oxidative agents in comparison to polymeric membranes. In fact, the work of Bruce et al. in 2006 used a glass fibre separator soaked into 1 M LiPF<sub>6</sub> in propylene carbonate [67]. However, the use of commercial glass fibre separators has notable

limitations due to the presence of redox mediators. Fig. 5a shows a simplified mechanism where upon the use of glass fibre separator the overpotential during charging is reduced (promoting Li<sub>2</sub>O<sub>2</sub> oxidation), also resulting in Li metal anode degradation due to parasitic reactions [30]. In this sense, the inherent characteristics of porous inorganic materials serve to face the shuttle of redox mediator molecules in Li–O<sub>2</sub>. As shown in Fig. 5b, a separator having a 15 μm thick MOF layer was exploited as a redox mediator molecular sieve to reduce the electron shuttling between the cathode and anode [83]. Specifically, the three-dimensional (3D) channel structure having highly ordered pores of 6.9–9 Å enable Li<sup>+</sup> crossing, while redox mediator molecules are blocked. In that way, the incomplete Li<sub>2</sub>O<sub>2</sub> decomposition and Li anode degradation in aprotic Li–O<sub>2</sub> cell is minimised, delivering a capacity of 5000 mAh·g<sup>−1</sup> after 100 cycles at 1 A·g<sup>−1</sup>. In a synthetically simpler approach, a thin polypyrrole could be introduced between a glass fibre separator and the air cathode to suppress the redox shuttle effect in Li–O<sub>2</sub> cells, enhancing the cycling life four times [84].

Further mesoporous materials such as the hydrophilic MCM-41 (Mobil Crystalline Material n° 41), a one-dimensional hexagonally ordered amorphous silica having a specific surface area of nearly 1000 m<sup>2</sup>·g<sup>−1</sup> and hierarchically arranged into hexagonally ordered narrow pore structures, have been applied into other metal air chemistries. For example, a 5 μm thick MCM-41 film was placed between a Zn anode and a Ni mesh cathode to provide ion exchange channels and act as a electrolyte matrix when soaked in KOH (maximum power density of 32 mW·cm<sup>−2</sup>, volumetric energy density of 300 Wh·L<sup>−1</sup>) [87]. As another example of an inorganic membrane soaked into a liquid electrolyte, lithium phosphorus oxynitride (LiPON, general formula of Li<sub>x</sub>PO<sub>y</sub>N<sub>z</sub>), an amorphous glassy material, can work as an electrolyte material in a Li-air battery as patented over 15 years ago [88]. LiPON is soaked into propylene carbonate/LiPF<sub>6</sub> organic electrolyte to act as a protective barrier against moisture and oxygen corrosion, reducing the rapid corrosion of Li anodes. A 40 μm thick freestanding LISICON separator was applied into Li–air batteries having a 2 M LiOH aqueous electrolyte [85]. This membrane resulted sufficiently thin to minimise ohmic losses in an aqueous Li–air cell while offering a watertight protection of the Li anode to prevent its oxidation by the water. Additionally, as shown in Fig. 5c, to limit Li metal attack, a LiPON coating was applied on the anode side of the separator. However, its poor ionic conductivity of  $1.6 \times 10^{-3} \text{ mS} \cdot \text{cm}^{-1}$  caused a relevant ohmic loss, resulting in relatively poor energy density and power density values.

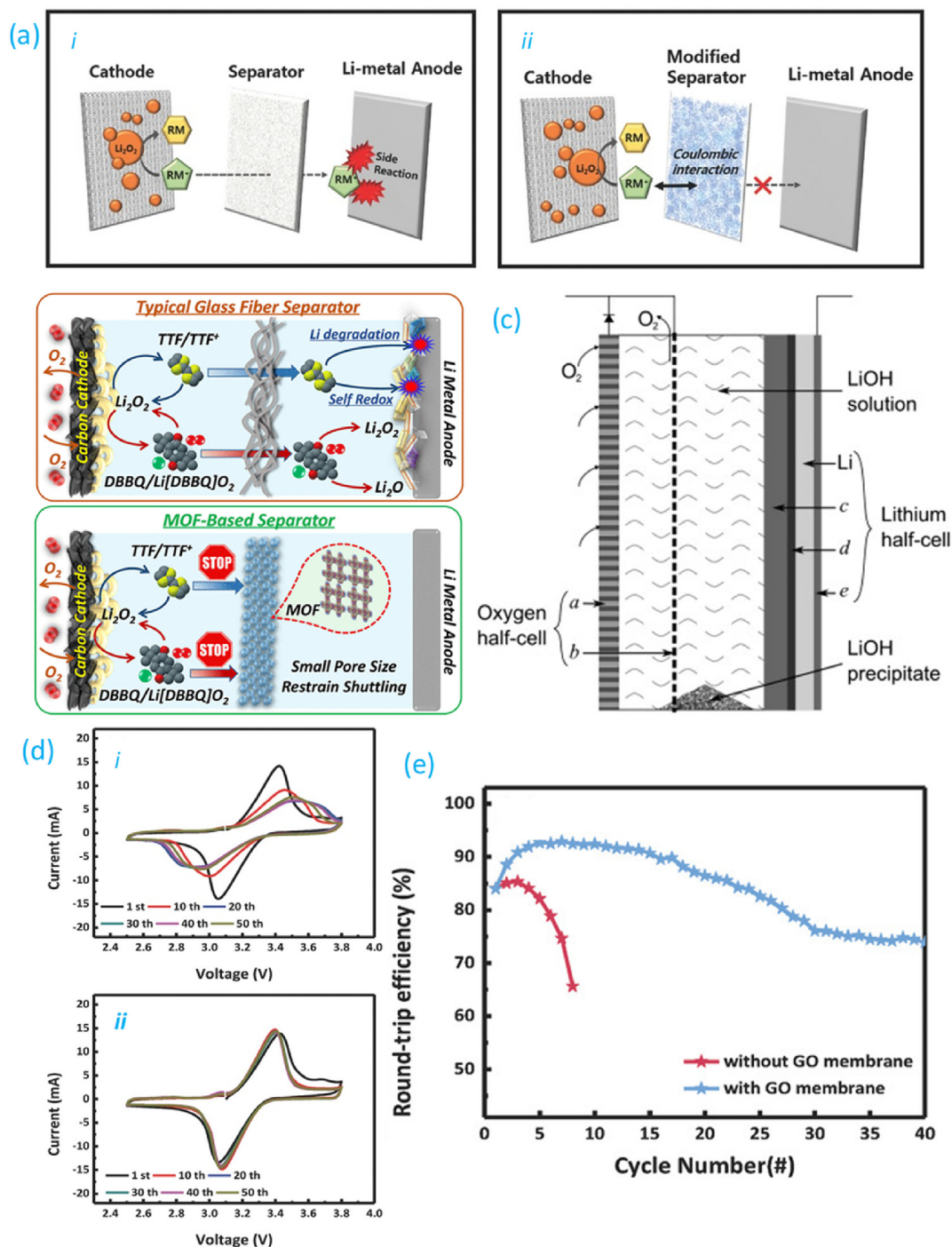
Similarly, to extend the life of Li–O<sub>2</sub> batteries, redox-mediator (RM)-sieving graphene oxide (GO) membranes were fabricated depositing a  $\approx 200 \text{ nm}$  thin GO layer onto a hydrophilic and porous 43 μm polytetrafluoroethylene filter [86]. Given the marginal resistance of the GO layer a negligible overpotential into Li–O<sub>2</sub> cells was observed. Importantly, the nano-channels provided by GO selectively reject 5,10-dihydro-5,10-dimethylphenazine (DMPZ) while enable Li<sup>+</sup> transport. Moreover, the negatively charged GO surfaces repel negative ions via Donnan exclusion, contributing to larger Li<sup>+</sup> transference numbers. As a result, the reversibility of the oxidation and reduction reaction between DMPZ and DMPZ<sup>+</sup> in Li–O<sub>2</sub> battery systems was notably improved as shown by CV curves in Fig. 10d. This is translated into a round-trip efficiency over 90% after 10 cycles as compared to the short cyclability when no GO is used (Fig. 5e).

### 3.1.1. Aqueous-based electrolytes

#### 3.1.1.1. Conventional water-based electrolytes.

Metals such as Zn, Fe, Al, and Mg are thermodynamically unstable in the aqueous medium and suffer from critical issues including electrode corrosion, passivation, hydrogen evolution, and dendrite formation [89]. The electrolyte material design can passivate their surfaces by different





**Fig. 5.** Porous membranes soaked into liquid electrolytes bearing inorganic materials. (a) Redox mediators promote the oxidation of Li<sub>2</sub>O<sub>2</sub> by reducing the overpotential in the charging process, also resulting in side reactions at the Li metal anode side: i) scenario using a commercial glass fibre separator and ii) coated glass fibre separator for avoid undesired redox mediator effects. Reproduced with permission [30]. Copyright © 2017, Wiley. (b) Scheme depicting the concept of a MOF-based separator acting as a physical layer inhibiting the shuttle of redox mediator molecules as opposed to the mechanisms in the presence of a glass microfibre separator. Reproduced with permission [83]. Copyright © 2018, American Chemical Society. (c) Scheme of an aqueous Li-air battery showing: a: O<sub>2</sub> reduction at the cathode, b: O<sub>2</sub> evolution electrode (stainless steel grid); c: a LiSICON separator; d: a protective lithium phosphorus oxynitride (LiPON) layer; e: current collector. Reproduced with permission [85]. Copyright © 2012, Elsevier. (d) CV curves in the voltage range of 2.5–3.8 V under with a bare PTFE membrane and a GO-coated PTFE membrane. (e) Electrochemical performance of Li–O<sub>2</sub> cells with 0.2 M 5,10-dihydro-5,10-dimethyl phenazine or DMPZ at a capacity of limit of 0.75 mAh·cm<sup>-2</sup> showing round-trip efficiency versus cycle number. Reproduced with permission [86]. Copyright © 2018, Wiley.

electrolyte additives, and thus makes them compatible with aqueous electrolytes to some extent.

In this context, the application of zinc sulphate (ZnSO<sub>4</sub>) and sodium alginate (SA) as electrolyte additives of 4 M NaOH was investigated with the aim to slow down the self-corrosion of Al

[90]. As result, not only an improvement of the stability of the Al anode was achieved, but also an increase of discharge capacity by 64.6% (from 162.46 to 267.41 mAh·cm<sup>-2</sup>) when compared with electrolytes with or without additives. In addition, Hosseini et al. studied the influence of sulphur–oxygen group additives in a 4 M

KOH electrolyte for Al–air batteries [91]. Among the different selected additives ( $\text{Na}_2\text{SO}_4$ ,  $\text{Na}_2\text{SO}_3$ ,  $\text{C}_2\text{H}_6\text{SO}$ , and  $\text{C}_6\text{H}_5\text{SO}_2\text{OH}$ ),  $\text{Na}_2\text{SO}_4$  and  $\text{C}_6\text{H}_5\text{SO}_2\text{OH}$  additives exhibited stable discharge/charge cycles with a discharge capacities of 2604 and 2048  $\text{mAh}\cdot\text{g}^{-1}$ , respectively, compared with bare electrolyte (2021  $\text{mAh}\cdot\text{g}^{-1}$ ). One step further, the self-corrosion of an Al electrode in an alkaline dual-electrolyte was investigated [92]. The novel cell configuration (Al anode | anolyte | anion exchange membrane | catholyte | air cathode) together with the addition of 5% (v/v) ethylene glycol to the 3 M KOH ethanol solution, a specific capacity of 2100  $\text{mAh}\cdot\text{g}^{-1}$  was achieved, bringing about a 70% utilisation efficiency. By this approach, not only anodic corrosion and passivation can be controlled, but also it reduced polarisation and charge transfer resistance.

Another interesting approach demonstrated that the combination of electrolyte additives greatly improves the discharging behaviour of Mg–air battery [93]. In particular, the use of sodium nitrate ( $\text{NO}_3^-$ ), salicylate (SAL) or a mixture (MIX) of both of them as electrolyte suppressed anode self-corrosion as well as uniform Mg dissolution under discharge conditions. By local pH gradient (measured from 50 to 2000  $\mu\text{m}$  above the Mg surface) it was possible to detect the formation of  $\text{Mg}(\text{OH})_2$  precipitates. Therefore, according to Fig. 6a, the pH of formation of precipitates is shifted to a more alkaline region (in the case of SAL and MIX) due to the formation of soluble Mg–SAL complexes. According to the proposed mechanism (Fig. 6b), the complex formation of dissolved  $\text{Fe}^{3+}$  with SAL avoids the iron re-deposition, leading to the decrease in the number of cathodically active spots.

The use of 1-octanethiol in an Fe–air battery results unfavourable as due to the reduction of the  $\text{O}_2$  transport [94]. The blocking of the active sites by the adsorbed alkane-thiols or thiols could be one of the possible reasons of this detrimental effect to the Fe–air battery performance. Bearing this in mind, further studies should be carried out to address the interaction of additives with metal–air components after several cycles.

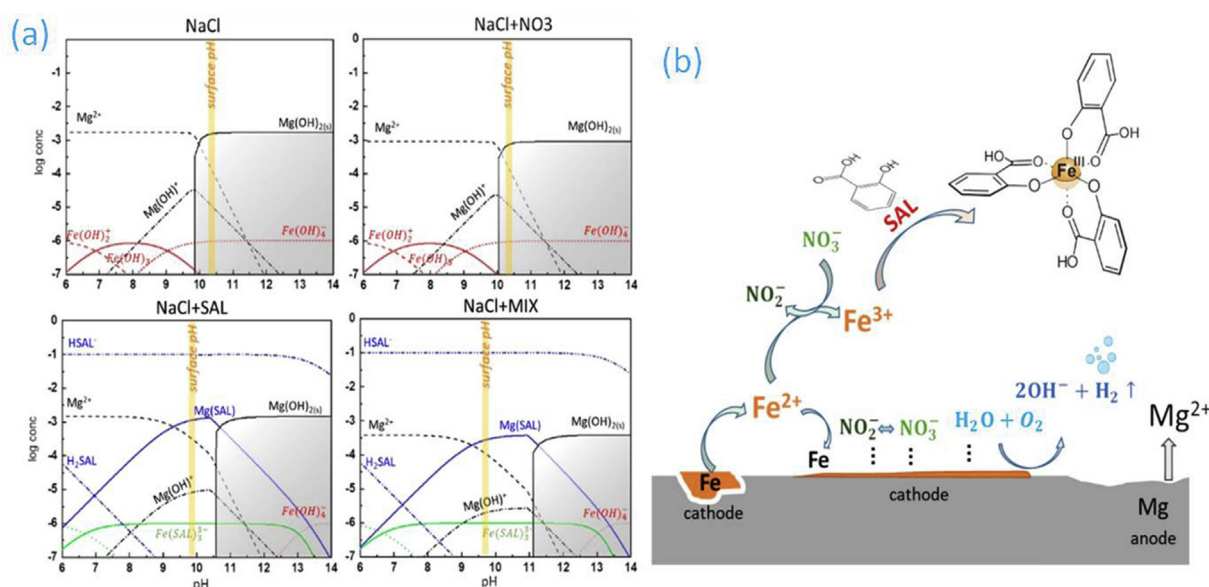
**3.1.1.2. High salt concentration electrolytes.** Water-in-salt electrolytes were firstly proposed in 2015, where the salt exceeded the

solvent in both weight and volume [95]. As a result, the rapid generation of a SEI in the anode, allowed many electrode materials to stably operate in aqueous electrolytes. Contrary to organic electrolytes, with the addition of salt to water, the volatility is notably reduced although the stability will be promoted. Very recently, the transport properties of water-in-salt lithium bis(trifluoromethane sulfonyl)imide (LiTFSI) aqueous electrolytes were studied using classical molecular dynamics simulations [96]. Results suggested that there is not a separation of TFSI<sup>-</sup>-rich or water-rich domains but a homogeneous electrolyte. A decrease in the diffusivity of the species (TFSI<sup>-</sup> anions > Li<sup>+</sup> cations) with increasing LiTFSI concentration was observed, obtaining a Li<sup>+</sup> apparent transference number of  $\sim 0.75$  at 20 m (mol·kg<sup>-1</sup> solvent).

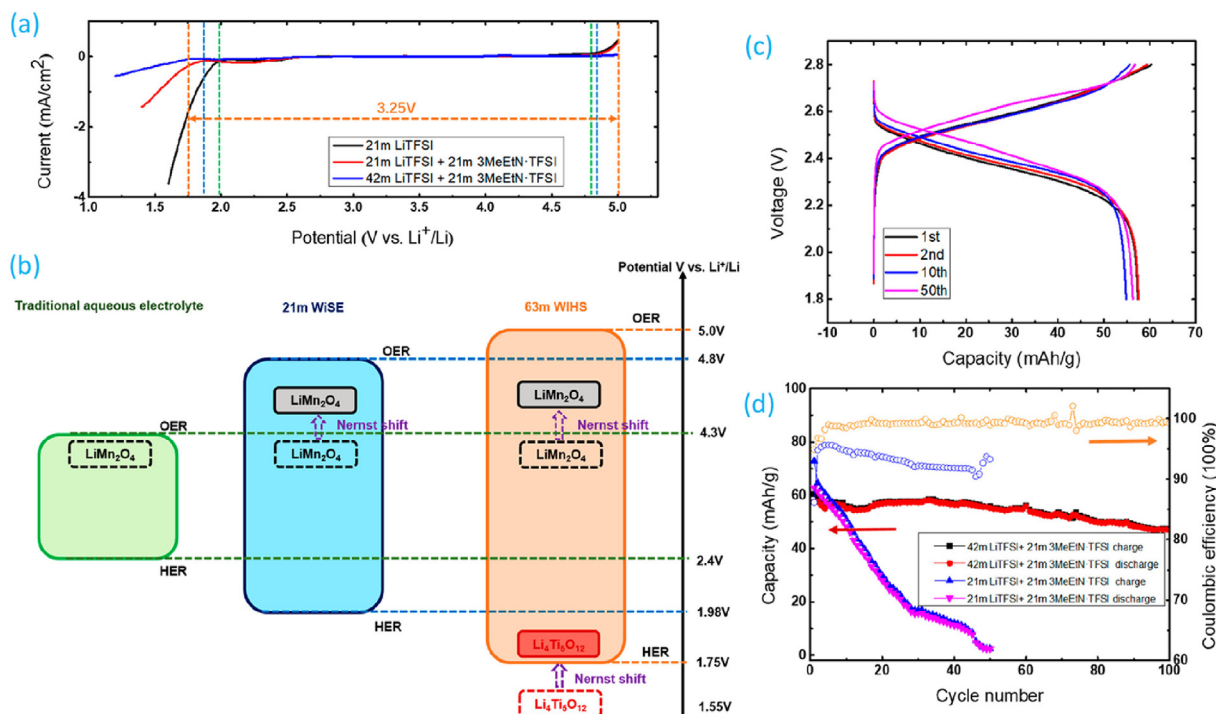
One step further was performed with the addition of 42 m LiTFSI + 21 m Me<sub>3</sub>EtN·TFSI, forming a water-in-high-salt electrolyte that expand the potential window from a standard 1.9 eV delivered by an aqueous electrolyte to a wide potential window of 3.25 V (Fig. 7a and b) [97]. This water-in-high-salt electrolyte provides (in a LiMn<sub>2</sub>O<sub>4</sub>//Li<sub>4</sub>Ti<sub>5</sub>O<sub>12</sub> battery), a discharge capacity of 56  $\text{mAh}\cdot\text{g}^{-1}$  (Fig. 7c), and an estimated energy density of 145  $\text{Wh}\cdot\text{kg}^{-1}$  over 150 cycles, with a capacity retention of 88% after 100 cycles at 1C (Fig. 7d).

Highly concentrated electrolytes based on other types of salts with high solubilities (e.g. 9 m NaOTf, 8 m NaTFSI, < 2 m KTFSI) have become an interesting research topic to extend the use of water-in-salt electrolytes. However, the lower charge density of these cations compared to Li<sup>+</sup>, entails the need of an even higher concentration than Li-based water-in-salt electrolytes to achieve similar strong cation–water and cation–anion interactions that enable an optimum electrochemical stability [98,99].

In this regard, Reber et al. [100], performed a comprehensive study of a set of Na-based salts (NaOAc, NaNO<sub>3</sub>, NaSCN, NaClO<sub>4</sub>, NaOTf, NaFSI, NaTFSI, NaTFSI, and NaPTFSI) to demonstrate the influence the anion has on solution structure and suitability for aqueous high-voltage batteries. Authors concluded that water/organic solvent systems, dual-cation electrolytes, and non-electrolyte approaches are needed to reach comparable electrochemical stability than Li<sup>+</sup> based batteries as no more than 10 m



**Fig. 6.** Combination of electrolyte additives to improve the discharge performance in a Mg–air battery. (a) Thermodynamic equilibrium of the electrolyte with different additives after 3 h of discharge at 5 mA·cm<sup>-2</sup> (the yellow vertical line shows the measured pH on the surface, and gray areas indicate the pH at which  $\text{Mg}(\text{OH})_2$  precipitates). (b) Proposed mechanism of synergistic inhibition of self-corrosion by  $\text{NO}_3^-$  and SAL mixture during discharge of the commercial purity (CP)–Mg anode. Fig. reproduced with permission from Snihirova et al. [93]. Copyright © 2020, Royal Society of Chemistry.



**Fig. 7.** Water-in-salt electrolytes. (a) Electrochemical windows of different aqueous electrolytes as measured with inactive current collectors (stainless steel) at scanning rate of  $5 \text{ mV} \cdot \text{s}^{-1}$ . (b) Illustration of expanded electrochemical stability window for 63 m water-in-high-salt electrolyte together with the modulated redox couples of  $\text{LiMn}_2\text{O}_4$  cathode and  $\text{Li}_4\text{Ti}_5\text{O}_{12}$  anode caused by high salt concentration. (c) Selected charge–discharge voltage profiles; and (d) Cycling stability and Coulombic efficiency of  $\text{LiMn}_2\text{O}_4/\text{Li}_4\text{Ti}_5\text{O}_{12}$  full cell with the 63 m water-in-high-salt aqueous electrolyte at the rate of 1 C. Fig. reproduced with permission from Chen et al. [97]. Copyright © 2020, American Chemical Society.

solubility was obtained. Recently, a ternary molten salt system ( $\text{Na}[\text{N}(\text{SO}_2\text{F})_2]-\text{Na}[\text{N}(\text{SO}_2\text{F})(\text{SO}_2\text{CF}_3)]-\text{Na}[\text{SO}_3\text{CF}_3]$ ) into propylene carbonate was studied to develop highly concentrated electrolytes (up to 8 m) for Na-ion batteries [101]. The best performance was obtained with a 5 m electrolyte, delivering a wide electrochemical window (5 V) (with a suppression of the aluminium corrosion).

Besides Na-based MABs, a hybrid high-concentration potassium acetate–potassium hydroxide electrolyte was proposed for Al–air battery [102]. An optimised concentration (16 m) results in a discharge capacity 3 times better than bare KOH (4 M) electrolyte, increasing the energy density to  $436.1 \text{ Wh} \cdot \text{kg}^{-1}$ . Considering the vast possible variations in the composition of concentrated electrolytes, this strategy can pave the way for the design of high-efficiency and stable alkaline MABs.

### 3.1.2. Organic-based electrolytes

The development of non-aqueous MABs is a relatively novel trend with the advent of Li–air technology, which is followed by other alkali and alkaline earth metals such as calcium (Ca)–, K–, and Na–air chemistries. These anode metals, when in contact with an aqueous environment, react vigorously to release  $\text{H}_2$  gas, making them unsafe for operation. To improve their stability, MABs with these specific anodes are designed based on organic carbonate-based or IL electrolytes with wide electrochemical stability windows.

Importantly, ORR in aprotic electrolytes proceeds through a mechanism drastically different from that in aqueous electrolytes. It is well established that the reaction involves an initial one-electron reduction of  $\text{O}_2$  on the catalyst surface to form a superoxide anion  $\text{O}_2^-$ , which then reacts with alkali metal cation ( $\text{M}^+$ ) to form peroxide  $\text{M-O}_2$  [103]. As for  $\text{Li}^+$ , its small size is unable to stabilise  $\text{O}_2^-$ .  $\text{LiO}_2$  subsequently disproportionate to form peroxide  $\text{Li}_2\text{O}_2$  as the discharge product. On the other hand, larger cations

( $\text{Na}^+$  and  $\text{K}^+$ ) can stabilise the superoxide anion according to hard-soft acid-base theory [104]. Accordingly, the discharge product of Na–air batteries is usually a mixture of  $\text{Na}_2\text{O}_2$  and  $\text{NaO}_2$ , and that of K– $\text{O}_2$  batteries is predominantly  $\text{KO}_2$ .

The main degradation process of non-aqueous MABs corresponds to the accumulation and gradual blockage of the available cathode surface area by the superoxides or peroxides, especially in carbon-based electrodes. In general, the blockage is a long-term effect, but there is also a flooding effect. This results in unstable triple-phase boundaries and therefore lower current densities [105]. In the case of larger cells, especially in vertical cell designs, the flooding is also influenced by hydrostatic effects, resulting in inhomogeneous current densities that inflict inhomogeneous degradation, for example, vanadium redox flow or zinc–air batteries [106]. As a result, the discharge capacity is determined by the storage capacity of the air cathode toward the discharge product, and is far smaller than the theoretical value. To unravel this negative effect, Pierini et al. performed *ab initio* calculation in order to analyse the energy landscape of the disproportionation of superoxide in aprotic media catalysed by alkali cations [107]. Unfortunately, the results revealed the existence of an additional parasitic redox process besides the expected disproportionation to peroxide and molecular oxygen, which leads to the production of solvated neutral metal atoms (that even in low quantity), affecting negatively the performance of aprotic metal– $\text{O}_2$  batteries. Nevertheless, many research groups consider K– $\text{O}_2$  batteries one of the most promising technologies to supplant Li– $\text{O}_2$  batteries due to their significantly lower over-potentials and costs. Basically, two are the main advantages that present these batteries. First, K– $\text{O}_2$  batteries eliminate the need for high-cost electrocatalysts (e.g. Pt) and second eliminates the superoxide disproportionation, sluggish two-electron process as a result of the facile single-electron process [108]. However, the reactivity and long-term stability of potassium

superoxide remains ambiguous, as is clearly not super reactive as was assumed [109]. So, further research need to be done in term to achieve a holistic comprehension as well as a high efficiency and long-term stability.

Another interesting approach to avoid the presence of superoxides entails the use of ether-based electrolytes incorporating 1,2 dimethoxyethane (DME or G1), diglyme (G2), triglyme (G3), or tetraglyme (G4). Although glyme-based electrolytes presents lower reactivity toward  $O_2^{\bullet-}$  radicals compared with carbonate-based electrolytes, they also suffer from stability problems such as electrochemical oxidation during charging and chemical decomposition on the  $Li_2O_2$  surfaces [110]. The influence of the anion (OTf vs. TFSI) in glyme-based systems was studied by Li et al. through *ab initio* molecular dynamics simulations [111]. Results indicate that all glyme-based electrolytes followed the so-called hopping or shuttling mechanisms for anion transport. However, minor anionic transport was achieved in the case of diglyme and monoglyme, proving the importance of anion concentration as well as glyme chain length.

**3.1.2.1. High salt concentration electrolytes.** A high concentration of LiTFSI cannot be generally obtained in aqueous chemistries based (e.g. Na, K, Al, or Zn). Essentially, electrolytes do not reach the electrochemical stability because of the relatively low solubility of the analogous imide and triflate salts. For example, maximum concentrations at room temperature are in the order of  $< 2$  m  $Zn(TFSI)_2$  [112], and  $< 1$  m  $Al(TFSI)_3$  [113].

To study the rate capability of high concentrated Li-conducting salt dissolved in organic solvents as well as the thickness of the electrodes (ultra-thick and thin  $LiNi_{0.6}Co_{0.2}Mn_{0.2}O_2$  (NCM-622) having a mass loading of  $49.5$   $mg \cdot cm^{-2}$  and  $5.6$   $mg \cdot cm^{-2}$ , respectively), Kremer et al. used  $LiPF_6$  concentrations up to  $2.3$  m [114]. Although concentrated electrolytes allow larger discharge capacities at current densities above  $3$   $mA \cdot cm^{-2}$  with thicker electrodes, the increase in viscosity results in a major polarisation, which leads to an overvoltage for concentrated electrolytes.

In the case of high concentration of  $3$  m sodium hexafluorophosphate ( $NaPF_6$ ) and sodium bis(trifluoromethanesulfonate) imide ( $NaTFSI$ ) dissolved in propylene carbonate, it was observed a widening of the electrochemical stability window as well as its ability to passivate the Al surface compared to  $1$  m Na-based electrolytes. However, the viscosity of  $3$  m is affected in the low-temperature range ( $20$ – $60$  °C), limiting the ionic conductivity most probably ascribed to the increasing amount of aggregates [115]. Also, the influence of Na salt concentration on the cathode–electrolyte interface of Na–air batteries was studied [116]. Similarly to previous studies aforementioned, the increment of Na salt concentration in the  $[C_4mpyr][TFSI]$  IL electrolyte enhances the discharge capacity, reduces the overpotential, and increases the cyclability of the Na– $O_2$  battery. It was concluded that the morphology of the air-cathode after the aggregates formed in the bulk of the electrolyte has strong impact in the final performance. In addition, they suggested a possible nucleation and growth mechanism (depicted in Fig. 8) of the discharge products on the electrode surface prone by the interaction of the superoxide anion ( $O_2^{\bullet-}$ ) with  $Na^+$  rather than with  $[C_4mpyr]^+$ .

**3.1.2.2. Binary or hybrid electrolytes.** Inspired by a combination of high salt concentration and water-in-salt electrolytes, a novel concept of hybrid electrolyte was proposed by Zhou [117], and Wang [118]. Basically, it consists on the introduction of the cathode in a water-in-salt electrolyte meanwhile the metal anode is immersed within an aprotic solvent separated by a ceramic superionic conductors (e.g. Lithium Super Ionic CONductor-LISICON, or

Na) Super Ionic CONductor-NASICON). In this sense, current drawbacks of conventional Li– $O_2$  batteries such as decomposition of organic electrolytes, corrosion of Li metal from humidity, and insoluble discharge product blocking the air electrode can be addressed. Although the concept is very attractive, extensive efforts toward developing a high catalytic activity of the cathode as well as enhancing the conductivity and stability of the hybrid electrolyte must be dedicated.

This configuration allowed Safanama et al. to assemble a hybrid cell with an anolyte of tetraethylene glycol dimethyl ether (TEGDME) and  $1$  M aqueous LiOH as the catholyte separated by a NASICON-type lithium aluminium germanium phosphate (LAGP) ceramics [119]. To verify whether higher temperature facilitates oxygen diffusion, cells were cycled from  $0$  to  $80$  °C as shown in Fig. 9a. Authors concluded that the possibility to work at high temperatures, resulted in a drop of the cell polarisation (Fig. 9b) and consequently the possibility to run it at high current densities of up to  $3$   $mA \cdot cm^{-2}$ .

Recently, Khan et al. summarised the state-of-the-art in hybrid electrolyte for Na–air batteries [120]. Several advantages have been observed such as low overpotential, high-energy efficiency, low-electrode polarisation, good cyclic stability, and use of ambient air as source of oxygen. Besides, we envision the need for further investigation in the electrolyte chemistry and other components of the cell (Fig. 10), interfacial chemistry between the organic electrolyte and NASICON membrane (key component in this type of cells) is not yet well understood and need to be addressed as it typically affects the resistance of the cell. For example, the crystal structure of NASICON can change when in contact with Li metal, yielding an interphase with a reduced ionic conductivity lowering the electrochemical performance during operation [121].

Regarding hybrid-electrolytes compositions, anolyte generally consist on Na-based salts (e.g.  $NaCF_3SO_3$ ,  $NaClO_4$ , etc.) dissolved in organic solvents (e.g. TEGDME and ethylene carbonate/dimethyl carbonate or EC/DMC). In the case of catholyte, aqueous NaOH and KOH are usually used. When an acidic catholyte is used, there is an improvement of the cell potential ( $3.94$  V), however, ceramic membrane suffers for low pH reducing the ionic conductivity [122]. Besides, catholyte remains the limiting component, as they are volatile when the battery works at high temperature. In order to overcome this issue, a quasi-solid-state Na–air battery based on single-wall-nanotubes (SWNTs)/IL (1-ethyl-3-methylimidazolium ( $[C_2C_1im]$ ) bis (trifluoromethylsulfonyl) imide( $[NTf_2]$ ), gel cathode was fabricated. The novelty of this work is based on the confinement of water molecules on the gel surface facilitating the generation of soluble discharge product (NaOH) and accordingly increasing the discharge capacity. An additional approach consists on the suppression of the ceramic membrane by a saline gel based on xanthan and KCl in combination with the PVA-HCl membrane in a dual electrolyte configuration for hybrid Al–air batteries [123]. An improvement in the discharge capacity with an electrochemical window wider than  $2.2$  V was observed.

### 3.2. Gel polymer electrolytes

*Gel polymer electrolytes combine the advantages of both liquid and solid electrolytes and have attracted increasing attention given their performance and safety trade-offs*

MABs comprising a solid porous membrane soaked into an electrolyte often present a fast-fading character due to solvent volatility across the air cathode (drying out effect), incorporation of

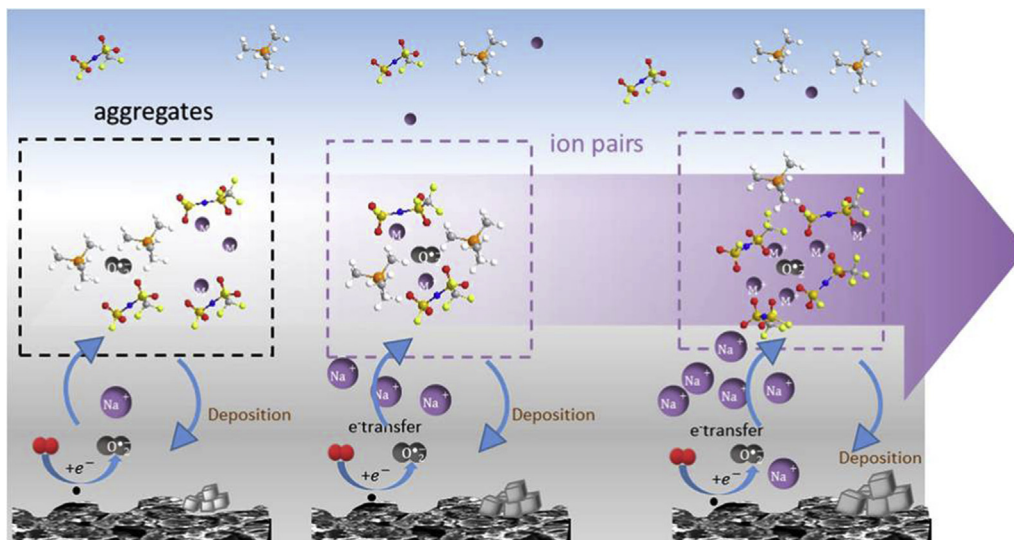


Fig. 8. Simplified schematic illustration of the effect of the concentration of NaTFSI/[C<sub>4</sub>mpyr][TFSI] electrolyte on the ORR process in the bulk electrolyte and subsequent deposit. Fig. reproduced with permission from Zhang et al. [116]. Copyright © 2018, American Chemical Society.

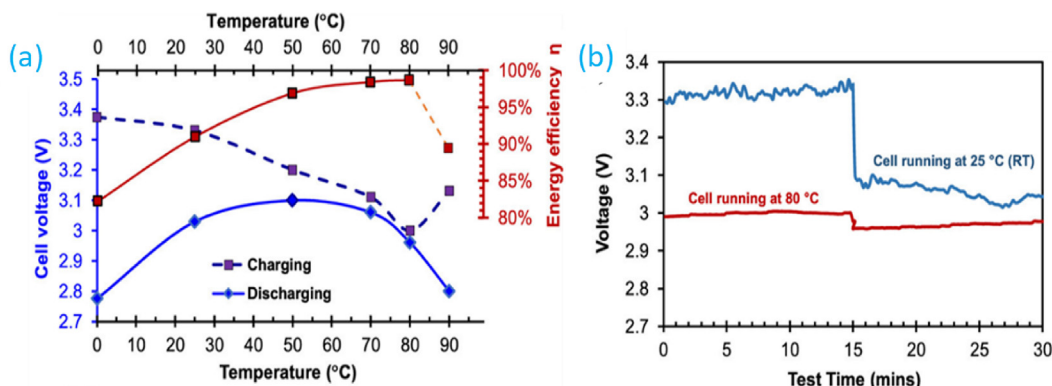


Fig. 9. Hybrid Li-air battery. (a) Effect of temperature on polarisation and energy efficiency of the hybrid Li-air cell. (b) First charge and discharge plateaus for the hybrid Li-air cell running at room temperature and 80 °C. Fig. reproduced with permission from Safanama et al. [119]. Copyright © 2020, American Chemical Society.

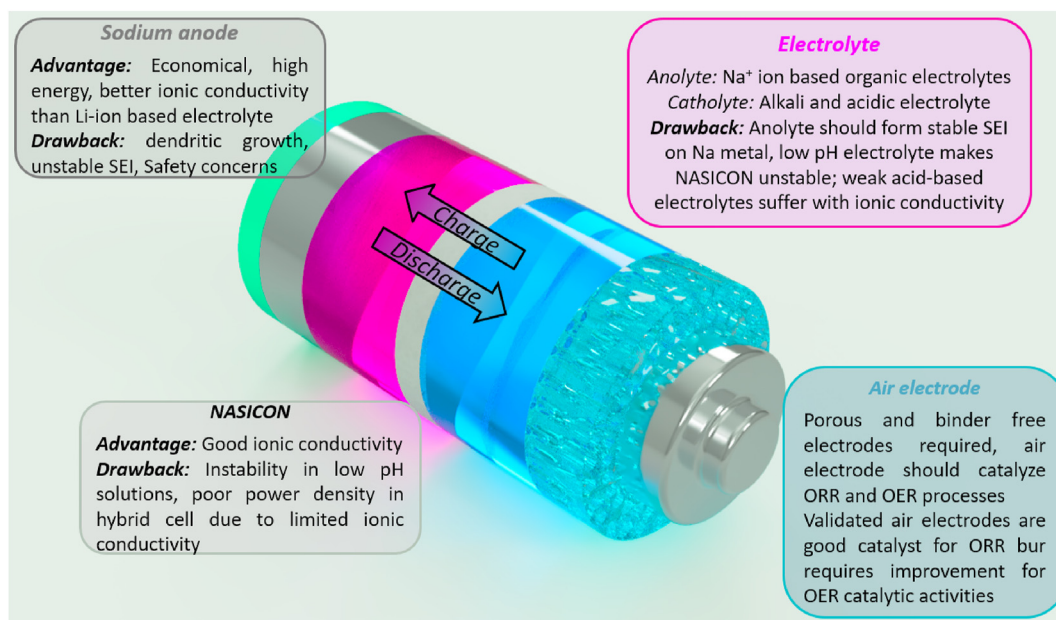


Fig. 10. Scheme illustrating various essential components in a hybrid Na-air cell. Main advantages and disadvantages are summarised.

contaminants such as H<sub>2</sub>O from the ambient air, and the formation of a passivating oxide film formed on the metal anode arising from the reaction of the anode with oxygen that has diffused from cathode through the liquid electrolyte and the micropores of the separator [124]. Moreover, the safety issues arising from a possible electrolyte leakage should also be considered. Replacing the liquid electrolyte by a gel polymer electrolyte (GPE) results an effective strategy to prevent oxygen diffusion while achieving relatively high ionic conductivities. After the pioneering works by Wright et al., in 1973 [125], poly(ethylene oxide) (PEO) has been the predominantly used material to develop GPEs and solid polymer electrolytes (SPEs) in lithium-based batteries given its high dielectric constant and ability for salt dissociation [126]. However, PEO presents low water absorption capacity, poor interfacial properties and high crystallinity. In fact, generally low  $T_g$  and predominantly amorphous polymers are preferred as they present a lower resistance to ion conduction [127].

GPEs can be used to restrict the liquid evaporation through the porous cathode. Accordingly, several GPEs having a polymer matrix swollen with a liquid electrolyte have been developed. The gel character efficiently delays electrolyte evaporation as proven by the fact that when submitted to thermogravimetric analyses, the weight loss of the poly(vinylidene fluoride-co-hexafluoropropylene)(PVDF-HFP)/cellulose acetate gel electrolyte is delayed by nearly 30 °C in comparison to liquid electrolyte (1 M LiTFSI in TEGDME) [128]. Similarly, a GPE composed by lignin fibres and EC/DMC/ethyl methyl carbonate (EMC) showed no weight loss when heated at 100 °C, indicating an enhanced stability of the organic solvent in the gel [129]. Lignin tightly restrains the liquid electrolyte thanks to the strong hydrogen bonds formed between the hydroxyl groups in lignin and the polar groups of carbonyl and ester in organic solvent. Interestingly, GPEs can be designed to be stretchable [130]. Considering the improved interface with the cathode and the anode provided by gels in comparison to conventional batteries bearing microporous membranes soaked into liquid electrolytes (which result in typically brittle batteries), flexible batteries could be constructed. In addition, these batteries enabled by GPEs can function under severe mechanical requirements as they are able to withstand repeated folding, bending and punching [131].

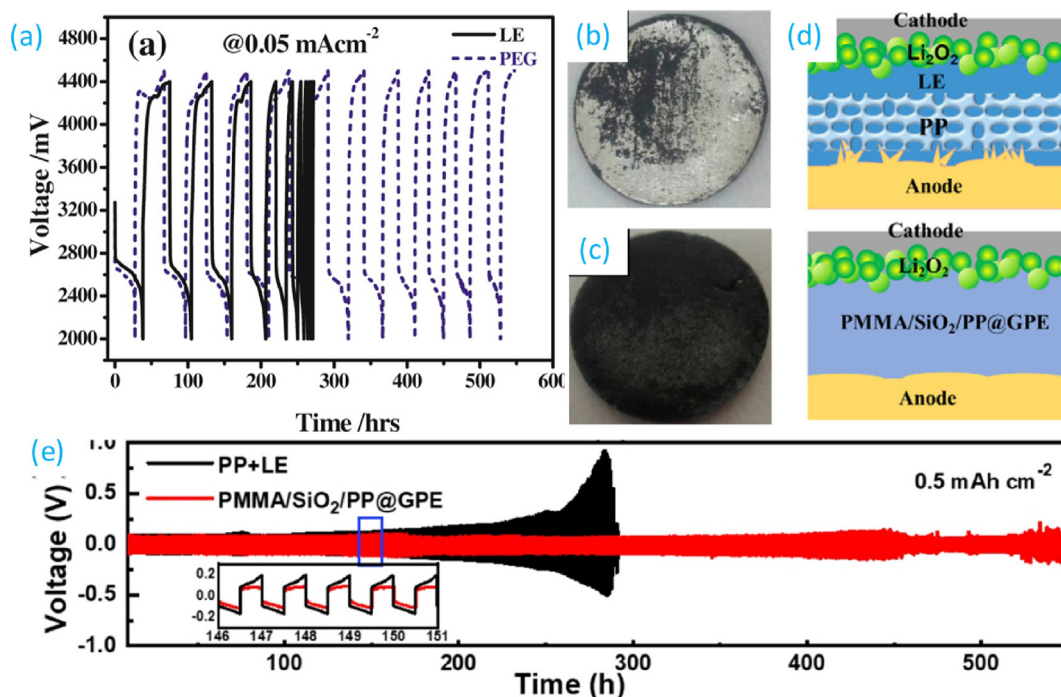
To solve the stability issues related to the irreversible decomposition of LiPF<sub>6</sub> when dissolved in EC/propylene carbonate (PC) [132], Hassoun et al. developed a solvent-free GPE based on PEO and LiCF<sub>3</sub>SO<sub>3</sub> [133]. In particular, the great ability of PEG to accommodate ions, the resistance of its ether linkage and the stability of LiCF<sub>3</sub>SO<sub>3</sub> towards nucleophile enables the development of solvent-free MABs. However, the low ionic conductivity values achieved resulted in batteries having a relatively poor electrochemical performance.

ILs, low temperature molten salts entirely composed of organic cations and anions, have been envisaged to develop GPEs given their non-volatility, non-flammability, and stability in contact with Li metal [134]. A dimensionally stable, mechanically flexible, and free-standing 90–100 μm thick GPE has been prepared mixing PVDF-HFP, an IL and LiTFSI [135]. An ionic conductivity of 0.36 mS·cm<sup>-1</sup> at 30 °C was reached, delivering a capacity (Li–O<sub>2</sub> battery) of 2525 mAh·g<sup>-1</sup> at 228 mA·g<sup>-1</sup> (cathode mass). Li<sub>2</sub>O<sub>2</sub> was reversibly formed and decomposed upon discharge and charge, respectively, and the formed SEI on the Li metal provided an effective barrier to water transport toward the Li anode. The battery was cycled up to 30 times, although the formed by-products (lithium fluoride, H<sub>2</sub>O, Li<sub>2</sub>O<sub>2</sub>, LiOH) increased the internal resistance of the battery during cycling. Benefiting from the green character of many ILs, Jia et al. embedded the choline nitrate IL within a chitosan matrix to obtain a biocompatible GPE offering an

ionic conductivity of 8.9 mS·cm<sup>-1</sup> [136]. Synthesised GPE was applied into a primary transient Mg-air battery capable of delivering a maximum volumetric power density of 3.9 W·L<sup>-1</sup>, which is enough to power diverse implanted medical devices. However, ~15% of the IL was leaked from the chitosan matrix after 160 h, and the battery could not be charged-discharged several times, which is one of the main bottlenecks of transient batteries [137]. In spite of the notable advances on the use of ILs to develop GPEs for MABs, it is important to bear in mind that the IL should be carefully selected as their potential window and ionic conductivity may limit battery life (for example, only 3 cycles have been reported for a GPE bearing 1 M LiTFSI-1-propyl-2,3-dimethylimidazolium bis(trifluoromethanesulfonyl)imide) [138]. In addition, the higher viscosity and increased surface tension of ILs in comparison with carbonate electrolytes results in a reduced wettability with the separator [139,140]. This non-efficient soaking of the IL with the polymeric membrane or gel hinder ion diffusion (generally yielding poor ionic conductivities and low ion transference numbers) and may jeopardise the long-term stability of the system.

Accordingly, ionically conducting GPEs are generally obtained after by adsorbing aqueous or organic electrolytes within a polymer matrix. Following this approach, cellulose acetate mixed with PVDF-HFP was impregnated into a 1 M LiTFSI TEGDME solution to obtain a 45 μm thick GPE [128]. PVDF-HFP offers good electrochemical stability, while cellulose acetate acts as an additive to enhance the wettability and ionic conductivity. With an ionic conductivity of 0.549 mS·cm<sup>-1</sup> (0.298 mS·cm<sup>-1</sup> for the commercial PE separator), and electrochemical stability up to 4.7 V vs. Li/Li<sup>+</sup>, a life-cycle of 530 h was obtained in comparison to the 250 h achieved for battery comprising the PE separator soaked into a liquid electrolyte (see discharge-charge curves in Fig. 11a). Post-mortem morphological and X-ray diffraction analyses were performed to understand such enhanced life of the batteries. As shown in Fig. 11b and c, the Li metal anode extracted from the Li–O<sub>2</sub> battery after 20 cycles showed a slightly shiny silver colour in contrast to the black film (identified as LiOH) observed for the battery comprising the liquid electrolyte solution. These analyses confirm that the improved electrochemical performance arises from the capacity of the GPE to slow down the oxygen diffusion from the air cathode to the Li metal anode (a 1.7-fold increase in the Gurley value indicating low air permeability is obtained in comparison to the PE separator) or the formation of a LiOH passivation film on the metal anode. Benefiting from the ability of carbohydrate polymers to form hydrogels, mechanically elastic and gummy xanthan and κ-carrageenan alkaline gels were applied to a primary Al–air battery [141]. The presence of KOH impairs an amorphous character to the GPE, facilitating ion motion and reaching a maximum ionic conductivity of 88 mS·cm<sup>-1</sup>. However, due to the formation and transfer of Al hydroxide particles in the electrolyte, the cell stopped operating at < 6 h.

GPEs functioning as both separator and electrolytes offer an enhanced protection against dendritic growth, which penetrate porous separators soaked into liquid electrolytes and result in an early failure of the battery (and associated safety issues) [143]. Additionally, their mechanically soft character effectively accommodates the electrode volume changes occurring during successive charge/discharge cycles [144]. However, the protection against dendrite puncture and the ionic conductivity still remain poor for practical applications. The incorporation of (nano)particles into a GPE offers additional benefits originating from the advantages of both organic and inorganic-based solid electrolytes. In this context, as schematically shown in Fig. 11d, a PMMA/SiO<sub>2</sub> composite GPE synthesised upon phase inversion method by a gelation process to protect the battery against undesired Li dendrite growth [142]. The abundant ester bonds of PMMA offer a good affinity with the liquid



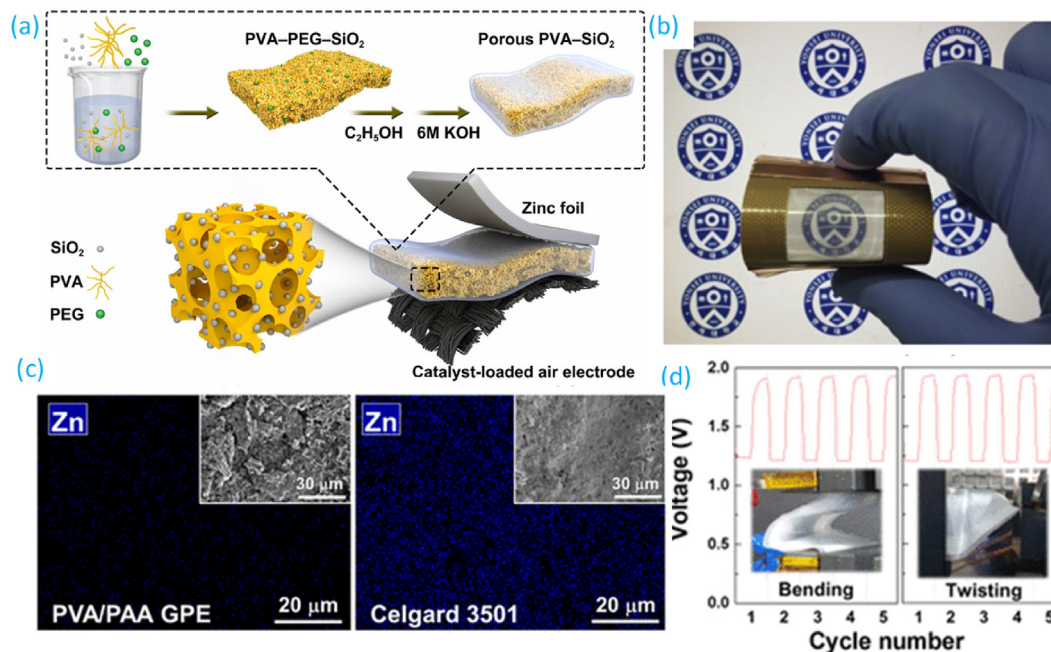
**Fig. 11.** Gel polymer electrolytes in metal-air batteries. (a) Constant current discharge-charge curves in a Li–O<sub>2</sub> battery having the cellulose acetate-PVDF-HFP gel electrolyte (termed as PEG) or the polyethylene separator soaked into a liquid electrolyte. Optical photograph of the Li anode disassembled from: (b) the GPE-containing battery after 20 cycles and (c) disassembled from the liquid electrolyte-containing battery after 20 cycles. Reproduced with permission [128]. Copyright © 2015, Elsevier. (d) Scheme shown the protection against dendrite growth provided by the PMMA/SiO<sub>2</sub> GPE in comparison to the scenario using a commercial PP separator soaked into a liquid electrolyte. Reproduced with permission [142]. Copyright © 2021, American Chemical Society. (e) Current polarisation curves of a coin-type symmetric Li cell at 0.5 mA·cm<sup>-2</sup> performed under an O<sub>2</sub> environment. Reproduced with permission [142]. Copyright © 2021, American Chemical Society.

electrolyte (1 M LiTFSI and 0.05 M LiBr in TEGDME), while the polar carbonyl groups interact with the Li salt to boost Li<sup>+</sup> dissociation. The cations of SiO<sub>2</sub> act as Lewis acids to replace Li<sup>+</sup> to react with oxygen or other groups on the polymer segment, while the oxygen can act as a Lewis base to interact with Li<sup>+</sup> and form a Li<sup>+</sup>-rich phase at the polymer-SiO<sub>2</sub> interface. As a result, a conductivity of 0.41 mS·cm<sup>-1</sup> and a Li<sup>+</sup> transference number of 0.54 were achieved. In addition to the remarkable cycle stability shown in Fig. 11e, a Li–O<sub>2</sub> battery with a first charge-discharge capacity of 6.8 mAh·cm<sup>-2</sup> and a stable cyclic performance of 116 cycles with 0.5 mAh·cm<sup>-2</sup> was obtained. However, when designing GPEs to protect against dendrites, it should be considered that an inverse relationship between the ionic conductivity and mechanical stiffness (able to resist dendrite puncture) in the GPE is obtained. Le et al. used a solution-casting method to mix PVDF-HFP with Al-doped Li<sub>0.33</sub>La<sub>0.56</sub>TiO<sub>3</sub> particles covered by silica and obtained a gel by simple activation in 1 M LiTFSI in TEGDME [145]. With an ionic conductivity of 1.22 mS·cm<sup>-1</sup>, electrochemical stability window up to 5 V vs. Li/Li<sup>+</sup>, and improved interfacial stability, the resistance against dendrite puncture was improved markedly and the contamination of the Li metal by oxygen gas or impurities diffused from the cathode side was prevented. As a result, a life cycle up to 72 cycles at 1000 mAh·g<sup>-1</sup> was obtained, exceeding by 25 cycles the lifecycle of the Li–O<sub>2</sub> cell using the GPE with no nanoparticles. Also for Al-air batteries, a poly(acrylic acid)-based freestanding GPE (KOH electrolyte) capable of preventing electrolyte leakage was achieved controlling the cross-linking degree to balance the ionic conductivity and mechanical strength. Paired with a ZnO additive as a corrosion inhibitor, synthesised GPE offered a maximum ionic conductivity of 460 mS·cm<sup>-1</sup> [146]. When assembled into an Al-air battery, a discharge capacity of

1166 mAh·g<sup>-1</sup> with an area density of 29.2 mAh·cm<sup>-2</sup> was achieved. PVA is commonly used to develop GPEs in MABs.

However, these electrolytes generally present a relatively poor electrolyte uptake, resulting in safety issues associated with electrolyte leakage during operation. To face this problem, Fan et al. designed a porous-structured PVA gel having silica nanoparticles [147]. As schematically shown in Fig. 12a, a phase-inversion approach involving the casting of a PVA-PEG-SiO<sub>2</sub> mixture followed by the dissolution of the pore-forming (PEG, polyethylene glycol) agent in absolute ethanol was followed. The porous structure was then immersed into an aqueous 6 M KOH solution to obtain the nanocomposite GPE. The hydroxyl groups onto SiO<sub>2</sub> and the pore-structure resulted beneficial for the retention of the electrolyte, enabling an ionic conductivity of 57.3 mS·cm<sup>-1</sup>. Importantly, the combination of SiO<sub>2</sub> and the porous structure provided by PEG resulted in a superior cycling stability of 48 h in comparison with the pure porous GPE or the non-porous electrolyte.

In addition to these functionalities, the implementation of permselective GPEs into MABs can avoid undesired side-reactions limiting the electrochemical stability of the batteries and as a consequence, enable longer lasting batteries. A good example of permselective GPEs applies in Zn-air batteries, where a full suppression of Zn(OH)<sub>4</sub><sup>2-</sup> crossover together with an easy OH<sup>-</sup> conduction is preferred. To that end, Kim et al. synthesised a 26 μm thick GPE with artificially engineered bi-continuous anion-conducting/-repelling phases using electrospun PVA/PAA nanofibre mat, and Nafion bearing pendant sulfonate groups, respectively [68]. Synthesised GPE showed an ionic conductivity of 6.6 mS·cm<sup>-1</sup>, and thanks to the Donnan exclusion effect provided by Nafion, the Zn(OH)<sub>4</sub><sup>2-</sup> diffusion coefficient was reduced from 232.4 × 10<sup>-7</sup> cm<sup>2</sup>·min<sup>-1</sup> for the Celgard membrane to



**Fig. 12.** Mechanically deformable gel polymer electrolytes in metal–air batteries. (a) Scheme depicting the fabrication of the PVA-based nanocomposite GPE. Reproduced with permission [147]. Copyright © 2019, Elsevier. (b) Optical photograph of a bended transparent Zn–air cell. Reproduced with permission [148]. Copyright © 2019, Springer-Nature. (c) Post-mortem surface energy-dispersive X-ray spectroscopy images (SEM at inset) of the air cathodes for the GPE and Celgard membrane soaked into a liquid electrolyte. Reproduced with permission [149]. Copyright © 2018, American Chemical Society. (d) In situ analysis of the galvanostatic discharge/charge cycling profiles upon bending (5 mm radius) and twisting (rotation angle of  $100^\circ$  at  $30^\circ \cdot s^{-1}$ ). Reproduced with permission [149]. Copyright © 2018, American Chemical Society.

$4.1 \times 10^{-7} \text{ cm}^2 \cdot \text{min}^{-1}$ . As a result, battery lifespan was increased from the 900 min of the conventional PP separator to  $> 2500$  min of the permselective GPE. Recently, gel electrolytes have been obtained by the dispersion of fumed silica in the aqueous electrolyte (where  $\text{Li}_2\text{SO}_4$  and  $\text{ZnSO}_4$  are present). The presence of  $\text{Li}_2\text{SO}_4$  facilitates the gel formation while  $\text{ZnSO}_4$  hinders gelling. Upon optimisation, the discharge capacity retention (after 300 charge-discharge cycles at 4C) was 10% enhanced over the liquid electrolyte [150].

GPEs also enable the development of multifunctional batteries useful for wearable electronics, transparent screens or smart windows [151]. An optically transparent Zn–air battery (see Fig. 12b) operating for more than 100 cycles and having a maximum power density of  $9.77 \text{ mW} \cdot \text{cm}^{-2}$  was fabricated using a 6 M KOH poly(acrylic acid) gel electrolyte [148]. Interestingly, the gel electrolyte avoids flooding the air electrode, and at the same time reduces the direct exposure of the cathode to the electrolyte saturated with zinc ions, which in turn could form an oxide coating which poisons the active catalyst. Lee et al. reported a secondary Zn–air battery with improved mechanical flexibility and stable cycling up to 1500 min using a cross-linked PVA/PAA (6 M KOH) gel polymer electrolyte [149]. The permselective GPE suppressed the zincate ion crossover by 3 times in comparison to that shown by the commercial polyolefin separator. As shown by the energy dispersive X-ray spectroscopy and SEM images in Fig. 12c, this was translated into a ZnO contamination-free air cathodes. Thanks to its design, the battery was able to withstand bending, twisting and even crumpling (Fig. 12d). In search of enhanced mechanical functionalities, a flexible and stretchable fibre-shaped Al–air battery having GEP and delivering a specific capacity of  $935 \text{ mAh} \cdot \text{g}^{-1}$  and an energy density of  $1168 \text{ Wh} \cdot \text{kg}^{-1}$  was reported [152]. Not only the mechanical performance and ionic conductivity ( $180 \text{ mS} \cdot \text{cm}^{-1}$ ) is remarkable, but also the corrosion of the Al anode was reduced by incorporating ZnO and  $\text{Na}_2\text{SnO}_3$  to the PVA/polyethylene oxide in KOH electrolyte.

### 3.3. Solid-state electrolytes

*Solid-state electrolytes have the potential to circumvent the complex water management and potential leakage issues. However, the electrochemical performance is somewhat poor due to low ionic conductivities and poor interfacial adhesion*

The configuration based on a porous membrane soaked into a liquid electrolyte results in bulky batteries with serious safety issues associated to electrolyte leakage and combustion risks. Transitioning from liquid-based electrolytes to solid-like electrolytes may simplify the design and fabrication process of the batteries and lower gas crossover [153]. However, the application of solid electrolytes has been limited by the ionic conductivities of one order lower than those of liquid electrolytes. Additionally, the chemical and electrochemical stability of solid electrolytes is relatively poor, which coupled with their brittleness and poor interfacial adhesion to metallic anode prevent them from being implemented in practical applications. To overcome these bottlenecks, the efforts have been mainly directed to develop polymeric (either in the form of mono-material or composite), solid inorganic and composite polymer electrolytes. Conventionally, polymer-containing solid electrolytes are achieved by cross-linking. The degree of cross-linking notably influences the physico-mechanical and electrochemical performance of polymeric electrolytes. An extended cross-linking restricts chain mobility of the matrix and usually reduces the crystallinity of the electrolyte [154,155]. A reduced crystallinity typically results in increased ion transport numbers and ionic conductivities, while a reduced macromolecular mobility increases the mechanical stability (with shear modulus increases), improving its resistance against dendritic growth. However, it



should be considered that an excessive cross-linking can also lower the ionic conductivity by restricting too much chain mobility.

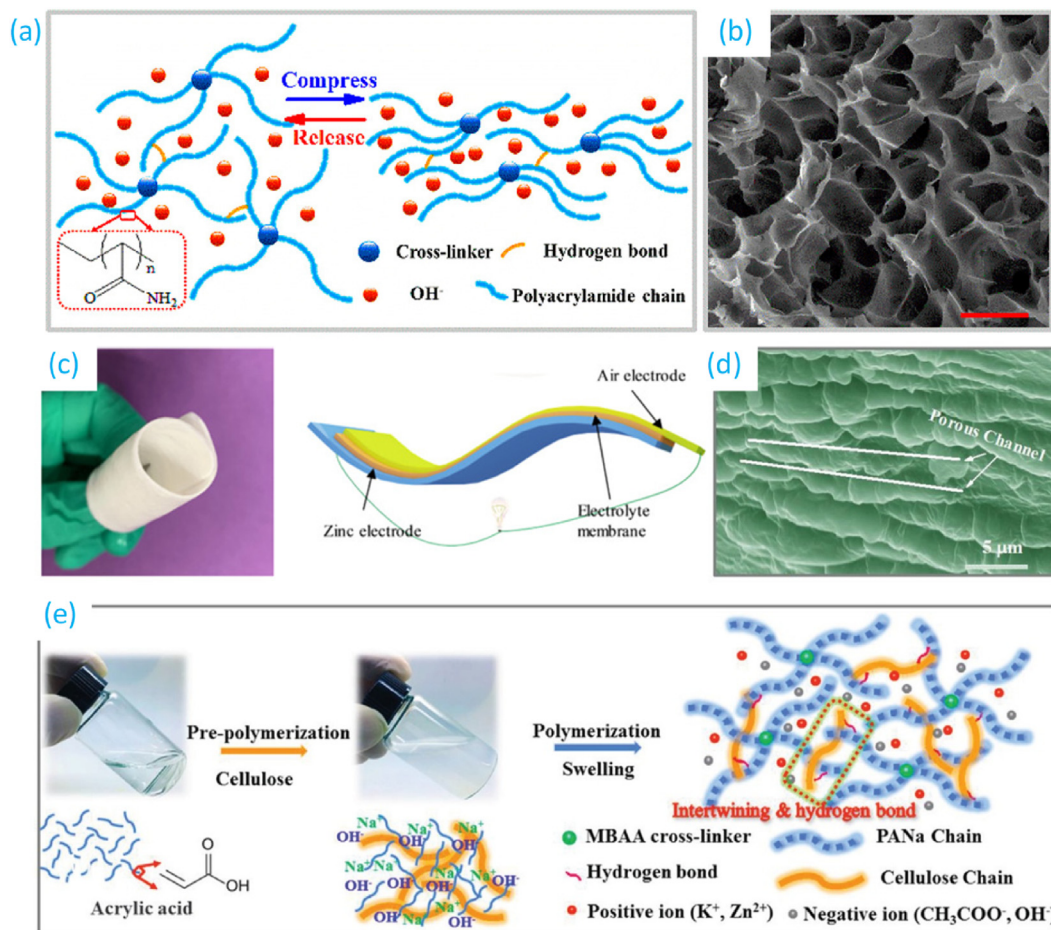
### 3.3.1. Solid polymer electrolytes (SPEs)

Similarly to GPEs, polymeric solid electrolytes are typically complexes of a salt and a high-molecular-weight polymer, but with theoretical absence of solvating liquids. However, many reports do not strictly distinguish gel or solid polymer electrolytes as SPEs may have more or less liquid as the conduction medium for ions to obtain satisfactory conductivities. To avoid misunderstanding, this section does not provide an exhaustive list of SPEs but it tries to briefly summarise the state-of-the-art in the field. Generally, due to the absence of solvating liquids, SPEs have low conductivities at room temperature ( $\sim 10^{-2} \text{ mS} \cdot \text{cm}^{-1}$ ), and their elastic modulus is in the order of several MPa, offering an insufficient protection against dendrite growth in comparison to inorganic solid electrolytes. However, their relatively soft character enables an easy battery handling and an intimate contact with the electrodes, which is translated into longer lifespans.

In spite of the widespread use of PEO as SPE for LIBs, the use of this polyether to fabricate SPEs for Li-air batteries has been somewhat limited. In this regard, Balaish et al. solved the inherent limitations of PEO (relatively poor interfacial properties and high crystallinity) by operating at  $80^\circ\text{C}$ , a temperature  $\sim 10^\circ\text{C}$  above the melting point of the polymer itself, reaching acceptable ionic

conductivity values for a PEO-lithium triflate SPE [156]. In comparison to Li-O<sub>2</sub> batteries having liquid electrolytes (charging voltage of 4–4.2 V), the charging voltage was lowered to 3.6 V, indicating a lower charging-over-potential. Additionally, as a liquid-free solution, this approach faces the long-term stability issues due to the autoxidation of liquid electrolytes under oxygenated radicals that are formed upon operation. In comparison to PEO, PVA offers improved liquid absorption thanks to its –OH groups attached to the carbon chain. An ionic conductivity of  $47 \text{ mS} \cdot \text{cm}^{-1}$  at room temperature has been reported for a PVA electrolyte, which increased discharge capacity of 792 mAh for the PE/PP separator to 1475 mAh when assembled into a Zn-air battery (percentage of utilisation increase from 49.5% to 92%) [157]. PVA can be further gelled in an aqueous 10 wt% glutaraldehyde solution (further addition of acetone and HCl) to obtain improved mechanically flexible electrolytes, although the ionic conductivity dropped to  $15 \text{ mS} \cdot \text{cm}^{-1}$  [158].

Poly(acrylic acid) generally offers higher ionic conductivities thanks to its low crystallinity and hydrophilic domains, although its mechanical properties can be poor. For example, an ionic conductivity as high as  $288 \text{ mS} \cdot \text{cm}^{-1}$  at room temperature has been reported of a poly(acrylic acid)-based electrolyte obtained after the cross-linking (in KOH) of acrylic acid with N,N'-methylene-bisacrylamide and K<sub>2</sub>S<sub>2</sub>O<sub>8</sub> as a polymerisation initiator [159]. Synthesised electrolyte showed a very similar electrochemical stability as the near alkaline solution. As schematically depicted in Fig. 13a, the



**Fig. 13.** Structure of solid polymer electrolytes used in metal-air batteries. (a) Diagram depicting the high compressibility for a polyacrylamide hydrogel electrolyte. The inset is the molecular formula of polyacrylamide; (b) SEM image of a freeze-dried polyacrylamide hydrogel. Reproduced with permission [160]. Copyright © 2018, American Chemical Society. (c) Optical photograph of the bacterial cellulose/PVA electrolyte highlighting its flexibility and diagram, of the assembled Zn-air battery. Reproduced with permission [164]. Copyright © 2019, American Chemical Society. (d) cross-section SEM image of the freeze-dried PANa-cellulose electrolyte; (e) synthetic procedure of the sodium polyacrylate-cellulose hydrogel electrolyte using the N,N'-Methylenebisacrylamide (MBAA) cross-linker, acrylate monomer and cellulose. Reproduced with permission [165]. Copyright © 2019, Wiley.

reversible intermolecular hydrogen bonds formed in polyacrylamide electrolytes polymerised by *N,N'*-methylenebis(acrylamide) enable the polyacrylamide chains to dynamically break and recombine to dissipate the applied energy, hindering the formation and propagation of cracks [160]. The interconnected macropores shown in Fig. 13b allow free ion transfer within the electrolyte. As a result, these electrolytes enable Zn-air batteries withstanding compressions up to 54% strain and bending up to 90° without losses in charge/discharge performance and output power. Other polymers such as poly(ethylene carbonate), poly(trimethylene carbonate), poly(propylene carbonate), PVDF-HFP, or PMMA are good candidates to develop SPEs as they typically present good salt dissociation, and thus, larger ionic conductivities [161].

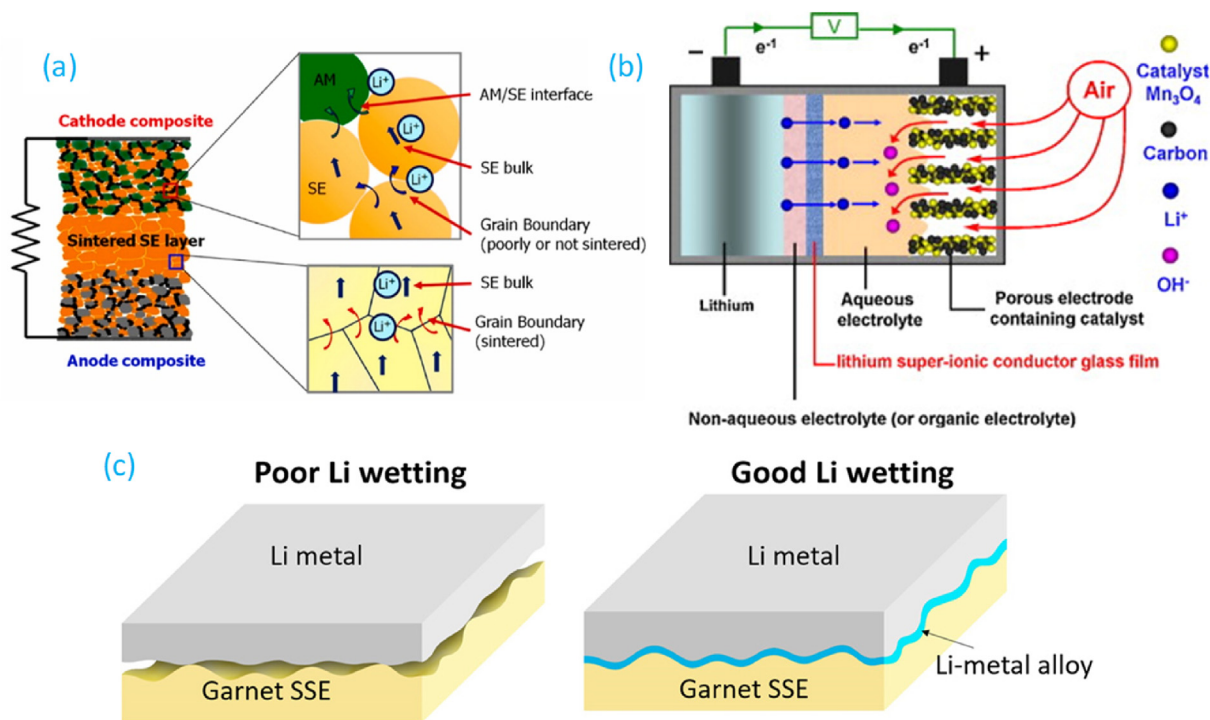
Biopolymers have also been used to develop SPEs for MABs. In this sense, Fu et al. reported the synthesis of an alkaline-exchange electrolyte membrane based on quaternary ammonia-functionalised cellulose nanofibres for solid-state Zn-air batteries [162]. The membrane with pore sizes of 25–300 nm facilitates the hydroxide ion hopping ( $21.2 \text{ mS}\cdot\text{cm}^{-1}$  in 1 M KOH), offers a large water retention capacity to avoid electrolyte loss by evaporation and is mechanically flexible. As a result, the specific capacity and the cycling stability of the battery improved in comparison to the commercial alkaline anion-exchange membrane, which showed a progressive water loss and ionic conductivity decay. In another example, a cellulose-based SPE has been fabricated using sodium polyacrylate, 10 M NaOH and a porous paper skeleton to store the gelled alkaline electrolyte [163]. When applied into an Al-air battery, a capacity up to  $901 \text{ mAh}\cdot\text{g}^{-1}$  was obtained with an open circuit voltage of 1.5 V and a peak power density of  $3.8 \text{ mW}\cdot\text{cm}^{-2}$ .

Importantly, biopolymers show synergetic properties when blended with other petroleum-based polymers. A flexible solid-state Zn-air battery was developed using bacterial cellulose, PVA, KOH,

and  $\text{Zn}(\text{CH}_3\text{COO})_2$  [164]. Thanks to the achieved microporous dual-network structure originating from the fibre-like shape of bacterial cellulose, ionic conductivities up to  $80.8 \text{ mS}\cdot\text{cm}^{-1}$  were observed, and a load-bearing percolating dual network is formed due to the hydrogen bonding between both electrolyte constituents. Interestingly, the solid electrolyte could fold and bent in any angle and restores its original size once mechanical stresses are removed, enabling flexible Zn-air batteries (Fig. 13c). The Zn-air battery could operate for more than 440 h with no notable capacity decrease. Ma et al. recently reported the fabrication of a highly-stretchable Zn-air battery comprising a sodium polyacrylate/cellulose electrolyte [165]. Cross-section SEM images of the freeze-dried solid electrolytes in Fig. 13d reveal a hierarchical structure with ordered porous channels distributed between layers. These basal spaces are expected to increase the water-retention and ionic conductivity of the hydrogel. As shown in Fig. 13e, the electrolyte was synthesised via free radical polymerisation of acrylic acid neutralised by a NaOH solution in the presence of cellulose and MBAA cross-linkers. A covalent cross-linking is formed between sodium polyacrylate/-OH groups of cellulose and PANA/MBAA, further reinforced by hydrogen bonds between sodium polyacrylate and cellulose chains. The synergy arising from chemical and physical cross-linking provides a strengthened mechanical robustness and stretchability to the electrolyte. Additionally, the electrolyte showed an enhanced alkaline tolerance, holding 6 M KOH which renders a conductivity of  $280 \text{ mS}\cdot\text{cm}^{-1}$ .

### 3.3.2. Solid inorganic electrolytes (SIEs)

Different types of SIEs have been reported, where sulfide-, oxide-, nitride- and phosphate-based ones are the most commonly found examples in lithium-metal batteries [166]. Generally, inorganic solid electrolytes exhibit satisfactory ionic conductivities



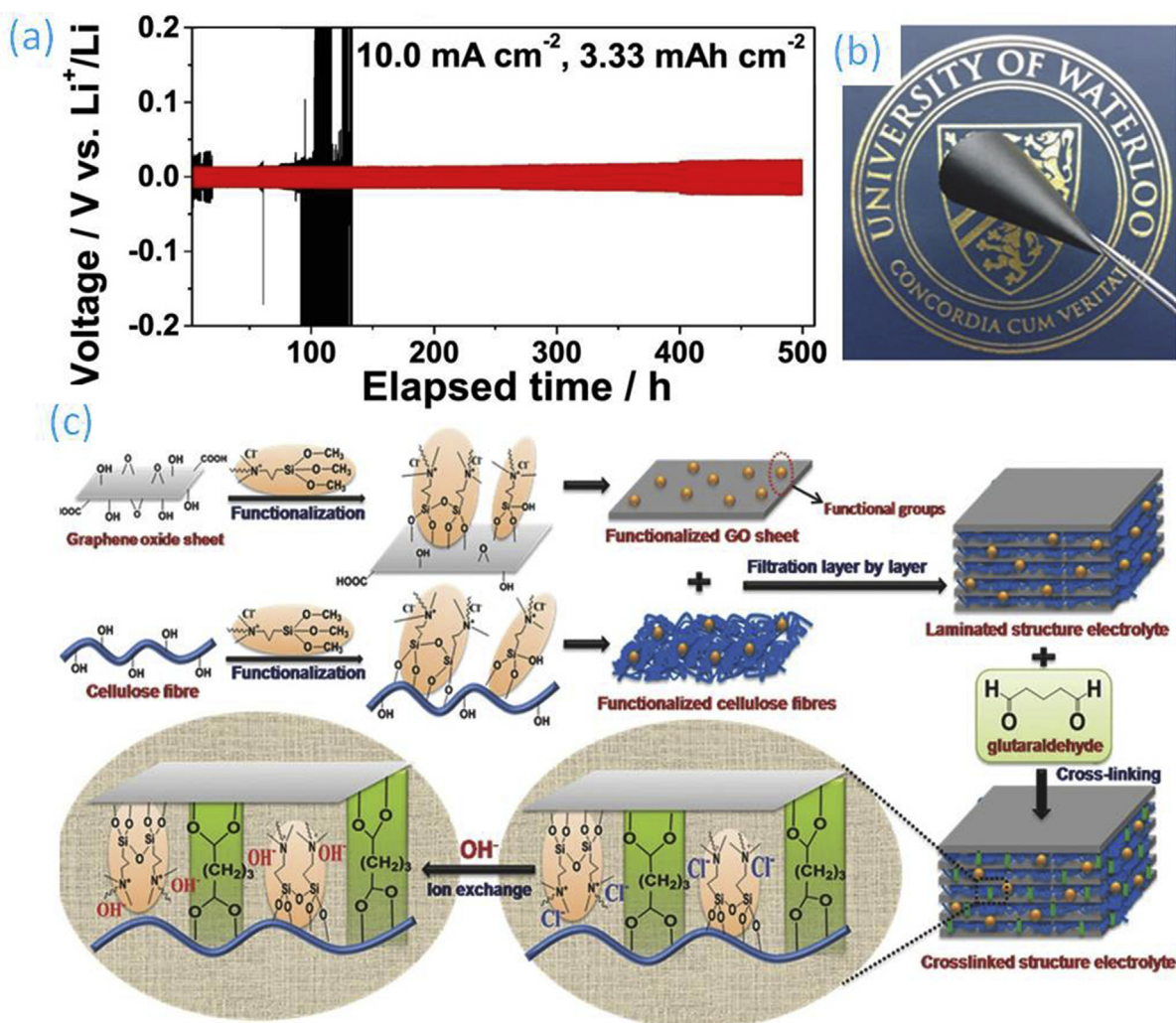
**Fig. 14.** Ceramic-based solid electrolytes in metal-air batteries. (a) Structure of a bulk-type all solid state battery and the resistance originated from solid electrolytes. AM: active materials; SE: solid electrolyte. Reproduced with permission [169]. Copyright © 2019, Elsevier. (b) A schematic representation of a Li-air battery containing a LISICON SIE. Reproduced with permission [171]. Copyright © 2010, Elsevier. (c) Schematic showing the improved wettability of the garnet-based SIE against Li metal using Li-metal alloy. Reproduced with permission [178]. Copyright © 2017, American Association for the Advancement of Science.

when comparing with polymeric solid electrolytes. Their elastic modulus is also higher, although surface adhesion with electrodes is compromised given their often rigid character, resulting in increased interfacial resistances upon cycling. The chemical and electrochemical stability of SIEs is also a concern. For example, some sulfides have good ionic conductivity properties, although they are unstable when exposed to moisture or oxygen, generating highly toxic  $\text{H}_2\text{S}$ .

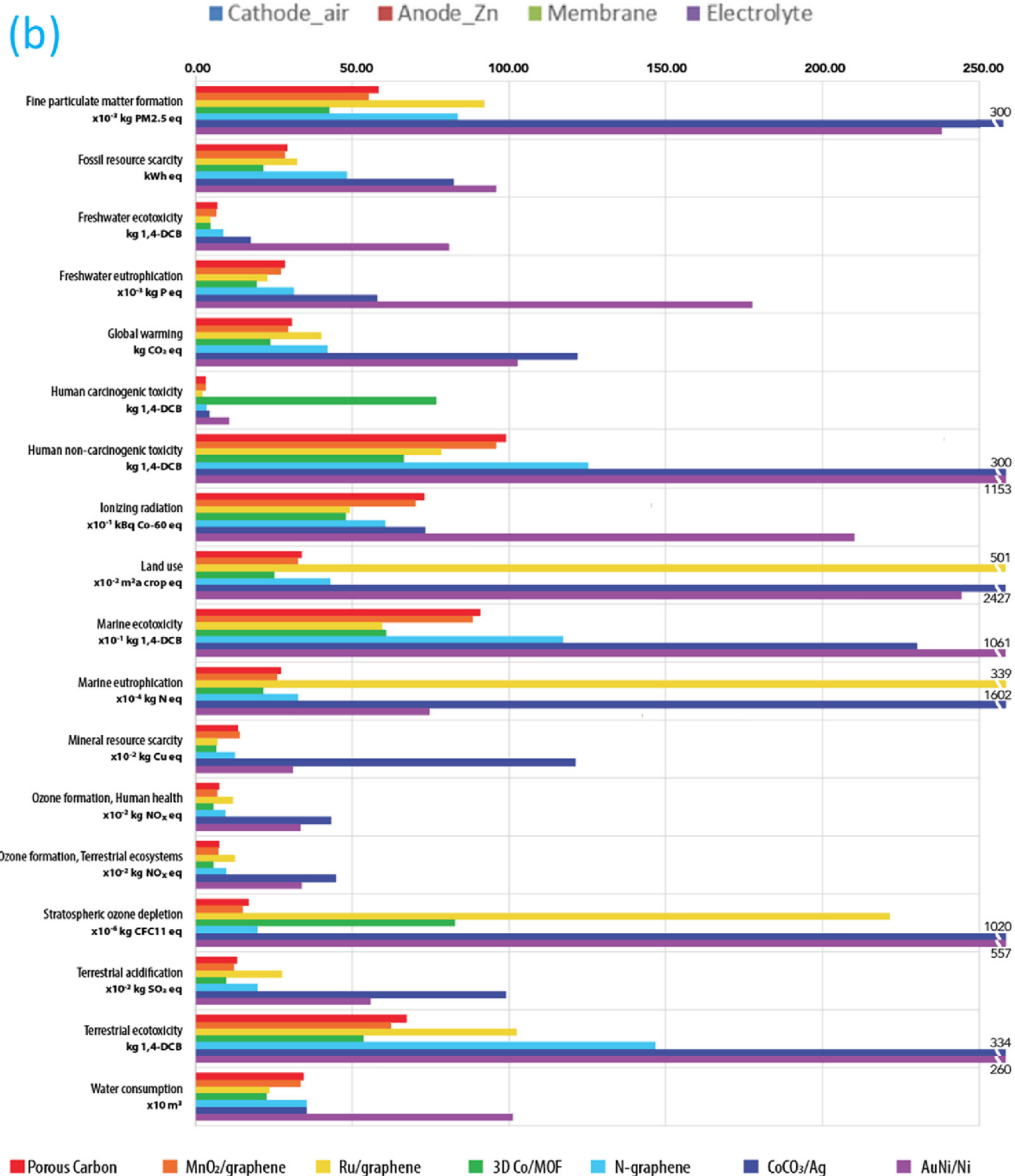
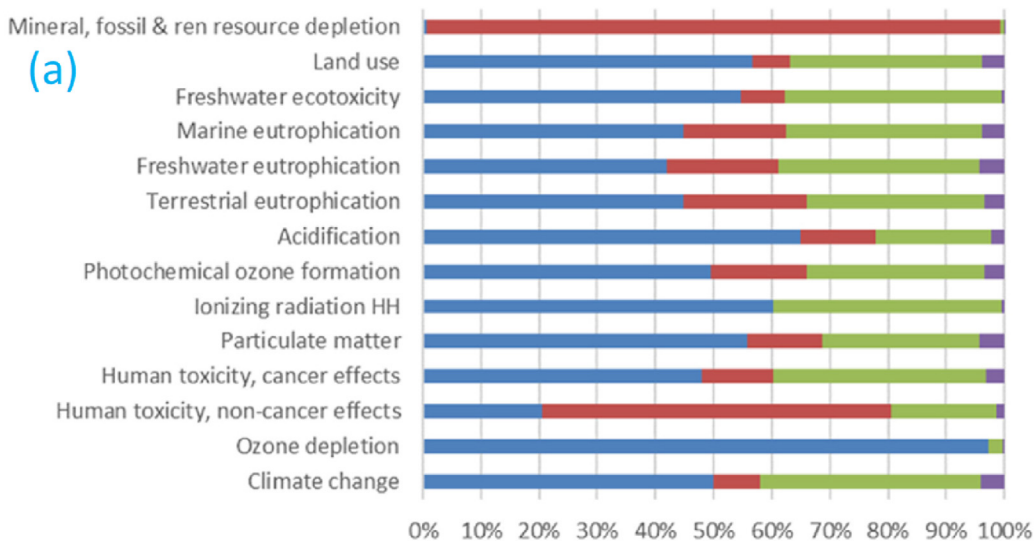
Oxides present a generally improved resistance to oxidation over sulfides. In fact, NASICON oxide electrolytes have been reported to be stable when exposed to air moisture, although their poor electrochemical stability at low voltages is a concern [3]. In 2004 Visco et al. proposed a  $\text{Li}^+$  conducting NASICON-type solid electrolyte to protect the Li anode in a Li–air battery [167]. This concept offers the advantage that the discharge reaction product (eg.  $\text{LiOH}$ ) is soluble in water. Following this approach, Li–air batteries with aqueous electrolytes separated by a water stable  $\text{Li}^+$  conducting glass ceramics have been reported [168]. Lithium titanium aluminium phosphate (LATP) in the composition of  $\text{Li}_{1+x}\text{Al}_x\text{Ti}_{2-x}(\text{PO}_4)_3$  are a promising group of solid-state electrolyte

materials thanks to their high-ionic conductivity and low-manufacturing cost [169]. As the bulk ionic conductivity of LATP ceramic is generally an order of magnitude greater than that of the grain boundary interface, the control of the grain boundaries on LATP enables enhancing the  $\text{Li}^+$  mobility. To that end, as shown in Fig. 14a, a high-temperature sintering process was applied to densify the solid-state electrolyte and remove the pores/voids/cracks.

A 200  $\mu\text{m}$  thick solid electrolyte separator of  $\text{Li}_{1.3}\text{Al}_{0.5}\text{Nb}_{0.2}\text{Ti}_{1.3}(\text{PO}_4)_3$  prepared by a tape-casting approach having a bending strength of 100 MPa and ionic conductivity of  $0.91 \text{ mS}\cdot\text{cm}^{-1}$  at  $25^\circ\text{C}$  was applied into a Li–air battery [170]. However, a polymeric porous separator with 4 M LiFSI in ethylene glycol dimethyl ether was used to solve the stability issues of the solid electrolyte when in contact with the Li anode, reducing the energy density of the cell. Although less attention in comparison to NASICON SIEs has been paid, LISICON ( $\text{Li}^+$  superionic conductor) SIEs are promising candidates for MABs given their high ionic diffusion in the mobile ion sub-lattice at room temperature. A LISICON solid electrolyte was implemented into Li–air batteries to separate organic and aqueous



**Fig. 15.** Composite polymer electrolytes in metal–air batteries. (a) Galvanostatic charge–discharge cycles of LLZTO-based CPE in symmetric 2032 coin cells at  $10.0 \text{ mA}\cdot\text{cm}^{-2}$  and  $3.33 \text{ mAh}\cdot\text{cm}^{-2}$ . Red line represents the CPE, while black line accounts for the bare LLZTO. Reproduced with permission [183]. Copyright © 2020, Elsevier. (b) Optical photograph of the flexible graphene oxide/CNF CPE. (c) Synthetic procedure for the synthesis of the graphene oxide/CNF CPE involving functionalisation, filtration, cross-linking, and hydroxide-exchange. Reproduced with permission [184]. Copyright © 2016, Wiley.



electrolytes obtain enhanced cycling stabilities [171]. In this system, the catalytic reduction of  $O_2$  occurs in an alkaline aqueous electrolyte, while Li remains in contact with a non-aqueous electrolyte (Fig. 14b). This design enables the continuous reduction of  $O_2$  from air to deliver energy.

NASICON-type LAGP solid electrolytes such as  $Li_{1.5}Al_{0.5}Ge_{1.5}(PO_4)_3$  have been used to inhibit the crossover of soluble products in Li– $O_2$  batteries, although a  $Li^+$  conducting interface between the Li metal and the solid electrolyte is generally required to prevent the direct reduction of the solid electrolyte [172]. In spite of this protecting layer, increased impedances are observed upon cycling due to localised reduction. Kamaya et al. reported a solid  $Li_{10}GeP_2S_{12}$  electrolyte reaching an ionic conductivity as high as  $12 \text{ mS}\cdot\text{cm}^{-1}$  at room temperature, even though the material was not tested into a MAB [173].

Apart from NASICON and LISICON solid electrolytes, there are also further materials suitable for MABs. In this context, Perovskite-type solid electrolytes are interesting given their high bulk ionic conductivities reaching several  $\text{mS}\cdot\text{cm}^{-1}$  at room temperature [174]. However, these materials present a low decomposition voltage against metallic Li and the grain boundary effect notably reduces the resulting ionic conductivity by one order of magnitude. To solve these issues, Inaguma and Nakashima prepared a lanthanum lithium titanate (LLTO) ceramic electrolyte ( $La_{0.57}Li_{0.29}TiO_3$ ) with a maximum conductivity of  $0.57 \text{ mS}\cdot\text{cm}^{-1}$  at  $27^\circ\text{C}$  eliminating the resistive grain-boundary by grain growth [175]. When applied as a separator into a Li–air battery having a 0.5 M LiOH aqueous and a Li organic electrolyte, one week stability was obtained, underlying the potential of LLTO ceramics in MABs.

Another remarkable example of oxide SIEs are garnet-type materials, which offer high ionic conductivities, adequate chemical stabilities with Li metal, and wide electrochemical potential windows [176]. Sue et al. showed the application of a garnet-type SIE having the nominal composition of  $Li_7La_3Zr_2O_{12}$  (LLZO) into a Li– $O_2$  battery [177]. A cutoff capacity of  $1000 \text{ mAh}\cdot\text{g}^{-1}$  carbon at  $20 \mu\text{A}\cdot\text{cm}^{-2}$  was achieved. However, the operating temperature was  $80^\circ\text{C}$  to improve the Li–SIE and the cathode–SIE interfacial contact. To modify the surface wettability of a garnet ( $Li_7La_{2.75}Ca_{0.25}Zr_{1.75}Nb_{0.25}O_{12}$ ) SIE from lithiophobic to lithiophilic, an intermediary Li–metal alloy could be applied between the SIE and the metallic Li as schematically depicted in Fig. 14c [178]. Thanks to the improved contact of the garnet SIE with metallic Li, a hybrid solid-liquid Li– $O_2$  cell could be cycled over 10 times.

In addition to these materials with remarkable properties, other inorganic materials are also being explored to develop solid electrolytes for MABs. An integrated solid-state Li–air battery having an ultrathin, high-ion-conductive zeolite-based solid electrolyte has been recently reported by Chi et al. [179]. The inherent microporous crystalline structure of zeolites facilitates the mass transport process while the good contact between the cathode and the zeolite-based solid electrolyte minimises the interfacial resistance of the cell. Moreover, the Gurley times (the time needed for  $100 \text{ cm}^3$  air to pass through a separator under an air pressure of  $0.862 \text{ kgf}\cdot\text{cm}^{-2}$ ) for the zeolite-electrolyte were too long to be within the detection range, in comparison with the 1410 s and 1s measured for the Celgard and the glass fibre separators, respectively. This much slower permeability suggests a notably reduced diffusion of  $O_2$ ,  $N_2$  or  $H_2O$  to the anode, limiting its corrosion. As a result, an extended lifecycle of 149 cycles at  $1000 \text{ mAh}\cdot\text{g}^{-1}$  was obtained, in

comparison to the 12 cycles obtained for a Li–air battery based on lithium aluminium germanium phosphate electrolytes and the 102 cycles for the battery bearing organic electrolytes.

### 3.3.3. Composite polymer electrolytes (CPEs)

Composite polymer electrolytes (CPEs) are formed by a polymer matrix incorporating chemically inert inorganic fillers that assist ion conductivity [180,181]. CPEs are developed to combine the advantages of solid polymer electrolytes and ion conductive inorganic ceramics. Although CPEs have been mainly applied into other technologies such as sodium-ion batteries (NIBs) or lithium-metal batteries (LMBs), some examples could also be found in MABs. For instance, a PVDF–HFP plasticised by a hydrophobic IL was used as a matrix to host 1–6 wt% hydrophobic silica nanoparticles [138]. The ionic conductivity increased from  $1.19 \text{ mS}\cdot\text{cm}^{-1}$  up to a maximum of  $1.83 \text{ mS}\cdot\text{cm}^{-1}$  with 3 wt% silica and designed CPE effectively stabilised the Li/CPE interface and diminish Li corrosion by water. Polydopamine-coated MOFs (CAU-1- $NH_2$ ) were incorporated into a PMMA matrix to obtain an  $O_2$  selective membrane thanks to the high surface area, controlled porosity and adjustable chemical functionality of the MOF [182]. The  $-NH_2$  groups in the MOF,  $-OH$  in polydopamine, and the  $-C=O$  double bond in PMMA preferably interact with  $CO_2$  and prevent its interaction with  $Li_2O_2$  to form  $Li_2CO_3$ , while the hydrophobicity of the CPE limits the ingress of water into the cell. As a result, when the terminal discharge voltage is set at 2 V, the Li–air battery lifecycle was extended from 6 to 66 cycles having the CPE. In another example, a CPEs containing 89.6 wt% LLZO garnet was included in a polyether sulfone matrix to obtain a ‘polymer-in-ceramic’ CPE having an ionic conductivity of  $0.69 \text{ mS}\cdot\text{cm}^{-1}$  at  $20^\circ\text{C}$  [183]. As depicted by galvanostatic charge/discharge cycles in symmetric Li cells in Fig. 15a, an improved compatibility with Li metal and acceptable capability against Li dendrite was obtained (red line for the CPE, black line for bare LLZO). Moreover, the discharge–charge voltage gap was reduced to 0.6 V in comparison with the nearly 1.5 V observed for the bare LLZO solid electrolyte.

A highly flexible laminate-structured functionalised GO/CNF membrane having highly hydroxide-conductive quaternary ammonium groups was developed for a stretchable Zn–air battery (Fig. 15b) [184]. As summarised in Fig. 15c, the CPE was obtained after a multi-step process involving chemical functionalisation, layer-by-layer filtration, cross-linking, and ion-exchange processes. The two aldehyde functional groups of glutaraldehyde reacts with the hydroxyl groups onto GO and CNFs to form an acetal structure with a cross-linked layered-structured membrane with hydroxide-conducting properties. CNFs offer an interconnected framework integrating graphene oxide into a flexible membrane with high water absorption ability. Ionic conductivities as high as  $39.0 \text{ mS}\cdot\text{cm}^{-1}$  ( $58.8 \text{ mS}\cdot\text{cm}^{-1}$  at  $70^\circ\text{C}$ ) are achieved as a result of the high mobility of hydroxide ions dissociated from the grafted quaternary ammonium groups. Those benefits are manifested into a peak power density of  $44.1 \text{ mW}\cdot\text{cm}^{-2}$  as opposed to the  $33.2 \text{ mW}\cdot\text{cm}^{-2}$  for the A201 membrane, while no performance loss after 600 h was observed (A201-based battery has large charge/discharge polarisations after 300 min). Overall, the work directed to the search of solid-state electrolytes to be implemented in MABs is notably lower when comparing with other battery configurations such as solid-state LMBs. Nevertheless, there are plethora of lessons that can be learned from these previous efforts.

**Fig. 16.** Environmental impacts of metal-air batteries. (a) The share of the different Zn–air battery subassemblies to the fourteen impact categories analysed according to the International Reference Life Cycle Data System (ILCD) methodology. Reproduced with permission [196]. Copyright © 2020, Elsevier. (b) Environmental impacts of seven Li– $O_2$  batteries normalised to 1 kWh of storage capacity based on life cycle assessment. Reproduced with permission [198]. Copyright © 2021, American Chemical Society.

#### 4. Environmental impacts

The development of sustainable energy storage systems is an inexcusable task that scientist and industry must undertake, particularly given the actual concerns over the depletion of non-renewable resources, global warming and battery waste management issues. Nowadays, LIB technology still has recognised environmental sustainability issues, mostly arising from the use of highly toxic and scarce materials [185]. In the sustainable energy storage landscape, MABs offer environmental benefits originating from their high energy efficiency that is 5–30 times greater than conventional LIBs. In addition, as opposed to LIBs or NIBs which use considerable amounts of materials found in the CRM list (Co, Mn, V, Ni, or graphite), MABs rarely use these materials, and when they do, small quantities are needed [186]. For example, heteroatom-doped hierarchical carbon with honeycomb structures function well as metal-free electrocatalyst for ORR [187], opening the door to design sustainable metal-air batteries free of catalysts such as Pt/C. These strategies can lessen the pressures over the extraction of CRMs for the battery industry, which encompasses serious environmental pressures, as for example, 1900 tons of H<sub>2</sub>O (diverted from essential agricultural activities) are consumed by evaporation for the extraction of 1 Li tone [188]. However, it should be considered that the catalysts in MAB are often composed by noble metals subjected to supply chain bottlenecks and environmental concerns (in spite of the relatively small quantity of metals required as opposed to LIBs/NIBs). Battery recycling is a plausible approach to recover those scarce materials as the net impact of LIB production can be reduced when the materials are recovered after battery end-of-life (EoL) [189].

Apart from these concepts, the full understanding the sustainability of MABs requires the determination of their environmental impacts. If the environmental burdens of pure metals are considered, Ca–air, Zn–air, and Mg–air batteries should be a priori preferred. Indeed, the production of pure Li has a global warming potential (GWP) of 7.1 kg CO<sub>2</sub>-equiv·kg<sup>-1</sup>, being the impacts of the other metals as follows: 8.2 kg CO<sub>2</sub>-equiv·kg<sup>-1</sup> for Al, 5.4 kg CO<sub>2</sub>-equiv·kg<sup>-1</sup> for Mg, 3.1 kg CO<sub>2</sub>-equiv·kg<sup>-1</sup> for Zn, and 1.0 kg CO<sub>2</sub>-equiv·kg<sup>-1</sup> for Ca [190]. Moreover, calcium is widely present in Earth's crust. Regarding cathode materials, pure cobalt shows a GWP of 8.3 kg CO<sub>2</sub>-equiv·kg<sup>-1</sup>, while vanadium encompasses 33.1 kg CO<sub>2</sub>-equiv·kg<sup>-1</sup>, manganese 1.0 kg CO<sub>2</sub>-equiv·kg<sup>-1</sup>, iron 1.5 kg CO<sub>2</sub>-equiv·kg<sup>-1</sup>, or nickel 6.5 kg CO<sub>2</sub>-equiv·kg<sup>-1</sup> [190].

The fabrication of energy storage systems is subjected to large amounts of raw materials and energy consumption, together with the emission of different wastes [191]. Accordingly, battery sustainability should go beyond the mere determination of the global warming involved during the use of raw materials, and should cover the different life cycle stages. In fact, the worldwide greenhouse gas emissions originating from battery manufacturing are estimated to be 182 Mt CO<sub>2</sub>-equivalents (a unit of measurement applied to standardise the climate effects of greenhouse gases) [192]. In this sense, a *cradle-to-grave* (the full life cycle, covering from resource extraction or cradle, manufacturing, distribution, use and end-of-life or grave), or at least *cradle-to-gate* (from raw material extraction to the processing, manufacturing and product fabrication or factory gate) approach needs to be considered to get the bigger picture [193]. Using the life cycle assessment (LCA) methodology, it is possible to quantify of environmental impact of a product or service through its life cycle, covering from the extraction and processing of the raw materials to the EoL and taking into account the manufacturing, distribution and use [194]. A priori, the main environmental burdens of MABs arise from the nature of cathode catalysts (which often require highly toxic and scarce elements). Aqueous electrolytes are environmentally preferred over

aprotic solvents, which entail notable environmental burdens in terms of CO<sub>2</sub> emissions and toxicity.

Zn-based batteries are stable towards moisture, so no inert atmosphere is required during battery manufacturing. This simplifies the production process and results in lower energy and material (argon) consumption typically needed to ensure a moisture-free inert atmosphere during cell assembly of conventional LIBs or NIBs (ensuring these conditions requires the 29.4% of the total energy for the production of a 32-Ah LMO/graphite cell) [195]. On this basis, Santos et al. studied the *cradle-to-gate* environmental impacts of a Zn–air battery bearing a PVA-KOH hydrogel electrolyte (termed as membrane in the study) and a carbon black/MnO<sub>2</sub> cathode [196]. A cumulative energy demand (CED) of 590.8 MJ·kg<sup>-1</sup> was obtained (where the cathode air, the membrane, the Zn anode and the electrolyte accounted for the 56, 39, 3 and 2%, respectively) as compared with the average of 152.9 MJ·kg<sup>-1</sup> (values ranging from 19.6 to 1416.0 for 76 different studies) corresponding to LIBs [197]. In spite of such larger value, the electricity consumption could be lower than that of a LIB given the laboratory-scale production of analysed Zn-air battery. An embedded emission of 61.2 kg CO<sub>2</sub>-equiv per 1 kWh of stored energy was obtained, where the cathode accounted for 50%, the membrane the 38%, the Zn anode 8% and the electrolyte solely 4%. As shown in Fig. 16a, this is the general trend except for the resource depletion category, where the Zn powder anode has the largest contribution. Overall, notable impacts in human toxicity (cancer and non-cancer effects), freshwater ecotoxicity and resource depletion are achieved. It should be noted that current LCA studies are mainly performed for laboratory-scale batteries, so small lab-scale configurations are analysed and no data regarding commercial cells is available.

Zackrisson et al. performed a *cradle-to-grave* analysis (including production, use and recycling) on Li–air battery cell for EVs [199]. The battery has a Li foil anode, a PP separator soaked in LiClO<sub>4</sub> in TEGDME, a CNT/Co<sub>3</sub>O<sub>4</sub> cathode, copper current collectors and PP housing. The cathode had a relative production-related CO<sub>2</sub> impact of 37%, followed by the 28% of the assembly energy and the 23% of the Li foil. A notable abiotic resource depletion (89% contribution) and ecotoxicity (67% contribution) during production arising from copper was observed. Interestingly, 10%–30% of production related environmental impacts could be avoided considering a recycling scenario. Although a complete sustainability-driven comparison with mature battery technologies is somehow difficult given the different technology readiness levels, Wang et al. compared the *cradle-to-grave* environmental impacts of a 63.5 kWh Li–O<sub>2</sub> battery (Li anode, CNT/MoS<sub>2</sub> cathode, LiClO<sub>4</sub> in TEGDME electrolyte) with a NMC-type LIB [200]. The negative electrode (Li foil) takes the largest share in most of the categories, largely attributed to the copper current collector used. On the contrary, thanks to its high porosity and lightness, the cathode contributes by less than 7% in most of the categories. Overall, with 149 g·CO<sub>2</sub>-equiv·km<sup>-1</sup>, the Li–O<sub>2</sub> battery system showed a 9.5% reduction in life cycle climate change due to the avoidance of manganese, nickel, and cobalt in the cathode. An additional environmental benefit when implemented into an electric vehicle may arise from the weight of Li–O<sub>2</sub> batteries, where decreases from 531 to 267 kg have been estimated by replacing a NMC (nickel, manganese, and cobalt) LIB [200]. Such weight saving can provide direct environmental benefits when implemented into an electric vehicle independently of the electricity grid type [201]. However, four orders of magnitude larger impacts for terrestrial ecotoxicity potential and 8 times larger for ozone depletion potential are achieved, highlighting the need for a holistic design of the battery.

Finally, Iturrondobeitia et al. analysed the *cradle-to-gate* impacts of 7 laboratory-scale aprotic Li–O<sub>2</sub> battery cathode chemistries having 60 kWh [198]. As shown in Fig. 16b, the impacts largely vary

depending on the battery type due to the variety of materials including nickel, MnO<sub>2</sub>, ruthenium, graphene, cobalt, MOFs, carbon nanotubes, Co<sub>3</sub>O<sub>4</sub>, Ag or AuNi. On average, the cathode is the major contributor to the GWP with a relative weight of 44.5%, matching the conclusions drawn by Santos et al. [196]. Li–O<sub>2</sub> batteries present an average value of 55.8 kg·CO<sub>2</sub>·equiv per 1 kWh, which remains below the 146.4 kg·CO<sub>2</sub>·equiv for NIBs, 146.4 kg·CO<sub>2</sub>·equiv for NIBs, the 58.4 kg·CO<sub>2</sub>·equiv for LIBs, or the 130.6 kg·CO<sub>2</sub>·equiv for Li–S (having a similar energy density). The impacts related to toxicological risks can be also reduced thanks to the simplicity/efficiency of the cathode fabrication, the use of abundant and safe materials, and limited amounts of electrolyte. Overall, reported LCA studies highlight the potential of MABs as a promising choice to fabricate sustainable energy storage systems, particularly given the low technical maturity.

It is important to bear in mind that battery performance (delivered energy) and lifetime are important variables determining the full sustainability. Environmentally sustainable MABs should be designed to avoid the phenomena resulting in early failure of the cell, such as those including dendrite formation, current collector corrosion, component volumetric changes, anode detachment from the current collector, and loss of electrode's electronic conductivity or electrolyte contamination or decomposition. This would avoid the extraction of new resources required for a new battery, would limit the CO<sub>2</sub> emission originating from battery manufacturing and would delay the entering of the batteries in the waste stream.

## 5. Summary and outlook

MABs are considered as one of the most significant contenders within the next-generation electrochemical energy storage systems. Given its particular relevance, till the date many efforts have been directed to the development of new cathode materials and designs (oxygen electrocatalysts). However, MABs should be studied from a holistic point of view, paying attention to the other battery components. In this sense, the application of polymers to develop electrolytes for MABs can certainly help to face the inherent drawbacks associated with the formation of undesired by-products [7], the ORR/OER overpotential, the reversibility of the metal electrode or the low round-trip efficiency. Microporous polyolefin membranes such as Celgard 2325 or 2500 revolutionised the commercial liquid electrolyte based LIBs thanks to their ease of fabrication, low cost, scalability and shutdown property [25]. However, the performance of these materials when implemented into MABs is far from practicability. In any case, it should be considered that given the versatility of polymers to obtain tailored chain structures, functional groups and physico-mechanical properties, these materials hold a bright future to improve the state-of-the-art energy storage systems both at fundamental and applied science level.

Gel–polymer electrolytes and solid–polymer electrolytes show relatively poor ionic conductivities in a similar way to their analogues applied in conventional LIBs or NIBs. In this sense, gel-polymer electrolytes bearing aqueous electrolytes should be explored in the near future given their potential to reach ionic conductivities up to few mS·cm<sup>-1</sup> at room temperature upon proper design, although poor transference number values may still be found. IL electrolytes provide wide electrochemical stability windows and offer an environmentally benign alternative to conventional carbonate-based electrolytes. However, obtained ionic conductivities cannot compete with the values obtained with conventional carbonate or water-based electrolytes. Solid polymer electrolytes have the benefit of providing enhanced mechanical properties while preventing undesired liquid electrolyte leakage.

Additionally, naturally-derived polymers such as cellulose hold a bright future for MAB electrolytes with enhanced electrochemical performance given their potential to dissolve salts, rich variety of functional groups including –NH<sub>2</sub>, –OH, –CONH<sup>-</sup>, –CONH<sub>2</sub>, and –SO<sub>3</sub>H, and ability to develop gel-like porous structures [79]. In addition, their inherent biodegradability, lack of toxicity and biocompatibility offer additional advantages that could not be ignored.

As the research on MABs is still in its infancy, their environmental sustainability and end-of-life scenarios have been largely neglected. In addition, certain funding agencies encourage the implementation circular economy and environmental impact metrics in project proposals. Accordingly, further works are needed to unequivocally quantify the environmental impacts during MAB production and use-phase. Methodologies such as life cycle assessment offer the means to do so by focusing on the whole life cycle [199]. The techno-economic assessment of MABs may offer interesting information to address the economic feasibility of new batteries, especially considering the capital-intensive materials and manufacturing equipment required sometimes [196]. In addition, the degradation of the materials building up the batteries, and their potential recycling should be considered in the coming years. This would not only lower the environmental footprint of batteries but also would help securing the access to critical raw materials, grating the establishment of more resilient supply chains for batteries materials. The conservation of natural resources and solving battery end-of-life issues are now being intensively studied in the LIB field due to the large amount of spent batteries being generated. Therefore, further research is needed in these neglected aspects in the development of MABs [202].

## CRedit authorship contribution statement

**Manuel Salado:** Conceptualization; Data curation; Formal analysis; Investigation; Project administration; Validation; Visualization; Writing - original draft; Writing - review & editing. **Erlantz Lizundia:** Conceptualization; Data curation; Formal analysis; Investigation; Project administration; Validation; Visualization; Writing - original draft; Writing - review & editing.

## Declaration of competing interest

The authors declare that they have no known competing financial interests or personal relationships that could have appeared to influence the work reported in this paper.

## References

- [1] J. Deng, C. Bae, A. Denlinger, T. Miller, Electric vehicles batteries: requirements and challenges, *Joule* 4 (2020) 511–515, <https://doi.org/10.1016/j.joule.2020.01.013>.
- [2] J. Wen, Y. Yu, C. Chen, A review on lithium-ion batteries safety issues: existing problems and possible solutions, *Mater. Express* 2 (2012) 197–212, <https://doi.org/10.1166/mex.2012.1075>.
- [3] S. Ferrari, M. Falco, A.B. Muñoz-García, M. Bonomo, S. Brutti, M. Pavone, C. Gerbaldi, Solid-state post Li metal ion batteries: a sustainable forthcoming reality? *Adv. Energy Mater.* 11 (2021), 2100785 <https://doi.org/10.1002/aenm.202100785>.
- [4] M. Garside, Global Projection of Total Lithium Demand 2016–2030, Available at: <https://www.Statista.Com/Statistics/452025/Projected-Total-Demand-for-Lithium-Globally/>. (accessed on May 2022).
- [5] I. Ore, I.O. Pigments, P. Rock, Q. Crystal, R. Earths, S. Ash, Mineral Commodity Summaries 2020, Available at: <https://pubs.usgs.gov/periodicals/mcs2020/mcs2020.pdf> (accessed on May 2022).
- [6] Y. Li, J. Lu, Metal-air batteries: future electrochemical energy storage of choice? *ACS Energy Lett.* 2 (2017) 1370–1377.
- [7] H.F. Wang, Q. Xu, Materials design for rechargeable metal-air batteries, *Matter* 1 (2019) 565–595, <https://doi.org/10.1016/j.matt.2019.05.008>.
- [8] F. Sun, R. Gao, D. Zhou, M. Osenberg, K. Dong, N. Kardjilov, A. Hilger, H. Markötter, P.M. Bieker, X. Liu, I. Manke, Revealing hidden facts of Li anode

- in cycled lithium–oxygen batteries through X-ray and neutron tomography, *ACS Energy Lett.* 4 (2019) 306–316, <https://doi.org/10.1021/acsenenergylett.8b02242>.
- [9] D.D. Macdonald, K.H. Lee, A. Moccari, D. Harrington, Evaluation of alloy anodes for aluminum–air batteries: corrosion studies, *Corrosion* 44 (1988) 652–657.
- [10] Y.N. Jo, K. Prasanna, S.H. Kang, P.R. Ilango, H.S. Kim, S.W. Eom, C.W. Lee, The effects of mechanical alloying on the self-discharge and corrosion behavior in Zn–air batteries, *J. Ind. Eng. Chem.* 53 (2017) 247–252.
- [11] Y. He, W. Shang, M. Ni, Y. Huang, H. Zhao, P. Tan, In-situ observation of the gas evolution process on the air electrode of Zn–air batteries during charging, *Chem. Eng. J.* 427 (2022), 130862.
- [12] J. Balamurugan, T.T. Nguyen, N.H. Kim, D.H. Kim, J.H. Lee, Novel core-shell CuMo–oxynitride@N-doped graphene nanohybrid as multifunctional catalysts for rechargeable zinc–air batteries and water splitting, *Nano Energy* 85 (2021), 105987, <https://doi.org/10.1016/j.nanoen.2021.105987>.
- [13] X. Zheng, X. Cao, K. Zeng, J. Yan, Z. Sun, M.H. Rummeli, R. Yang, A self-jet vapor-phase growth of 3D FeNi@NCNT clusters as efficient oxygen electrocatalysts for zinc–air batteries, *Small* 17 (2021), 2006183, <https://doi.org/10.1002/smll.202006183>.
- [14] Q. Liu, Z. Pan, E. Wang, L. An, G. Sun, Aqueous metal–air batteries: fundamentals and applications, *Energy Storage Mater.* 27 (2020) 478–505, <https://doi.org/10.1016/j.ensm.2019.12.011>.
- [15] H. Wang, Z. Yu, X. Kong, W. Huang, Z. Zhang, D.G. Mackanic, X. Huang, J. Qin, Z. Bao, Y. Cui, Dual-solvent Li-ion solvation enables high-performance Li-metal batteries, *Adv. Mater.* 33 (2021), 2008619, <https://doi.org/10.1002/adma.202008619>.
- [16] Y. Zhou, J. Pan, X. Ou, Q. Liu, Y. Hu, W. Li, R. Wu, J. Wen, F. Yan, CO<sub>2</sub> ionized poly(vinyl alcohol) electrolyte for CO<sub>2</sub>-tolerant Zn–air batteries, *Adv. Energy Mater.* 11 (2021), 2102047, <https://doi.org/10.1002/aenm.202102047>.
- [17] F. Duffner, N. Kronmeyer, J. Tübke, J. Leker, M. Winter, R. Schmich, Post-lithium-ion battery cell production and its compatibility with lithium-ion cell production infrastructure, *Nat. Energy* 6 (2021) 123–134.
- [18] D. Monti, A. Ponrouch, R.B. Araujo, F. Barde, P. Johansson, M.R. Palacián, Multivalent batteries—prospects for high energy density: Ca batteries, *Front. Chem.* 7 (2019) 79, <https://doi.org/10.3389/fchem.2019.00079>.
- [19] T. Kim, W. Song, D.-Y. Son, L.K. Ono, Y. Qi, Lithium-ion batteries: outlook on present, future, and hybridized technologies, *J. Mater. Chem. A* 7 (2019) 2942–2964, <https://doi.org/10.1039/C8TA10513H>.
- [20] S. Clark, A. Latz, B. Horstmann, A review of model-based design tools for metal–air batteries, *Batteries* 4 (2018) 5.
- [21] G. Houchins, V. Pande, V. Viswanathan, Mechanism for singlet oxygen production in Li-ion and metal–air batteries, *ACS Energy Lett.* 5 (2020) 1893–1899.
- [22] Y. Li, J. Lu, Metal–air batteries: will they be the future electrochemical energy storage device of choice? *ACS Energy Lett.* 2 (2017) 1370–1377, <https://doi.org/10.1021/acsenenergylett.7b00119>.
- [23] Y. Son, N. Kim, T. Lee, Y. Lee, J. Ma, S. Chae, J. Sung, H. Cha, Y. Yoo, J. Cho, Calendering-compatible macroporous architecture for silicon–graphite composite toward high-energy lithium-ion batteries, *Adv. Mater.* 32 (2020), 2003286.
- [24] T. Leisegang, F. Meutzner, M. Zschornak, W. Münchgesang, R. Schmid, T. Nestler, R.A. Eremin, A.A. Kabanov, V.A. Blatov, D.C. Meyer, The aluminum-ion battery: a sustainable and seminal concept? *Front. Chem.* 7 (2019) 268, <https://doi.org/10.3389/fchem.2019.00268>.
- [25] P. Arora, Z. Zhang, Battery separators, *Chem. Rev.* 104 (2004) 4419–4462, <https://doi.org/10.1021/cr020738u>.
- [26] C. Hänsel, E. Lizundia, D. Kundu, A single Li-ion conductor based on cellulose, *ACS Appl. Energy Mater.* 2 (2019) 5686–5691, <https://doi.org/10.1021/acsaem.9b00821>.
- [27] X. Casas, M. Niederberger, E. Lizundia, A sodium ion battery separator with reversible voltage response based on water-soluble cellulose derivatives, *ACS Appl. Mater. Interfaces* 12 (2020) 29264–29274, <https://doi.org/10.1021/acsaami.0c05262>.
- [28] A. Avoundjian, V. Galvan, F.A. Gomez, An inexpensive paper-based aluminum–air battery, *Micromachines* 8 (2017), <https://doi.org/10.3390/mi8070222>.
- [29] X.-B. Cheng, R. Zhang, C.-Z. Zhao, Q. Zhang, Toward safe lithium metal anode in rechargeable batteries: a review, *Chem. Rev.* 117 (2017) 10403–10473, <https://doi.org/10.1021/acs.chemrev.7b00115>.
- [30] S.H. Lee, J.-B. Park, H.-S. Lim, Y.-K. Sun, An advanced separator for Li–O<sub>2</sub> batteries: maximizing the effect of redox mediators, *Adv. Energy Mater.* 7 (2017), 1602417, <https://doi.org/10.1002/aenm.201602417>.
- [31] Y. Hu, X. Zhu, L. Wang, Two-dimensional material-functionalized separators for high-energy-density metal–sulfur and metal-based batteries, *ChemSusChem* 13 (2020) 1366–1378, <https://doi.org/10.1002/cssc.201902758>.
- [32] W.-K. Shin, A.G. Kannan, D.-W. Kim, Effective suppression of dendritic lithium growth using an ultrathin coating of nitrogen and sulfur codoped graphene nanosheets on polymer separator for lithium metal batteries, *ACS Appl. Mater. Interfaces* 7 (2015) 23700–23707, <https://doi.org/10.1021/acsaami.5b07730>.
- [33] J. Jindra, J. Mrha, M. Musilová, Zinc–air cell with neutral electrolyte, *J. Appl. Electrochem.* 3 (1973) 297–301, <https://doi.org/10.1007/BF00613036>.
- [34] F.W. Thomas Goh, Z. Liu, T.S.A. Hor, J. Zhang, X. Ge, Y. Zong, A. Yu, W. Khoo, A near-neutral chloride electrolyte for electrically rechargeable zinc–air batteries, *J. Electrochem. Soc.* 161 (2014) A2080–A2086, <https://doi.org/10.1149/2.0311414jes>.
- [35] A. Sumboja, X. Ge, G. Zheng, F.W.T. Goh, T.S.A. Hor, Y. Zong, Z. Liu, Durable rechargeable zinc–air batteries with neutral electrolyte and manganese oxide catalyst, *J. Power Sources* 332 (2016) 330–336, <https://doi.org/10.1016/j.jpowsour.2016.09.142>.
- [36] A. Kube, N. Wagner, K.A. Friedrich, Influence of organic additives for zinc–air batteries on cathode stability and performance, *J. Electrochem. Soc.* 168 (2021), 050531, <https://doi.org/10.1149/1945-7111/abff63>.
- [37] S. Clark, A.R. Mainar, E. Iruin, L.C. Colmenares, J.A. Blázquez, J.R. Tolchard, Z. Jusys, B. Horstmann, Designing aqueous organic electrolytes for zinc–air batteries: method, simulation, and validation, *Adv. Energy Mater.* 10 (2020), 1903470, <https://doi.org/10.1002/aenm.201903470>.
- [38] C.-X. Zhao, J.-N. Liu, J. Wang, D. Ren, B.-Q. Li, Q. Zhang, Recent advances of noble-metal-free bifunctional oxygen reduction and evolution electrocatalysts, *Chem. Soc. Rev.* 50 (2021) 7745–7778.
- [39] C. Lv, Y. Zhu, W. Zhang, W. Xu, J. Ren, H. Liu, X. Yang, R. Cai, S. Jin, D. Li, D. Yang, Interfacial enhancement of O\* protonation for Fe<sub>2</sub>N/Fe<sub>3</sub>C nanoparticles to boost oxygen reduction reaction and the fuel cell in acidic electrolyte, *Mater. Today Energy* 21 (2021), 100834, <https://doi.org/10.1016/j.mtener.2021.100834>.
- [40] Y. Wu, S. Nagata, Y. Nabee, Genuine four-electron oxygen reduction over precious-metal-free catalyst in alkaline media, *Electrochim. Acta* 319 (2019) 382–389, <https://doi.org/10.1016/j.electacta.2019.06.174>.
- [41] S.S. Shinde, C.H. Lee, J.-Y. Jung, N.K. Wagh, S.-H. Kim, D.-H. Kim, C. Lin, S.U. Lee, J.-H. Lee, Unveiling dual-linkage 3D hexaiminobenzene metal–organic frameworks towards long-lasting advanced reversible Zn–air batteries, *Energy Environ. Sci.* 12 (2019) 727–738, <https://doi.org/10.1039/C8EE02679C>.
- [42] A. Kundu, A. Samanta, C.R. Raj, Hierarchical hollow MOF-derived bamboo-like N-doped carbon nanotube-encapsulated Co<sub>0.25</sub>Ni<sub>0.75</sub> alloy: an efficient bifunctional oxygen electrocatalyst for zinc–air battery, *ACS Appl. Mater. Interfaces* 13 (2021) 30486–30496, <https://doi.org/10.1021/acsaami.1c01875>.
- [43] J. Xu, Y. Xu, C. Lai, T. Xia, B. Zhang, X. Zhou, Challenges and perspectives of covalent organic frameworks for advanced alkali-metal ion batteries, *Sci. China Chem.* 64 (2021) 1267–1282.
- [44] Y. Zhang, R.-L. Zhong, M. Lu, J.-H. Wang, C. Jiang, G.-K. Gao, L.-Z. Dong, Y. Chen, S.-L. Li, Y.-Q. Lan, Single metal site and versatile transfer channel merged into covalent organic frameworks facilitate high-performance Li–CO<sub>2</sub> batteries, *ACS Cent. Sci.* 7 (2021) 175–182, <https://doi.org/10.1021/acscentsci.0c1390>.
- [45] J. Cao, H. Gong, L. Xie, Y. Li, N. Zhang, W. Tian, R. Zhang, J. Zhou, T. Wang, Y. Zhai, N. Li, M. Luo, K. Liang, P. Chen, B. Kong, Super-assembled carbon nanofibers decorated with dual catalytically active sites as bifunctional oxygen catalysts for rechargeable Zn–air batteries, *Mater. Today Energy* 20 (2021), 100682, <https://doi.org/10.1016/j.mtener.2021.100682>.
- [46] A.R. Mainar, E. Iruin, L.C. Colmenares, A. Kvasha, I. de Metzta, M. Bengochea, O. Leonet, I. Boyano, Z. Zhang, J.A. Blázquez, An overview of progress in electrolytes for secondary zinc–air batteries and other storage systems based on zinc, *J. Energy Storage* 15 (2018) 304–328, <https://doi.org/10.1016/j.est.2017.12.004>.
- [47] C.-S. Yang, K.-N. Gao, X.-P. Zhang, Z. Sun, T. Zhang, Rechargeable solid-state Li–air batteries: a status report, *Rare Met.* 37 (2018) 459–472.
- [48] J. Zhang, Q. Zhou, Y. Tang, L. Zhang, Y. Li, Zinc–air batteries: are they ready for prime time? *Chem. Sci.* 10 (2019) 8924–8929, <https://doi.org/10.1039/C9SC04221K>.
- [49] S.P. Penteado, R.F. Bento, Performance analysis of ten brands of batteries for hearing aids, *Int. Arch. Otorhinolaryngol.* 17 (2013) 291–304.
- [50] Z. Liu, S.Z. El Abedin, F. Endres, Electrodeposition of zinc films from ionic liquids and ionic liquid/water mixtures, *Electrochim. Acta* 89 (2013) 635–643, <https://doi.org/10.1016/j.electacta.2012.11.077>.
- [51] F. Ilyas, M. Ishaq, M. Jabeeb, M. Saeed, A. Ihsan, M. Ahmed, Recent trends in the benign-by-design electrolytes for zinc batteries, *J. Mol. Liq.* 343 (2021), 117606, <https://doi.org/10.1016/j.molliq.2021.117606>.
- [52] C. Wang, J. Li, Z. Zhou, Y. Pan, Z. Yu, Z. Pei, S. Zhao, L. Wei, Y. Chen, Rechargeable zinc–air batteries with neutral electrolytes: recent advances, challenges, and prospects, *EnergyChem* 3 (2021), 100055, <https://doi.org/10.1016/j.enchem.2021.100055>.
- [53] X. Zhao, X. Liang, Y. Li, Q. Chen, M. Chen, Challenges and design strategies for high performance aqueous zinc ion batteries, *Energy Storage Mater.* 42 (2021) 533–569, <https://doi.org/10.1016/j.ensm.2021.07.044>.
- [54] R. Buckingham, T. Asset, P. Atanassov, Aluminum–air batteries: a review of alloys, electrolytes and design, *J. Power Sources* 498 (2021), 229762, <https://doi.org/10.1016/j.jpowsour.2021.229762>.
- [55] R.D. McKerracher, C. Ponce de Leon, R.G.A. Wills, A.A. Shah, F.C. Walsh, A review of the iron–air secondary battery for energy storage, *Chempluschem* 80 (2015) 323–335, <https://doi.org/10.1002/cplu.201402238>.
- [56] W.K. Tan, G. Kawamura, H. Muto, A. Matsuda, Chapter 3 - Current Progress in the Development of Fe–Air Batteries and their Prospects for Next-Generation Batteries, Elsevier, 2021, pp. 59–83, <https://doi.org/10.1016/B978-0-12-820628-7.00003-4>.
- [57] L. Li, H. Chen, E. He, L. Wang, T. Ye, J. Lu, Y. Jiao, J. Wang, R. Gao, H. Peng, Y. Zhang, High-energy-density magnesium–air battery based on dual-layer gel electrolyte, *Angew. Chem. Int. Ed.* 60 (2021) 15317–15322, <https://doi.org/10.1002/anie.202104536>.



- [58] T. Zhang, Z. Tao, J. Chen, Magnesium–air batteries: from principle to application, *Mater. Horiz.* 1 (2014) 196–206, <https://doi.org/10.1039/C3MH00059A>.
- [59] J.-S. Lee, S. Tai Kim, R. Cao, N.-S. Choi, M. Liu, K.T. Lee, J. Cho, Metal–air batteries with high energy density: Li–air versus Zn–air, *Adv. Energy Mater.* 1 (2011) 34–50, <https://doi.org/10.1002/aenm.201000010>.
- [60] L. Liu, H. Guo, L. Fu, S. Chou, S. Thiele, Y. Wu, J. Wang, Critical advances in ambient air operation of nonaqueous rechargeable Li–air batteries, *Small* 17 (2021), 1903854, <https://doi.org/10.1002/sml.201903854>.
- [61] K. Chen, G. Huang, X.-B. Zhang, Efforts towards practical and sustainable Li/Na-air batteries, *Chin. J. Chem.* 39 (2021) 32–42, <https://doi.org/10.1002/cjoc.202000408>.
- [62] X. Bi, R. Wang, Y. Yuan, D. Zhang, T. Zhang, L. Ma, T. Wu, R. Shahbazian-Yassar, K. Amine, J. Lu, From sodium–oxygen to sodium–air battery: enabled by sodium peroxide dihydrate, *Nano Lett.* 20 (2020) 4681–4686, <https://doi.org/10.1021/acs.nanolett.0c01670>.
- [63] W. Wang, Y.-C. Lu, The potassium–air battery: far from a practical reality? *Accounts Mater. Res.* 2 (2021) 515–525, <https://doi.org/10.1021/accounts.mr.1c00061>.
- [64] Y.-T. Lu, A.R. Neale, C.-C. Hu, L.J. Hardwick, Divalent nonaqueous metal–air batteries, *Front. Energy Res.* 8 (2021) 357, <https://doi.org/10.3389/fenrg.2020.602918>.
- [65] P. Chen, K. Zhang, D. Tang, W. Liu, F. Meng, Q. Huang, J. Liu, Recent progress in electrolytes for Zn–air batteries, *Front. Chem.* 8 (2020) 372, <https://doi.org/10.3389/fchem.2020.00372>.
- [66] M. He, P. Zhang, L. Liu, B. Liu, S. Xu, Hierarchical porous nitrogen doped three-dimensional graphene as a free-standing cathode for rechargeable lithium–oxygen batteries, *Electrochim. Acta* 191 (2016) 90–97, <https://doi.org/10.1016/j.electacta.2016.01.026>.
- [67] T. Ogasawara, A. Débart, M. Holzapfel, P. Novák, P.G. Bruce, Rechargeable Li<sub>2</sub>O<sub>2</sub> electrode for lithium batteries, *J. Am. Chem. Soc.* 128 (2006) 1390–1393, <https://doi.org/10.1021/ja056811q>.
- [68] H.-W. Kim, J.-M. Lim, H.-J. Lee, S.-W. Eom, Y.T. Hong, S.-Y. Lee, Artificially engineered, bicontinuous anion-conducting/-repelling polymeric phases as a selective ion transport channel for rechargeable zinc–air battery separator membranes, *J. Mater. Chem. A* 4 (2016) 3711–3720, <https://doi.org/10.1039/C5TA09576J>.
- [69] K.M. Abraham, Z. Jiang, A polymer electrolyte-based rechargeable lithium/oxygen battery, *J. Electrochem. Soc.* 143 (1996) 1–5, <https://doi.org/10.1149/1.1836378>.
- [70] T. Kawamura, S. Okada, J. Yamaki, Decomposition reaction of LiPF<sub>6</sub>-based electrolytes for lithium ion cells, *J. Power Sources* 156 (2006) 547–554, <https://doi.org/10.1016/j.jpowsour.2005.05.084>.
- [71] C.V. Amanchukwu, J.R. Harding, Y. Shao-Horn, P.T. Hammond, Understanding the chemical stability of polymers for lithium–air batteries, *Chem. Mater.* 27 (2015) 550–561, <https://doi.org/10.1021/cm5040003>.
- [72] B.G. Kim, J.-S. Kim, J. Min, Y.-H. Lee, J.H. Choi, M.C. Jang, S.A. Freunberger, J.W. Choi, A moisture- and oxygen-impermeable separator for aprotic Li–O<sub>2</sub> batteries, *Adv. Funct. Mater.* 26 (2016) 1747–1756, <https://doi.org/10.1002/adfm.201504437>.
- [73] W.C. Tan, L.H. Saw, M.C. Yew, D. Sun, Z. Cai, W.T. Chong, P.-Y. Kuo, Analysis of the polypropylene-based aluminum–air battery, *Front. Energy Res.* 9 (2021) 32, <https://doi.org/10.3389/fenrg.2021.599846>.
- [74] G.M. Wu, S.J. Lin, J.H. You, C.C. Yang, Study of high-anionic conducting sulfonated microporous membranes for zinc–air electrochemical cells, *Mater. Chem. Phys.* 112 (2008) 798–804, <https://doi.org/10.1016/j.matchemphys.2008.06.058>.
- [75] H.J. Hwang, W.S. Chi, O. Kwon, J.G. Lee, J.H. Kim, Y.-G. Shul, Selective ion transporting polymerized ionic liquid membrane separator for enhancing cycle stability and durability in secondary zinc–air battery systems, *ACS Appl. Mater. Interfaces* 8 (2016) 26298–26308, <https://doi.org/10.1021/acsami.6b07841>.
- [76] L.-L. Shen, G.-R. Zhang, M. Biesalski, B.J.M. Etzold, Paper-based microfluidic aluminum–air batteries: toward next-generation miniaturized power supply, *Lab Chip* 19 (2019) 3438–3447, <https://doi.org/10.1039/C9LC00574A>.
- [77] E. Lizundia, C.M. Costa, R. Alves, S. Lanceros-Méndez, Cellulose and its derivatives for lithium ion battery separators: a review on the processing methods and properties, *Carbohydr. Polym. Technol. Appl.* 1 (2020), 100001, <https://doi.org/10.1016/j.carpta.2020.100001>.
- [78] P. Katsoufis, M. Katsaiti, C. Mourelas, T.S. Andrade, V. Dracopoulos, C. Politis, G. Avgouropoulos, P. Lianos, Study of a thin film aluminum–air battery, *Energies* 13 (2020), <https://doi.org/10.3390/en13061447>.
- [79] E. Lizundia, D. Kundu, Advances in natural biopolymer-based electrolytes and separators for battery applications, *Adv. Funct. Mater.* 31 (2021), 2005646, <https://doi.org/10.1002/adfm.202005646>.
- [80] W. Xie, W. Liu, Y. Dang, A. Tang, T. Deng, W. Qiu, Investigation on electrolyte-immersed properties of lithium-ion battery cellulose separator through multi-scale method, *J. Power Sources* 417 (2019) 150–158, <https://doi.org/10.1016/j.jpowsour.2019.02.002>.
- [81] D.E. Turney, J.W. Gallaway, G.G. Yadav, R. Ramirez, M. Nyce, S. Banerjee, Y.K. Chen-Wiegart, J. Wang, M.J. D’Ambrose, S. Kolhekar, J. Huang, X. Wei, Rechargeable zinc alkaline anodes for long-cycle energy storage, *Chem. Mater.* 29 (2017) 4819–4832, <https://doi.org/10.1021/acs.chemmater.7b00754>.
- [82] J. Liu, D. Wang, D. Zhang, L. Gao, T. Lin, Synergistic effects of carboxymethyl cellulose and ZnO as alkaline electrolyte additives for aluminum anodes with a view towards Al–air batteries, *J. Power Sources* 335 (2016) 1–11, <https://doi.org/10.1016/j.jpowsour.2016.09.060>.
- [83] Y. Qiao, Y. He, S. Wu, K. Jiang, X. Li, S. Guo, P. He, H. Zhou, MOF-based separator in an Li–O<sub>2</sub> battery: an effective strategy to restrain the shuttling of dual redox mediators, *ACS Energy Lett.* 3 (2018) 463–468, <https://doi.org/10.1021/acsenerylett.8b00014>.
- [84] N. Togasaki, R. Shibamura, T. Naruse, T. Momma, T. Osaka, Prevention of redox shuttle using electropolymerized polypyrrole film in a lithium–oxygen battery, *APL Mater.* 6 (2018), 47704, <https://doi.org/10.1063/1.5011135>.
- [85] L. Puech, C. Cantau, P. Vinatier, G. Toussaint, P. Stevens, Elaboration and characterization of a free standing LiSiCON membrane for aqueous lithium–air battery, *J. Power Sources* 214 (2012) 330–336, <https://doi.org/10.1016/j.jpowsour.2012.04.064>.
- [86] S.H. Park, T.H. Lee, Y.J. Lee, H.B. Park, Y.J. Lee, Graphene oxide sieving membrane for improved cycle life in high-efficiency redox-mediated Li–O<sub>2</sub> batteries, *Small* 14 (2018), 1801456, <https://doi.org/10.1002/sml.201801456>.
- [87] H. Saputra, R. Othman, A.G.E. Sutjipto, R. Muhida, MCM-41 as a new separator material for electrochemical cell: application in zinc–air system, *J. Membr. Sci.* 367 (2011) 152–157, <https://doi.org/10.1016/j.memsci.2010.10.061>.
- [88] Jody Klaassen, *Lithium/Air Batteries with LiPON as Separator and Protective Barrier and Method*, US20050095506A1, 2005.
- [89] S. Huang, P. Pei, Z. Wang, Anode corrosion of Zn–air fuel cell: mechanism and protection, *J. Electrochem. Soc.* 167 (2020), 90538.
- [90] L. Yang, Y. Wu, S. Chen, Y. Xiao, S. Chen, P. Zheng, J. Wang, J.-E. Qu, A promising hybrid additive for enhancing the performance of alkaline aluminum–air batteries, *Mater. Chem. Phys.* 257 (2021), 123787, <https://doi.org/10.1016/j.matchemphys.2020.123787>.
- [91] S. Hosseini, Z.-Y. Liu, C.-T. Chuan, S.M. Soltani, V.V.K. Lanjapalli, Y.-Y. Li, The role of SO<sub>3</sub>-group-based additives in improving the rechargeable aluminum–air batteries, *Electrochim. Acta* 375 (2021), 137995, <https://doi.org/10.1016/j.electacta.2021.137995>.
- [92] T. Phusittananan, W. Kao-Ian, M.T. Nguyen, T. Yonezawa, R. Pornprasertsuk, A.A. Mohamad, S. Kheawhom, Ethylene glycol/ethanol anolyte for high capacity alkaline aluminum–air battery with dual-electrolyte configuration, *Front. Energy Res.* 8 (2020) 189, <https://doi.org/10.3389/fenrg.2020.00189>.
- [93] D. Snihrova, L. Wang, S.V. Lamaka, C. Wang, M. Deng, B. Vaghefinazari, D. Höche, M.L. Zheludkevich, Synergistic mixture of electrolyte additives: a route to a high-efficiency Mg–air battery, *J. Phys. Chem. Lett.* 11 (2020) 8790–8798, <https://doi.org/10.1021/acs.jpclett.0c02174>.
- [94] R.D. McKerracher, H.A. Figueredo-Rodríguez, K. Dimogiannis, C. Alegre, N.I. Villanueva-Martínez, M.J. Lázaro, V. Baglio, A.S. Aricó, C. Ponce de León, Effect of 1-octanethiol as an electrolyte additive on the performance of the iron–air battery electrodes, *J. Solid State Electrochem.* 25 (2021) 225–230, <https://doi.org/10.1007/s10008-020-04738-4>.
- [95] L. Suo, O. Borodin, T. Gao, M. Olguin, J. Ho, X. Fan, C. Luo, C. Wang, K. Xu, “Water-in-salt” electrolyte enables high-voltage aqueous lithium-ion chemistries, *Science* 350 (2015), <https://doi.org/10.1126/science.aab1595>, 938 LP – 943.
- [96] Y. Zhang, E.J. Maginn, Water-in-salt LiTFSI aqueous electrolytes (2): transport properties and Li<sup>+</sup> dynamics based on molecular dynamics simulations, *J. Phys. Chem. B* (2021), <https://doi.org/10.1021/acs.jpcc.1c07581>.
- [97] L. Chen, J. Zhang, Q. Li, J. Vatamanu, X. Ji, T.P. Pollard, C. Cui, S. Hou, J. Chen, C. Yang, L. Ma, M.S. Ding, M. Garaga, S. Greenbaum, H.-S. Lee, O. Borodin, K. Xu, C. Wang, A 63 m superconcentrated aqueous electrolyte for high-energy Li-ion batteries, *ACS Energy Lett.* 5 (2020) 968–974, <https://doi.org/10.1021/acsenerylett.0c00348>.
- [98] L. Suo, O. Borodin, Y. Wang, X. Rong, W. Sun, X. Fan, S. Xu, M.A. Schroeder, A.V. Cresce, F. Wang, C. Yang, Y.-S. Hu, K. Xu, C. Wang, “Water-in-Salt” electrolyte makes aqueous sodium-ion battery safe, green, and long-lasting, *Adv. Energy Mater.* 7 (2017), 1701189, <https://doi.org/10.1002/aenm.201701189>.
- [99] D. Reber, R. Figi, R.-S. Kühnel, C. Battaglia, Stability of aqueous electrolytes based on LiFSI and NaFSI, *Electrochim. Acta* 321 (2019), 134644, <https://doi.org/10.1016/j.electacta.2019.134644>.
- [100] D. Reber, R. Grissa, M. Becker, R.-S. Kühnel, C. Battaglia, Anion selection criteria for water-in-salt electrolytes, *Adv. Energy Mater.* 11 (2021), 2002913, <https://doi.org/10.1002/aenm.202002913>.
- [101] J. Hwang, A.N. Sivasengaran, H. Yang, H. Yamamoto, T. Takeuchi, K. Matsumoto, R. Hagiwara, Improvement of electrochemical stability using the eutectic composition of a ternary molten salt system for highly concentrated electrolytes for Na-ion batteries, *ACS Appl. Mater. Interfaces* 13 (2021) 2538–2546.
- [102] S. Wu, S. Hu, Q. Zhang, D. Sun, P. Wu, Y. Tang, H. Wang, Hybrid high-concentration electrolyte significantly strengthens the practicability of alkaline aluminum–air battery, *Energy Storage Mater.* 31 (2020) 310–317, <https://doi.org/10.1016/j.ensm.2020.06.024>.
- [103] T. Zhang, R. Amine, X. Bi, Y. Qin, M. Li, S. Al-Hallaj, F. Huo, J. Lu, K. Amine, Exploring the charge reactions in a Li–O<sub>2</sub> system with lithium oxide cathodes and nonaqueous electrolytes, *J. Mater. Chem. A* 7 (2019) 15615–15620, <https://doi.org/10.1039/C9TA03763B>.

- [104] M.K. Kim, Y.J. Lee, N.J. Jo, The effect of HSAB principle on electrochemical properties of polymer-in-salt electrolytes with aliphatic polymer. *Surf. Rev. Lett.* 17 (2010) 63–68, <https://doi.org/10.1142/S0218625X10013825>.
- [105] A. Ikezawa, K. Miyazaki, T. Fukutsuka, T. Abe, Investigations of electrochemically active regions in bifunctional air electrodes using partially immersed platinum electrodes, *J. Electrochem. Soc.* 162 (2015) A1646–A1653, <https://doi.org/10.1149/2.0971508jes>.
- [106] A. Kube, J. Meyer, D. Kopljär, N. Wagner, K.A. Friedrich, A segmented cell measuring technique for current distribution measurements in batteries, exemplified by the operando investigation of a Zn-air battery, *J. Electrochem. Soc.* 168 (2021), 120530, <https://doi.org/10.1149/1945-7111/ac4059>.
- [107] A. Pierini, S. Brutti, E. Bodo, Reactive pathways toward parasitic release of singlet oxygen in metal-air batteries, *Npj Comput. Mater.* 7 (2021) 126, <https://doi.org/10.1038/s41524-021-00597-3>.
- [108] N. Xiao, X. Ren, W.D. McCulloch, G. Gourdin, Y. Wu, Potassium superoxide: a unique alternative for metal-air batteries, *Acc. Chem. Res.* 51 (2018) 2335–2343, <https://doi.org/10.1021/acs.accounts.8b00332>.
- [109] N. Xiao, R.T. Rooney, A.A. Gewirth, Y. Wu, The long-term stability of  $\text{KO}_2$  in  $\text{K-O}_2$  batteries, *Angew. Chem.* 130 (2018) 1241–1245, <https://doi.org/10.1002/ange.201710454>.
- [110] M. Saito, *Electrolytes and General Properties of Glyme-Based Electrolytes for Rechargeable Li-Air Batteries BT - Next Generation Batteries: Realization of High Energy Density Rechargeable Batteries*, iSpringer Singapore, Singapore, 2021, pp. 461–477, [https://doi.org/10.1007/978-981-33-6668-8\\_40](https://doi.org/10.1007/978-981-33-6668-8_40).
- [111] K. Li, V. Subasinghe, C.S. Gupta, R. David, R. Kumar, Effect of anion identity on ion association and dynamics of sodium ions in non-aqueous glyme based electrolytes—OTf vs TFSI, *J. Chem. Phys.* 154 (2021), 184505, <https://doi.org/10.1063/5.0046073>.
- [112] L. Zhang, Z. Liu, G. Wang, J. Feng, Q. Ma, Developing high voltage Zn(TFSI)<sub>2</sub>/Pyr14TFSI/AN hybrid electrolyte for a carbon-based Zn-ion hybrid capacitor, *Nanoscale* 13 (2021) 17068–17076, <https://doi.org/10.1039/D1NR03879F>.
- [113] J. Krummacker, A. Balducci, Al, TFSI)<sub>3</sub> as a conducting salt for high-voltage electrochemical double-layer capacitors, *Chem. Mater.* 30 (2018) 4857–4863, <https://doi.org/10.1021/acs.chemmater.8b02253>.
- [114] L.S. Kremer, T. Danner, S. Hein, A. Hoffmann, B. Prifling, V. Schmidt, A. Latz, M. Wohlfahrt-Mehrens, Influence of the electrolyte salt concentration on the rate capability of ultra-thick NCM 622 electrodes, *Batter. Supercaps.* 3 (2020) 1172–1182, <https://doi.org/10.1002/batt.202000998>.
- [115] C. Geng, D. Buchholz, G.-T. Kim, D.V. Carvalho, H. Zhang, L.G. Chagas, S. Passerini, Influence of salt concentration on the properties of sodium-based electrolytes, *Small Methods* 3 (2019), 1800208, <https://doi.org/10.1002/smt.201800208>.
- [116] Y. Zhang, N. Ortiz-Vitoriano, B. Acebedo, L. O'Dell, D.R. MacFarlane, T. Rojo, M. Forsyth, P.C. Howlett, C. Pozo-Gonzalo, Elucidating the impact of sodium salt concentration on the cathode-electrolyte interface of Na-air batteries, *J. Phys. Chem. C* 122 (2018) 15276–15286, <https://doi.org/10.1021/acs.jpcc.8b02004>.
- [117] A. Zhou, L. Jiang, J. Yue, Y. Tong, Q. Zhang, Z. Lin, B. Liu, C. Wu, L. Suo, Y.-S. Hu, Water-in-Salt electrolyte promotes high-capacity FeFe(CN)<sub>6</sub> cathode for aqueous Al-ion battery, *ACS Appl. Mater. Interfaces* 11 (2019) 41356–41362.
- [118] H. Wang, R. Tan, Z. Yang, Y. Feng, X. Duan, J. Ma, Stabilization perspective on metal anodes for aqueous batteries, *Adv. Energy Mater.* 11 (2021), 2000962, <https://doi.org/10.1002/aenm.202000962>.
- [119] D. Safanama, D. Ji, K.C. Phuah, S. Ramakrishna, S. Adams, Round-trip efficiency enhancement of hybrid Li-air battery enables efficient power generation from low-grade waste heat, *ACS Sustain. Chem. Eng.* 8 (2020) 18500–18505, <https://doi.org/10.1021/acssuschemeng.0c06202>.
- [120] Z. Khan, M. Vagin, C. Crispin, Can hybrid Na-air batteries outperform nonaqueous Na-O<sub>2</sub> batteries? *Adv. Sci.* 7 (2020), 1902866 <https://doi.org/10.1002/advs.201902866>.
- [121] W. Cao, Y. Yang, J. Deng, Y. Li, C. Cui, T. Zhang, Localization of electrons within interlayer stabilizes NASICON-type solid-state electrolyte, *Mater. Today Energy* 22 (2021), 100875, <https://doi.org/10.1016/j.mtener.2021.100875>.
- [122] Y. Kang, F. Su, Q. Zhang, F. Liang, K.R. Adair, K. Chen, D. Xue, K. Hayashi, S.C. Cao, H. Yadegari, X. Sun, Novel high-energy-density rechargeable hybrid sodium-air cell with acidic electrolyte, *ACS Appl. Mater. Interfaces* 10 (2018) 23748–23756, <https://doi.org/10.1021/acsami.8b04278>.
- [123] M.F. Galee, F. Migliardini, T.M. Di Palma, Dual solid electrolytes for aluminum-air batteries based on polyvinyl alcohol acidic membranes and neutral hydrogels, *J. Solid State Electrochem.* 25 (2021) 1207–1216, <https://doi.org/10.1007/s10008-021-04900-6>.
- [124] L. Grande, E. Paillard, J. Hassoun, J.-B. Park, Y.-J. Lee, Y.-K. Sun, S. Passerini, B. Scrosati, The lithium/air battery: still an emerging system or a practical reality? *Adv. Mater.* 27 (2015) 784–800, <https://doi.org/10.1002/adma.201403064>.
- [125] D.E. Fenton, J.M. Parker, P.V. Wright, Complexes of alkali metal ions with poly(ethylene oxide), *Polymer (Guildf.)* 14 (1973) 589, [https://doi.org/10.1016/0032-3861\(73\)90146-8](https://doi.org/10.1016/0032-3861(73)90146-8).
- [126] W.-Q. Ding, F. Lv, N. Xu, M.-T. Wu, J. Liu, X.-P. Gao, Polyethylene oxide-based solid-state composite polymer electrolytes for rechargeable lithium batteries, *ACS Appl. Energy Mater.* 4 (2021) 4581–4601, <https://doi.org/10.1021/acsaem.1c00216>.
- [127] Z. Gadjourova, Y.G. Andreev, D.P. Tunstall, P.G. Bruce, Ionic conductivity in crystalline polymer electrolytes, *Nature* 412 (2001) 520–523, <https://doi.org/10.1038/35087538>.
- [128] L. Leng, X. Zeng, P. Chen, T. Shu, H. Song, Z. Fu, H. Wang, S. Liao, A novel stability-enhanced lithium-oxygen battery with cellulose-based composite polymer gel as the electrolyte, *Electrochim. Acta* 176 (2015) 1108–1115, <https://doi.org/10.1016/j.electacta.2015.07.111>.
- [129] S.-D. Gong, Y. Huang, H.-J. Cao, Y.-H. Lin, Y. Li, S.-H. Tang, M.-S. Wang, X. Li, A green and environment-friendly gel polymer electrolyte with higher performances based on the natural matrix of lignin, *J. Power Sources* 307 (2016) 624–633, <https://doi.org/10.1016/j.jpowsour.2016.01.030>.
- [130] D. Wei, W. Shen, T. Xu, K. Li, L. Yang, Y. Zhou, M. Zhong, F. Yang, X. Xu, Y. Wang, M. Zheng, Y. Zhang, Q. Li, Z. Yong, H. Li, Q. Wang, Ultra-flexible and foldable gel polymer lithium-ion batteries enabling scalable production, *Mater. Today Energy* 23 (2022), 100889, <https://doi.org/10.1016/j.mtener.2021.100889>.
- [131] Y. Zuo, K. Wang, M. Wei, S. Zhao, P. Zhang, P. Pei, Starch gel for flexible rechargeable zinc-air batteries, *Cell Reports Phys. Sci.* 3 (2022), 100687, <https://doi.org/10.1016/j.xcrp.2021.100687>.
- [132] S.A. Freunberger, Y. Chen, Z. Peng, J.M. Griffin, L.J. Hardwick, F. Bardé, P. Novák, P.G. Bruce, Reactions in the rechargeable lithium-O<sub>2</sub> battery with alkyl carbonate electrolytes, *J. Am. Chem. Soc.* 133 (2011) 8040–8047, <https://doi.org/10.1021/ja2021747>.
- [133] J. Hassoun, F. Croce, M. Armand, B. Scrosati, Investigation of the O<sub>2</sub> electrochemistry in a polymer electrolyte solid-state cell, *Angew. Chem. Int. Ed.* 50 (2011) 2999–3002, <https://doi.org/10.1002/anie.201006264>.
- [134] T. Zhou, Y. Zhao, J.W. Choi, A. Coskun, Ionic liquid functionalized gel polymer electrolytes for stable lithium metal batteries, *Angew. Chem. Int. Ed.* 60 (2021), <https://doi.org/10.1002/anie.202106237>.
- [135] K.-N. Jung, J.-I. Lee, J.-H. Jung, K.-H. Shin, J.-W. Lee, A quasi-solid-state rechargeable lithium-oxygen battery based on a gel polymer electrolyte with an ionic liquid, *Chem. Commun.* 50 (2014) 5458–5461, <https://doi.org/10.1039/C4CC01243G>.
- [136] X. Jia, Y. Yang, C. Wang, C. Zhao, R. Vijayaraghavan, D.R. MacFarlane, M. Forsyth, G.G. Wallace, Biocompatible ionic liquid-biopolymer electrolyte-enabled thin and compact magnesium-air batteries, *ACS Appl. Mater. Interfaces* 6 (2014) 21110–21117, <https://doi.org/10.1021/am505985z>.
- [137] N. Mittal, A. Ojaguren, M. Niederberger, E. Lizundia, Degradation behavior, biocompatibility, electrochemical performance and circularity potential of transient batteries, *Adv. Sci.* 8 (2021), 2004814.
- [138] D. Zhang, R. Li, T. Huang, A. Yu, Novel composite polymer electrolyte for lithium air batteries, *J. Power Sources* 195 (2010) 1202–1206, <https://doi.org/10.1016/j.jpowsour.2009.08.063>.
- [139] Y. Xie, H. Zou, H. Xiang, R. Xia, D. Liang, P. Shi, S. Dai, H. Wang, Enhancement of lithium battery separator toward nonaqueous electrolytes, *J. Membr. Sci.* 503 (2016) 25–30, <https://doi.org/10.1016/j.memsci.2015.12.025>.
- [140] R. Gonçalves, E. Lizundia, M.M. Silva, C.M. Costa, S. Lanceros-Méndez, Mesoporous cellulose nanocrystal membranes as battery separators for environmentally safer lithium-ion batteries, *ACS Appl. Energy Mater.* 2 (2019) 3749–3761, <https://doi.org/10.1021/acsaem.9b00458>.
- [141] T.M. Di Palma, F. Migliardini, D. Caputo, P. Corbo, Xanthan and κ-carrageenan based alkaline hydrogels as electrolytes for Al/air batteries, *Carbohydr. Polym.* 157 (2017) 122–127, <https://doi.org/10.1016/j.carbpol.2016.09.076>.
- [142] X. Liu, X. Xin, L. Shen, Z. Gu, J. Wu, X. Yao, Poly(methyl methacrylate)-based gel polymer electrolyte for high-performance solid state Li-O<sub>2</sub> battery with enhanced cycling stability, *ACS Appl. Energy Mater.* 4 (2021) 3975–3982, <https://doi.org/10.1021/acsaem.1c00344>.
- [143] W. Chen, W. Yin, Y. Shen, Z. Huang, X. Li, F. Wang, W. Zhang, Z. Deng, Z. Zhang, Y. Huang, High areal capacity, long cycle life Li-O<sub>2</sub> cathode based on highly elastic gel granules, *Nano Energy* 47 (2018) 353–360, <https://doi.org/10.1016/j.nanoen.2018.03.005>.
- [144] Y. Wang, L. Fu, L. Shi, Z. Wang, J. Zhu, Y. Zhao, S. Yuan, Gel polymer electrolyte with high Li<sup>+</sup> transference number enhancing the cycling stability of lithium anodes, *ACS Appl. Mater. Interfaces* 11 (2019) 5168–5175, <https://doi.org/10.1021/acsami.8b21352>.
- [145] H.T.T. Le, D.T. Ngo, R.S. Kalubarme, G. Cao, C.-N. Park, C.-J. Park, Composite gel polymer electrolyte based on poly(vinylidene fluoride-hexafluoropropylene) (PVDF-HFP) with modified aluminum-doped lithium lanthanum titanate (A-LTTO) for high-performance lithium rechargeable batteries, *ACS Appl. Mater. Interfaces* 8 (2016) 20710–20719, <https://doi.org/10.1021/acsami.6b05301>.
- [146] Z. Zhang, C. Zuo, Z. Liu, Y. Yu, Y. Zuo, Y. Song, All-solid-state Al-air batteries with polymer alkaline gel electrolyte, *J. Power Sources* 251 (2014) 470–475, <https://doi.org/10.1016/j.jpowsour.2013.11.020>.
- [147] X. Fan, J. Liu, Z. Song, X. Han, Y. Deng, C. Zhong, W. Hu, Porous nano-composite gel polymer electrolyte with high ionic conductivity and superior electrolyte retention capability for long-cycle-life flexible zinc-air batteries, *Nano Energy* 56 (2019) 454–462, <https://doi.org/10.1016/j.nanoen.2018.11.057>.
- [148] O. Kwon, H.J. Hwang, Y. Ji, O.S. Jeon, J.P. Kim, C. Lee, Y.G. Shul, Transparent bendable secondary zinc-air batteries by controlled void ionic separators, *Sci. Rep.* 9 (2019) 3175, <https://doi.org/10.1038/s41598-019-38552-4>.
- [149] D. Lee, H.-W. Kim, J.-M. Kim, K.-H. Kim, S.-Y. Lee, Flexible/rechargeable Zn-air batteries based on multifunctional heteronanomaterial architecture, *ACS*

- Appl. Mater. Interfaces 10 (2018) 22210–22217, <https://doi.org/10.1021/acami.8b05215>.
- [150] N. Nguyen, T.N.L. Doan, T.K.A. Hoang, H. Zhao, P. Chen, Effect of fumed silica concentration and separator type on the electrochemical performance of gel electrolyte in the rechargeable hybrid aqueous battery, *Mater. Today Energy* 8 (2018) 73–79, <https://doi.org/10.1016/j.mtener.2018.03.002>.
- [151] L.A. Wehner, N. Mittal, T. Liu, M. Niederberger, Multifunctional batteries: flexible, transient, and transparent, *ACS Cent. Sci.* 7 (2021) 231–244, <https://doi.org/10.1021/acscentsci.0c01318>.
- [152] Y. Xu, Y. Zhao, J. Ren, Y. Zhang, H. Peng, An all-solid-state fiber-shaped aluminum–air battery with flexibility, stretchability, and high electrochemical performance, *Angew. Chem. Int. Ed.* 55 (2016) 7979–7982, <https://doi.org/10.1002/anie.201601804>.
- [153] P. Zhang, Y. Zhao, X. Zhang, Functional and stability orientation synthesis of materials and structures in aprotic Li–O<sub>2</sub> batteries, *Chem. Soc. Rev.* 47 (2018) 2921–3004, <https://doi.org/10.1039/C8CS00009C>.
- [154] H. Ben youcef, O. Garcia-Calvo, N. Lago, S. Devaraj, M. Armand, Cross-linked solid polymer electrolyte for all-solid-state rechargeable lithium batteries, *Electrochim. Acta* 220 (2016) 587–594, <https://doi.org/10.1016/j.electacta.2016.10.122>.
- [155] C. Xin, K. Wen, S. Guan, C. Xue, X. Wu, L. Li, C.-W. Nan, A cross-linked poly(ethylene oxide)-based electrolyte for all-solid-state lithium metal batteries with long cycling stability, *Front. Mater.* 9 (2022), <https://doi.org/10.3389/fmats.2022.864478>.
- [156] M. Balaish, E. Peled, D. Golodnitsky, Y. Ein-Eli, Liquid-free lithium–oxygen batteries, *Angew. Chem. Int. Ed.* 54 (2015) 436–440, <https://doi.org/10.1002/anie.201408008>.
- [157] C.-C. Yang, S.-J. Lin, Preparation of alkaline PVA-based polymer electrolytes for Ni–MH and Zn–air batteries, *J. Appl. Electrochem.* 33 (2003) 777–784, <https://doi.org/10.1023/A:1025514620869>.
- [158] J. Fu, D.U. Lee, F.M. Hassan, L. Yang, Z. Bai, M.G. Park, Z. Chen, Flexible high-energy polymer–electrolyte-based rechargeable zinc–air batteries, *Adv. Mater.* 27 (2015) 5617–5622, <https://doi.org/10.1002/adma.201502853>.
- [159] X. Zhu, H. Yang, Y. Cao, X. Ai, Preparation and electrochemical characterization of the alkaline polymer gel electrolyte polymerized from acrylic acid and KOH solution, *Electrochim. Acta* 49 (2004) 2533–2539, <https://doi.org/10.1016/j.electacta.2004.02.008>.
- [160] L. Ma, S. Chen, Z. Pei, Y. Huang, G. Liang, F. Mo, Q. Yang, J. Su, Y. Gao, J.A. Zapien, C. Zhi, Single-site active iron-based bifunctional oxygen catalyst for a compressible and rechargeable zinc–air battery, *ACS Nano* 12 (2018) 1949–1958, <https://doi.org/10.1021/acsnano.7b09064>.
- [161] D. Zhou, D. Shanmukaraj, A. Tkacheva, M. Armand, G. Wang, Polymer electrolytes for lithium-based batteries: advances and prospects, *Inside Chem.* 5 (2019) 2326–2352, <https://doi.org/10.1016/j.chempr.2019.05.009>.
- [162] J. Fu, J. Zhang, X. Song, H. Zarrin, X. Tian, J. Qiao, L. Rasen, K. Li, Z. Chen, A flexible solid-state electrolyte for wide-scale integration of rechargeable zinc–air batteries, *Energy Environ. Sci.* 9 (2016) 663–670, <https://doi.org/10.1039/C5EE03404C>.
- [163] Y. Wang, W. Pan, H. Kwok, X. Lu, D.Y.C. Leung, Low-cost Al–air batteries with paper-based solid electrolyte, *Energy Proc.* 158 (2019) 522–527, <https://doi.org/10.1016/j.egypro.2019.01.146>.
- [164] N. Zhao, F. Wu, Y. Xing, W. Qu, N. Chen, Y. Shang, M. Yan, Y. Li, L. Li, R. Chen, Flexible hydrogel electrolyte with superior mechanical properties based on poly(vinyl alcohol) and bacterial cellulose for the solid-state zinc–air batteries, *ACS Appl. Mater. Interfaces* 11 (2019) 15537–15542, <https://doi.org/10.1021/acami.9b00758>.
- [165] L. Ma, S. Chen, D. Wang, Q. Yang, F. Mo, G. Liang, N. Li, H. Zhang, J.A. Zapien, C. Zhi, Super-stretchable zinc–air batteries based on an alkaline-tolerant dual-network hydrogel electrolyte, *Adv. Energy Mater.* 9 (2019), 1803046, <https://doi.org/10.1002/aenm.201803046>.
- [166] K.J. Kim, M. Balaish, M. Wadaguchi, L. Kong, J.L.M. Rupp, Solid-state Li–metal batteries: challenges and horizons of oxide and sulfide solid electrolytes and their interfaces, *Adv. Energy Mater.* 11 (2021), 2002689, <https://doi.org/10.1002/aenm.202002689>.
- [167] C.M. Visco SJ, E. Nimon, L.C. De Jonghe, B. Katz, Lithium fuel cells, in: *Proceedings of the 12th International Meeting on Lithium Batteries, Electrochem. Soc., 2004*.
- [168] T. Zhang, N. Imanishi, Y. Shimonishi, A. Hirano, Y. Takeda, O. Yamamoto, N. Sammes, A novel high energy density rechargeable lithium/air battery, *Chem. Commun.* 46 (2010) 1661–1663, <https://doi.org/10.1039/B920012F>.
- [169] W. Xiao, J. Wang, L. Fan, J. Zhang, X. Li, Recent advances in  $\text{Li}_{1-x}\text{Al}_x\text{Ti}_{2-x}(\text{PO}_4)_3$  solid-state electrolyte for safe lithium batteries, *Energy Storage Mater.* 19 (2019) 379–400, <https://doi.org/10.1016/j.ensm.2018.10.012>.
- [170] H. Nemori, X. Shang, H. Minami, S. Mitsuoka, M. Nomura, H. Sonoki, Y. Morita, D. Mori, Y. Takeda, O. Yamamoto, N. Imanishi, Aqueous lithium–air batteries with a lithium-ion conducting solid electrolyte  $\text{Li}_1.3\text{Al}_0.5\text{Nb}_0.2\text{Ti}_{1.3}(\text{PO}_4)_3$ , *Solid State Ionics* 317 (2018) 136–141, <https://doi.org/10.1016/j.ssi.2018.01.020>.
- [171] Y. Wang, H. Zhou, A lithium–air battery with a potential to continuously reduce O<sub>2</sub> from air for delivering energy, *J. Power Sources* 195 (2010) 358–361, <https://doi.org/10.1016/j.jpowsour.2009.06.109>.
- [172] X. C. K.C. Y., N.L. F., A high-energy-density lithium–oxygen battery based on a reversible four-electron conversion to lithium oxide, *Science* 361 (2018) 777–781, <https://doi.org/10.1126/science.aas9343>.
- [173] N. Kamaya, K. Homma, Y. Yamakawa, M. Hirayama, R. Kanno, M. Yonemura, T. Kamiyama, Y. Kato, S. Hama, K. Kawamoto, A. Mitsui, A lithium superionic conductor, *Nat. Mater.* 10 (2011) 682–686, <https://doi.org/10.1038/nmat3066>.
- [174] J. Lu, Y. Li, Perovskite-type Li-ion solid electrolytes: a review, *J. Mater. Sci. Mater. Electron.* 32 (2021) 9736–9754, <https://doi.org/10.1007/s10854-021-05699-8>.
- [175] Y. Inaguma, M. Nakashima, A rechargeable lithium–air battery using a lithium ion–conducting lanthanum lithium titanate ceramics as an electrolyte separator, *J. Power Sources* 228 (2013) 250–255, <https://doi.org/10.1016/j.jpowsour.2012.11.098>.
- [176] A. Kim, S. Woo, M. Kang, H. Park, B. Kang, Research progresses of garnet-type solid electrolytes for developing all-solid-state Li batteries, *Front. Chem.* 8 (2020) 468, <https://doi.org/10.3389/fchem.2020.00468>.
- [177] J. Sun, N. Zhao, Y. Li, X. Guo, X. Feng, X. Liu, Z. Liu, G. Cui, H. Zheng, L. Gu, H. Li, A rechargeable Li–air fuel cell battery based on garnet solid electrolytes, *Sci. Rep.* 7 (2017), 41217, <https://doi.org/10.1038/srep41217>.
- [178] F.K. (Kelvin), G. Yunhui, L. Boyang, Z. Yizhou, X. Shaomao, Y. Yonggang, L. Wei, W. Chengwei, L.S. D. D. Jiaqi, C. Yanan, M. Yifei, W. Eric, H. Liangbing, Toward garnet electrolyte–based Li metal batteries: an ultrathin, highly effective, artificial solid-state electrolyte/metallic Li interface, *Sci. Adv.* 3 (2017), e1601659, <https://doi.org/10.1126/sciadv.1601659>.
- [179] X. Chi, M. Li, J. Di, P. Bai, L. Song, X. Wang, F. Li, S. Liang, J. Xu, J. Yu, A highly stable and flexible zeolite electrolyte solid-state Li–air battery, *Nature* 592 (2021) 551–557, <https://doi.org/10.1038/s41586-021-03410-9>.
- [180] W. Liu, N. Liu, J. Sun, P.-C. Hsu, Y. Li, H.-W. Lee, Y. Cui, Ionic conductivity enhancement of polymer electrolytes with ceramic nanowire fillers, *Nano Lett.* 15 (2015) 2740–2745, <https://doi.org/10.1021/acs.nanolett.5b00600>.
- [181] W. Zhou, S. Wang, Y. Li, S. Xin, A. Manthiram, J.B. Goodenough, Plating a dendrite-free lithium anode with a polymer/ceramic/polymer sandwich electrolyte, *J. Am. Chem. Soc.* 138 (2016) 9385–9388, <https://doi.org/10.1021/jacs.6b05341>.
- [182] L. Cao, F. Lv, Y. Liu, W. Wang, Y. Huo, X. Fu, R. Sun, Z. Lu, A high performance O<sub>2</sub> selective membrane based on CAU-1-NH<sub>2</sub>@polydopamine and the PMMA polymer for Li–air batteries, *Chem. Commun.* 51 (2015) 4364–4367, <https://doi.org/10.1039/C4CC09281C>.
- [183] X. Pan, J. Sun, C. Jin, Z. Wang, R. Xiao, L. Peng, L. Shen, C. Li, R. Yang, A flexible composite electrolyte membrane with ultrahigh LLZTO garnet content for quasi solid state Li–air batteries, *Solid State Ionics* 351 (2020), 115340, <https://doi.org/10.1016/j.ssi.2020.115340>.
- [184] J. Zhang, J. Fu, X. Song, G. Jiang, H. Zarrin, P. Xu, K. Li, A. Yu, Z. Chen, Laminated cross-linked nanocellulose/graphene oxide electrolyte for flexible rechargeable zinc–air batteries, *Adv. Energy Mater.* 6 (2016), 1600476, <https://doi.org/10.1002/aenm.201600476>.
- [185] M.-M. Titirici, Sustainable batteries—quo vadis? *Adv. Energy Mater.* (2021) 2003700, <https://doi.org/10.1002/aenm.202003700>, n/a.
- [186] J. Piątek, S. Afyon, T.M. Budnyak, S. Budnyk, M.H. Sipponen, A. Slabon, Sustainable Li-ion batteries: chemistry and recycling, *Adv. Energy Mater.* (2020) 2003456, <https://doi.org/10.1002/aenm.202003456>, n/a.
- [187] Y. Li, Y. Liu, S. Chen, P. Wang, S. Yuan, X. Li, H. Song, C. Chen, Self-templating synthesis nitrogen and sulfur co-doped hierarchical porous carbons derived from crab shells as a high-performance metal-free oxygen electroreduction catalyst, *Mater. Today Energy* 10 (2018) 388–395, <https://doi.org/10.1016/j.mtener.2018.09.012>.
- [188] The spiralling environmental cost of our lithium battery addiction, n.d. <https://www.wired.co.uk/article/lithium-batteries-environment-impact>.
- [189] G. Harper, R. Sommerville, E. Kendrick, L. Driscoll, P. Slater, R. Stolkin, A. Walton, P. Christensen, O. Heidrick, S. Lambert, A. Abbott, K. Ryder, L. Gaines, P. Anderson, Recycling lithium-ion batteries from electric vehicles, *Nature* 575 (2019) 75–86, <https://doi.org/10.1038/s41586-019-1682-5>.
- [190] P. Nuss, M.J. Eckelman, Life cycle assessment of metals: a scientific synthesis, *PLoS One* 9 (2014), e101298, <https://doi.org/10.1371/journal.pone.0101298>.
- [191] A.R. Dehghani-Sani, E. Tharumalingam, M.B. Dusseault, R. Fraser, Study of energy storage systems and environmental challenges of batteries, *Renew. Sustain. Energy Rev.* 104 (2019) 192–208, <https://doi.org/10.1016/j.rser.2019.01.023>.
- [192] World Economic Forum, A Vision for a Sustainable Battery Value Chain in 2030. Available at: <https://www.weforum.org/reports/a-vision-for-a-sustainable-battery-value-chain-in-2030> (accessed on May 2022).
- [193] T.M. Kousemaker, G.H. Jonker, A.I. Vakis, LCA practices of plastics and their recycling: a critical review, *Appl. Sci.* 11 (2021) 3305, <https://doi.org/10.3390/app11083305>.
- [194] A. Serra, X. Domènech, E. Brillas, J. Peral, Life cycle assessment of solar photo-Fenton and solar photoelectro-Fenton processes used for the degradation of aqueous  $\alpha$ -methylphenylglycine, *J. Environ. Monit.* 13 (2011) 167–174, <https://doi.org/10.1039/c0em00552e>.
- [195] M. Iturrondobetia, O. Akizu-Gardoki, O. Amondarain, R. Minguez, E. Lizundia, Environmental impacts of aqueous zinc ion batteries based on life cycle assessment, *Adv. Sustain. Syst.* 6 (2021) 2100308, <https://doi.org/10.1002/advsu.202100308>.
- [196] F. Santos, A. Urbina, J. Abad, R. López, C. Toledo, A.J. Fernández Romero, Environmental and economical assessment for a sustainable Zn/air battery, *Chemosphere* 250 (2020), 126273, <https://doi.org/10.1016/j.chemosphere.2020.126273>.
- [197] E. Zhao, P.D. Walker, N.C. Surawski, N.S. Bennett, Assessing the life cycle cumulative energy demand and greenhouse gas emissions of lithium-ion

- batteries, *J. Energy Storage* 43 (2021), 103193, <https://doi.org/10.1016/j.est.2021.103193>.
- [198] M. Iturrondobeitia, O. Akizu-Gardoki, R. Minguez, E. Lizundia, Environmental impact analysis of aprotic Li–O<sub>2</sub> batteries based on life cycle assessment, *ACS Sustain. Chem. Eng.* 9 (2021) 7139–7153, <https://doi.org/10.1021/acssuschemeng.1c01554>.
- [199] M. Zackrisson, K. Fransson, J. Hildenbrand, G. Lampic, C. O'Dwyer, Life cycle assessment of lithium-air battery cells, *J. Clean. Prod.* 135 (2016) 299–311, <https://doi.org/10.1016/j.jclepro.2016.06.104>.
- [200] F. Wang, Y. Deng, C. Yuan, Life cycle assessment of lithium oxygen battery for electric vehicles, *J. Clean. Prod.* 264 (2020), 121339, <https://doi.org/10.1016/j.jclepro.2020.121339>.
- [201] A. Mayyas, M. Omar, M. Hayajneh, A.R. Mayyas, Vehicle's lightweight design vs. electrification from life cycle assessment perspective, *J. Clean. Prod.* 167 (2017) 687–701, <https://doi.org/10.1016/j.jclepro.2017.08.145>.
- [202] E.A. Olivetti, G. Ceder, G.G. Gaustad, X. Fu, Lithium-ion battery supply chain considerations: analysis of potential bottlenecks in critical metals, *Joule* 1 (2017) 229–243, <https://doi.org/10.1016/j.joule.2017.08.019>.